Development of a new technique for determining the RTD of a dispersed solid phase and its application in a deep fluidized bed

Atena Dehghani Kiadehi

Par **Atena DEHGHANI KIADEHI**

Development of a new technique for determining the RTD of a dispersed solid phase and its application in a deep fluidized bed

Thèse présentée
pour l'obtention du grade
de Docteur de l'UTC

Soutenue le 28 mai 2019
Spécialité : Génie des Procédés Industriels : Transformations intégrées de la matière renouvelable (EA-4297)
D2491

THESIS

Presented to obtaining the

DOCTOR OF UNIVERSITY OF TECHNOLOGY OF COMPIEGNE

Specialty: Industrial Process Engineering

Génie des Procédés Industriels

By

Atena DEHGHANI KIADEHI

Development of a new technique for determining the RTD of a dispersed solid phase and its application in a deep fluidized bed

Date of defense 28 may 2019 in front of jury :

K. SALEH et Aissa OULD-DRIS	Professeurs	Directeurs de Thèse
N. FATAH	Professeur, ENSCL-UCCS, Lille	Rapporteur
L. BALLAND	Maître de conférences HDR, Université de Rouen Normandie (IUT de Rouen)	Rapporteur
N. MOUHAB	Professeur de l'Université de Rouen Normandie (IUT de Rouen)	Membre
K. SHAKOURZADEH	Dr.Ingénieur, UTC Compiègne	Membre
M. LETURIA	Dr.Ingénieur, UTC Compiègne	Membre invité

THESE

En vue de l'obtention du titre du

DOCTORAT DE L'UNIVERSITE de TECHNOLOGIE de COMPIEGNE

Spécialité : Génie des Procédés Industriels

Unité de recherche : TIMR

Par

Atena DEHGHANI KIADEHI

Développement d'une nouvelle technique de détermination de la DTS d'une phase solide dispersée et application à l'écoulement dans un lit fluidisé profond

Soutenue le 28 mai 2019 devant le jury composé de:

K. SALEH et A. OULD-DRIS	Professeurs	Directeurs de Thèse
N. FATAH	Professeur, ENSCL-UCCS, Lille	Rapporteur
L. BALLAND	Maître de conférences HDR, Université de Rouen Normandie (IUT de Rouen)	Rapporteur
N. MOUHAB	Professeur de l'Université de Rouen Normandie (IUT de Rouen)	Membre
K. SHAKOURZADEH	Dr.Ingénieur, UTC Compiègne	Membre
M. LETURIA	Dr.Ingénieur, UTC Compiègne	Membre invité

Abstract

The aim of the present thesis is to develop a novel experimental technique for determining the residence time distribution (RTD) of solid particles in solid unit operations as well as model development. Initially, a novel optical method was developed to measure the particle RTD. Experiments are carried out with Silicon Carbide (SiC) and the pigment phosphorescent (Lumilux® Green SN-F50 WS) as tracer particle. A preliminary experimental study was conducted in a simple bubbling fluidized bed in order to validate the proposed RTD measurement methodology. In the second step, the developed technique of the concentration measurement was applied to measure the RTD of a deep fluidized bed. The particle RTD curves are determined experimentally in different operating conditions. Finally, a model consisting of the combination of the ideal reactors is proposed to predict the particle residence time distribution in the studied fluidized bed. The predicted output values are then compared with the experimental data to establish a good model fitting data.

Keywords: Residence time distribution; fluidized bed; optical method; phosphorescent tracer

Résumé

L'objectif de cette thèse est le développement d'une nouvelle technique expérimentale de détermination de la distribution des temps de séjour (DTS) des particules solides dans les enceintes de manutention et de transformation de solides particulaires ainsi que le développement d'un modèle. Dans un premier temps, une nouvelle méthode optique a été développée pour mesurer la DTS des particules. Les expériences sont réalisées avec le carbure de silicium (SiC) et le pigment phosphorescent (Lumilux® Green SN-F50 WS) a été utilisé en tant que traceur. Une étude expérimentale préliminaire a été réalisée dans un lit fluidisé bouillonnant simple afin de valider la méthodologie proposée de mesure de la DTS. Dans un deuxième temps, la technique développée de la mesure de concentration a été appliquée à la détermination de la DTS dans un lit fluidisé profond. Les courbes de la DTS des particules sont déterminées expérimentalement dans différentes conditions opératoires. Dans un troisième temps, un modèle basé sur une combinaison de réacteurs idéaux est proposé pour prédire la DTS des particules du lit fluidisé étudié. Les valeurs de sortie prédites sont ensuite comparées aux données expérimentales pour l'ajustement du modèle.

Mots-clés : Distribution des temps de séjour; lit fluidisé; méthode optique; traceur phosphorescent

`

Acknowledgement

The completion of this degree would not have been possible if it were not for those people, who truly believed in my potential and provided me with opportunities; who landed help whenever I needed; and who unconditionally supported me. I would like to thank the many people, supervisors, family and friends who helped me to reach this level of achievement.

I would like to express my deepest gratefulness to my chief supervisor Pr. SALEH for his encouragement, guidance, inspiration and continuous to support throughout this endeavor. He encouraged me and challenged me every step of the way, professionally and personally, allowing for my own developments.

Much appreciation is extended to my co-supervisor Pr. OULD-DRIS for his helpful guidance, constructive suggestions, kind encouragement during the progress of this work.

My special thank you is directed to Dr. Mikel LETURIA for his unconditional support, invaluable encouragement, advice and friendship throughout these years.

I would like to thank all the members of TIMR team for their kind welcome, for their time allocated to cooperating with me in sharing information and the production of ideas and knowledge that allowed me to enrich this thesis.

Finally, I acknowledge my family; my parents who provided not only wonderful examples of hard work, but without your dedication in my education all these would not be possible. I would never be able to pay back the love and affection showered upon by my parents.

I also appreciate my little girl Anahita for the patience she showed during my thesis. Lastly, thanks to my dear husband, Vahid, for his continued and unconditional love, support and patience and makes the completion of this thesis possible. Words would never say how grateful I am to both of you.

Contents

Nomenclature

Greek Letters		**Unit**
ψ_s	sphericity of the solid particles	
σ	variance	
ε	porosity of particle	
ε_{mf}	minimum fluidization porosity	
μ	viscosity of gas	Pa s
ρ	density	kg m^{-3}
ρ_p	density of solid	kg m^{-3}
ρ_g	density of gas	kg m^{-3}
ρ_f	density of flow	kg m^{-3}
ν	volumetric flow rate	m^3/s
τ_s	mean residence time in the CSTR	s
τ_p	mean residence time in the PFR	s
τ_i	average residence time in each stage	s
Θ	dimensionless time	
∞	infinity	

Latin letters		
A	cross-sectional area	m^2
Ar	Archimedes number	
$C_{Pigment}$	concentration of the tracer particle	
C_V	combinations of moments	
CSTR	continuous stirred-tank reactor	
CFB	circulating fluidized bed	
D	dispersion coefficient	$m^2\ s^{-1}$
d	column diameter	m
D_B	bubble diameter at the bed surface	m
d_p	particle diameter	m
d_p^*	dimensionless particle diameter	
E(t)	residence time distribution function	
$E_{i\infty}$	elutriation rate constant	
$E(\Theta)$	normalized RTD function	
E_1	residence time distribution of the block-injection	
E_2	residence time distribution of the bed	
E_m	residence time distribution of model	
F(t)	cumulative distribution	
F	mean cumulative distribution value	

F_0	entrainment rate of particles at the bed surface	m^3s^{-1}
F_∞	total amount of particles elutriated	g
$F_{i\infty}$	amount of particles elutriated	g
F_{i0}	amount of fine particles in the freeboard	g
F_D	fluid drag	N
g	standard gravity	$m\ s^{-2}$
H	bed height	m
I	integral of the detected signal	
L	reactor height	m
L_{mf}	minimum bed height	m
m	masse of tracer	g
N	number of ideal tank in series	
n	sample size	
N_0	amount of injected tracer	mole
Pe	Peclet number	
PMT	photomultiplicator	
PFR	plug flow reactor	
ΔP	pressure drop	
R	radius of the tube	m
RTD	residence time distribution	
RMS	root mean square	
Re	Reynolds number	
Re_{mf}	Reynolds number in minimum fluidization	
R	radial distance from the center of the tube	m
S	skewness	
SD	standard deviation	
t	time	s
t^*	dimensionless time	
t_1	half of the injection time	s
t_m	mean residence time	s
TDH	transport disengaging height	m
Δt	time step interval	s
U	fluid velocity	$m.\ s^{-1}$
U_{mf}	minimum fluidization velocity	$m.\ s^{-1}$
U_{mb}	minimum bubbling velocity	$m.\ s^{-1}$
U^*	dimensionless fluidization velocity	
V	reactor volume	m^3
x	longitudinal abscissa of the flow	
X_i	weight fraction of fine particles present in the bed	
z	longitudinal abscissa of the flow	
$Z_{\alpha/2}$	confidence coefficient	

List of figures

List of tables

General introduction

The present thesis is conducted at "*Laboratoire des Transformations Intégrées de la Matière Renouvelable-TIMR*" University of Technology of Compiègne (UTC) under the supervision of Professor SALEH, co-directed by Professor OULD-DRIS.

A novel technique for particle Residence Time Distribution (RTD) measurement in solid unit operations is developed in this work.

An introduction to the research background, objectives and thesis structure are presented in this section while leaving detailed introductions on specific topics to later chapters.

Context

In the study and design of a solid unit operation, characterization of overall flow behavior by means of particle RTD and the solid flow pattern and mixing are major issues. The solid flow patterns in these units are very complex. The solids in a continuous solid-flow system leave the system after a period of time approximating mean residence time.
Consequently, in solid unit operations there is a wide range of particle residence time distribution, which can be a serious disadvantage if, as in many commercial applications, good control of solid mixing, fast reaction rate, quick catalyst activation and uniform treatment of solids is desired. Knowledge of the RTD enables the exact prediction of yield for first order reactions and allows close estimation for reactions of order other than first.
Even though the RTD does not carry complete information about the flow and structure of a particular bed, it is possible to affirm that the RTD is a characteristic of the mixing which occurs in the solid unit operations and is vital for solid unit design and scale-up, plant operation and optimization.
Fluidized bed reactors, a type of solid unit operation, are present in many applications and gas-solid processes. These reactors are widely used in numerous industries such as biomass gasification, reforming and chemical looping combustion.
The process efficiency depends on the efficiency of contact and the contact time between gas and solid phases. Therefore, knowledge of solid mixing and particle residence time distribution is essential in order to describe, design and model the fluidized bed reactors. Several tracer methods have been used for particle residence time distribution measurement or for mixing investigation purpose. These methods are summarized in Table1.

Table 1: Summery of solid residence time distribution methods.

Method	Author	System	Details of method
Radioactive tracer	Abellon et al. [1]	Four interconnected fluidized bed	Bed material: Glass beads Tracer: ^{24}Na and ^{192}Ir
	Ambler et al.[2]	CFB	Pulse tracer technique with Gallium-68 tracer
	Bhusarapu et al.[3]	Riser of CFB	Single radioactive particle (^{46}Sc)
	Lin et al. [4]	CFB boiler	^{56}Mn as tracer
	Mahmoudi et al.[5]	CFB riser	Positron emission particle tracking using ^{18}F as tracer

	Pant et al. [6]	Pilot scale fluidized bed reactor	Gold-198 as tracer
	Chan et al. [7]	Riser of fluidized bed	Positron emission particle tracking using ^{18}F as tracer
Magnetic tracer	Avidan and Yerushalmi[8]	Expanded top fluidized bed	Ferromagnetic particle tracer
	Guío-Pérez et al. [9], [10]	Dual circulating fluidized bed	Steel particles as tracer
	Legile et al.[11]	Thin channel type gas-solid fluidized bed	Ferromagnetic particle tracer
Chemical particle tracer	Andreux et al. [12]	Riser of cold fluidized bed	NaCl crystals injected in the connecting point between L-valve and the riser
	Cui et al. [13]	Stripper of fluidized bed	FCC particles were impregnated with a saturated solution of table salt and then dried to remove all moisture
	Rhodes et al. [14]	Riser of CFB	NaCl as tracer; Tracer sampling was performed in three locations in the riser
	Smolders and Baeyens[15]	Riser of CFB	NaCl tracer
Phosphor particle tracer	Wei and Du [16]	Riser of CFB	The tracer particles are made by coating of fin phosphor particles on the surface of different property particles with nitryl-varnish as the bond.
	Harris et al. [17]–[21]	Riser of CFB	All particle have phosphorescent properties
	Huang et al.[22]	Down-flow CFB	A pneumatic injection phosphor tracer technique (PIPTT) was used to determine the axial and lateral solids dispersion by measuring the solids RTD at same axial but different lateral positions.
	Wei et al.[23]	CFB downer	A unique phosphor tracer technique measures the solids tracer concentration with time at different radial and axial positions within the co-current down flow circulating fluidized bed.
	Yan et al.[24]	Riser of CFB	The solids mixing in a riser with a height of 10 m and 0.186 m inner diameter was investigated by using the pneumatic phosphor tracer technique.
	Chen et al. [25]	Extruder	A He-Ne laser as a light source with carbon black as the tracer

From the review of the reported experimental methods, several research groups [16], [19]–[25] prefer to employ phosphorescent tracer particles thanks to its simplicity and high accuracy. In these works, the properties of phosphorescent tracer particles were similar to the average properties of the bulk particles.
The principal of the impulse injection phosphorescent tracer technique is shown in Figure 1. It consists of two main parts: tracer activation and tracer detection. When the light source is turned on, the phosphorescent particles surrounding the light are excited. The excited phosphorescent particles emit light and the afterglow is captured by a detector and collected by a computer data acquisition system as a function of time.

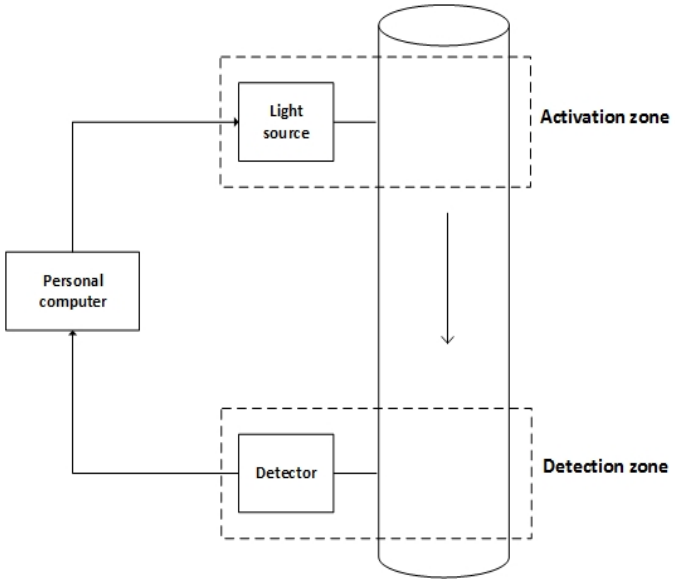

Figure 1: Schematic diagram of impulse injection phosphorescent tracer technique.

This optical method has been perfected by Harris et al. [19]–[21]. In these phosphorescent tracer experiments, phosphorescent particles were used as both bulk and tracer particles. In fact, just a small amount of phosphorescent particles were illuminated and became tracers. The detection is then carried out without disturbance of hydrodynamic behavior by means of a light detector. In these works, the phosphorescent tracer particle consumption was quite high due to the large amount of the bulk particles. It is also possible to coat the outside of the bulk particles using the pigment and a binder or glue. In this way, any particles that can be coated may be used for RTD experiments. Wei et al. [23],Yan et al. [24]and Du et al. [16]used a phosphorescent material, typically alumina powder coated with a phosphorescent compound as a tracer particle. Kulah et al. [26] investigated the solid mixing and motion in a riser of circulating fluidized bed utilizing phosphorescent-coated FCC particles as a tracer. The key advantage of this method according to the authors was its cost effectiveness. The major disadvantage was the need for a perfect coating which could reduce the detection efficiency.
In order to limit the amount of tracer particles used, a pneumatic injection phosphorescent tracer technique (PIPTT) was proposed by Du et al. [16]. The similar technique was undertaken by Huang et al. [22]. A small amount of phosphorescent tracer particles with similar properties to the bulk particles were injected into the fluidized bed so that wasteful amount of phosphorescent particles was reduced significantly.

Since the intensity of the light emitted by the activated tracer decays with time, there is an upper residence time limit for phosphorescent tracer techniques (for example 3 minutes for the tracer particle used by Harris et al. [20]). Therefore, the particle RTD measurement using this technique has been extensively studied in short solid residence time units (like previous PhD thesis done by Dr. Ahmed BELLIL, GPI department member at UTC). Due to the significance of total particle RTD of the unit operations, as an example of long residence time, on their optimization and design; finding an accurate technique able to detect very low intensity is a non-trivial matter. It was necessary to consider that with using this technique, which detects very low concentration, the tracer consumption will be reduced, and the hydrodynamic patterns of the unit operation will be changed as little as possible.
It should be mentioned that the particle RTD measurement in dispersed phases of solid unit operations is difficult to measure since the particle velocities vary. The particle size distribution leads to different velocities in activation part. Thus, the particles which pass through the activation part do not necessarily get detected at the detection part. Consequently, this inhomogeneity in size distribution and particle velocities makes it difficult to measure the particle RTD.

Research objectives

The objectives of the present study are:

- To develop a novel system for particle RTD measurement able to detect very low tracer concentration which allows the RTD experimental studies to be carried out in solid unit operations with long residence time and also with very low tracer consumption. The low consumption of the tracer enables the experiment to be conducted without separating the tracer particles and bulk particles.
- To create a calibration curve that provides the experimental relationship between the tracer concentration and the integral of the detected signal with high accuracy in systems with very low concentrations.
- To fully characterize and evaluate this novel particle RTD measurement technique by RTD studies of a simple bubbling fluidized bed reactor in order to validate the measurement methodology.
- To apply this novel technique to the particle RTD measurement of a deep fluidized bed in order to present an application of the developed technique.
- To model the particle RTD in the deep fluidized bed that provides predictions of the particle RTD with a reasonable accuracy. The model consists of a combination of ideal reactor models for which the E-functions are known. The simulated results are then compared with the experimental results.

Thesis structure

The thesis report consists of 4 chapters. The following chapter includes the literature review related to RTD theory and different ways to conduct RTD measurements in solid unit operations as well as RTD modeling in fluidized bed reactors.

Chapter 2 provides the details about the experimental apparatus of a new technique developed for tracer concentration measurement, the measurement technique and the experimental procedure. In this technique, a calibration curve is developed which provided the empirical relationship between the integral of the detected signal and the concentration of pigment. This chapter also describes a series of experiments which were performed in a bubbling fluidized bed. The results were compared with the theoretical results in order to validate this RTD measurement technique.

Chapter 3 presents a novel approach to a mixing process in a deep fluidized bed based on the developed RTD measurement technique. The main aim of the work presented in this chapter is to apply this novel technique for particle RTD measurement in a deep fluidized bed as an example.

Chapter 4 presents a model combining the ideal plug flow and stirred tank reactors for the fluidized bed described in Chapter 3. The interest is on predicting the RTD of a fluidized bed in order to formulate the modifications to obtain more information about the flow pattern inside the bed and also to serve in further investigations of this topic.

The general conclusion of this study and the list of recommendations for future work on particle RTD measurement are given at the end of this thesis.

Chapter 1

Literature survey

1.1 Introduction

In chemical engineering and related fields, the residence time distribution (RTD) is described as the probability distribution of time that solid or fluid materials stay inside one or more unit operations in a continuous flow system [27]. Residence time distribution is a key parameter to understand the profile of flow in the solid unit operations and is used in different industrial processes like the continuous manufacturing of chemicals, plastics, polymers, food, catalysts, and pharmaceutical products. To have the desired output from a specific unit operation, raw materials are designed to stay inside the unit operation under a specified period of time and specific operation conditions. Then, the residence time distribution is a necessary factor to complete the reaction or process in the unit operations.

Therefore, the RTD characterization is the first stage in optimization, design and scale up of process in different unit operations [27]. Fluidized bed as a type of solid unit operation is used as a solid-gas contacting system in a wide range of industries. Fluidized beds are used in chemical and mineral processing, gasification and combustion for power generation, environmental technologies, in the petrochemical industry as fluidized catalytic crackers, pharmaceuticals, biotechnology and other solid handling industries [28]. Compared to other solid-fluid contacting systems, fluidized beds have many advantages such as ease in solids handling and high heat and mass transfer. The disadvantages of fluidized bed is that it approaches a continuous stirred tank reactor rather than a plug flow reactor, resulting in the large amount of attrition caused by the strong mixing and high velocities of the solids. To study the hydrodynamic behavior in fluidized bed reactors, risers and downers, experimental and measurement methods have been developed. There are two study models in the experimental work in fluidized bed reactors: cold-model and hot-model. In the cold-model, the study of the experimental work has been devoted to hydrodynamic studies without reactions. In contrast, in the hot-model study the hydrodynamic studies have been done with reactions in order to obtain the reactor performance. Hydrodynamics are usually described by studies of solid holdup and gas and solid velocities. Studies on solid residence time distribution in fluidized bed reactors are crucial as interactions are often influenced by hydrodynamics [29].

The goal of the present chapter is to extend our basic understanding of the motion of solid phase (particles) in solid unit operations through the study of the particle residence time distribution and to make the state of the art on the methods used for the particle residence time determination. Unlike the residence time in a gas or a liquid, residence time determination in solids poses special problems related to the existence of the concentration and velocity profiles and a sliding velocity between gas and solid phases.

This chapter consists of a review of topics necessary to understand the concepts applied in the research. The first section is about the RTD theory in solid unit operations and RTD measurement techniques (RTD definition, RTD function, RTD of ideal and real reactors, RTD models, reported experimental RTD techniques). The second part will present a general description of fluidized bed reactors as a widely used solid unit operation.

1.2 Residence Time Distribution (RTD) theory

1.2.1 RTD definition

When the material flow passes the inlet of the reactor in steady state, the various fractions of the stream do not pass through the outlet section of the reactor at the same time, reflecting the fact that there is a distribution of the residence times in the reactor. This phenomenon can be represented by a residence time distribution, abbreviated to RTD [30]. The residence time distribution of a unit operation is one of the characteristics of the mixing process.

In lot of processes, the fast reaction rate, quick deactivation of catalyst and high heat and mass transfer, there is a need of a good control of solid mixing and residence time. Therefore, residence time distribution data help in the understanding of fluid dynamics. These data are essential for reactor design, scale-up, plant operation and optimization [19].

As mentioned earlier, the residence time distribution measurement in solids poses specific problems. The residence time distribution in solids related to the concentration and velocity profiles and sliding velocity between particles and gas phase. Besides, finding the best tracer materials and detection methods is very difficult.

Regarding to the measurement system, some of the most important RTD measurement requirements are [31]:

- Sensitivity of the measurement must be as high as possible; use of a small amount of tracer is beneficial.
- The measurement should be repeatable and reproducible within reasonable time.
- In ideal condition, the tracer concentration should be calculated without need of intricate assumptions or corrections.
- Any disruption of the internal flow pattern should not be affected by the detection device or method. Exclusively, pressure and solid inventory should not be affected.
- RTD measurement should be possible under steady state operation conditions.
- The detection method should be fast enough. In this way the features of RTD in fast beds with very short residence time can be captured.

The experimental determination of RTD, also called the tracing method, is a general method and can be implemented on a wide variety of industrial systems [5],[32] or on a laboratory scale in microstructure reactors [33].

1.2.2 Residence time distribution function E(t)

The RTD is commonly measured experimentally by tracer injection into the feed stream at time *t=0* and then the tracer concentration *C* is measured in the exit stream as a function of time (stimulus-response injection technique) [34]. The tracer should be an inert chemical, molecule or atom and should have physical properties similar to those of the bulk particles and be completely soluble in the

bulk. The tracer also should not to be adsorbed on the surfaces of the reactor like walls. The pulse input and step input are the most common and simplest tracer injection techniques [35]. In a pulse input, an amount of tracer is suddenly injected into the unit operation in a short time interval. The outlet concentration is then measured as a function of time. Typical concentration curves for a step input and pulse input are given in Figure 1.1.

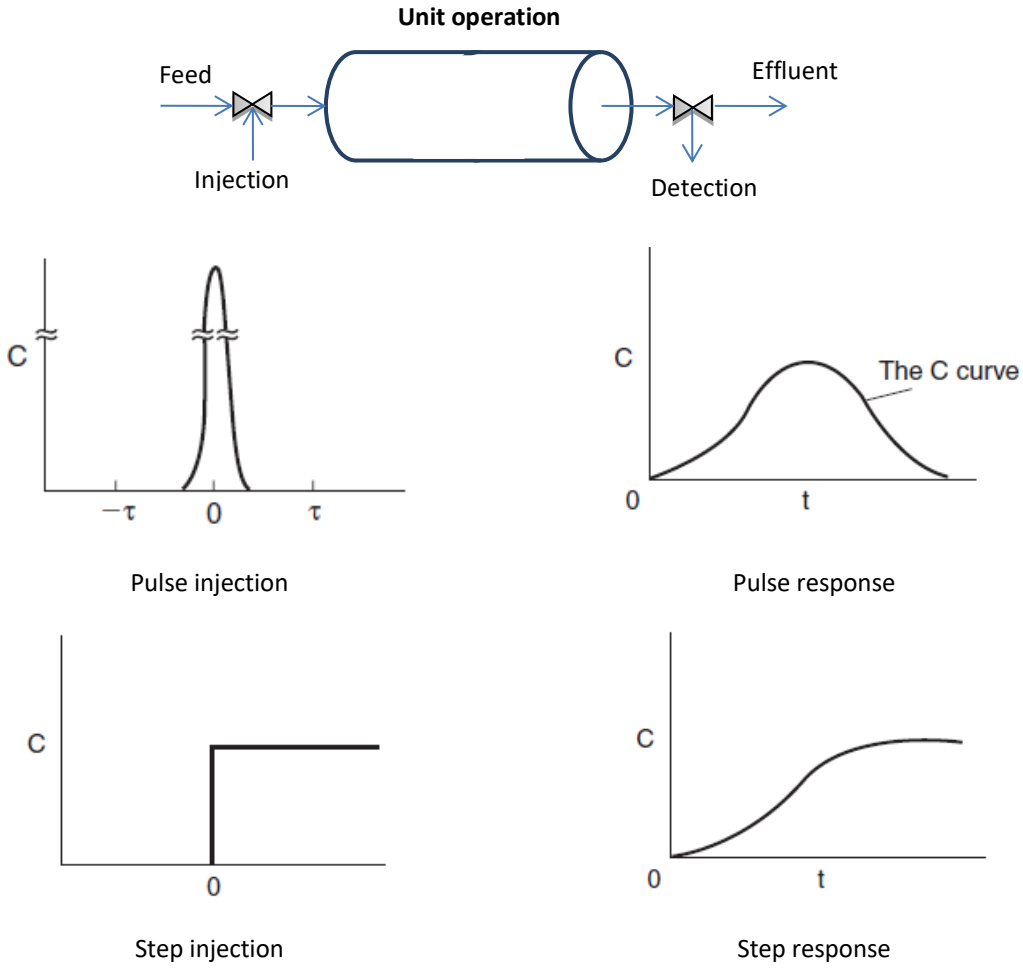

Figure 1.1: RTD measurements for a step input (bottom) and pulse input (top) [34].

The pulse input is usually more difficult to carry out experimentally than the step input. In step input tracer injection technique, the total amount of tracer must be known in the input stream over the experimental time contrary to the pulse test. On the other side, in step input injection technique is sometimes complicate to maintain a constant tracer concentration in the input stream [34].

Another drawback in step input tracer injection technique is that the obtained RTD involves differentiation of the data which leads to large errors. It should be noted that in step input technique

the large amount of tracer is required. Therefore, for the expensive tracer a pulse test is always used to minimize the cost [34].

The amount of tracer material, *ΔN*, leaving the reactor between time *t* and *t+Δt* is:

$$\Delta N = C(t) v\, \Delta t \qquad (1.\ 1)$$

where v is the volumetric flow rate, *C(t)* is the concentration of the tracer particles in the exit at time *t* and ΔN is the amount of material passing the reactor which has spent an amount of time between *t* and *t+Δt* in the reactor. It should be noted that the equation (1. 1) is valid for a tracer miscible in all proportions with the fluid and when there is no relative velocity between the tracer and the fluid. Therefore, the amount of tracer material in two-phase systems, particularly for a solid phase, is difficult to measure experimentally.

The residence time distribution function for pulse injection is defined by [34]:

$$E(t) = \frac{v\, C(t)}{N_0} \qquad (1.\ 2)$$

or,

$$E(t) = \frac{C(t)}{\int_0^\infty C(t)dt} \qquad (1.\ 3)$$

when *C(t)* is the concentration of the exit tracer particles at time *t* and N_0 is the amount of tracer injected into the reactor. It must be mentioned that the equation (1. 2) is valid for a piston flow and when there is no slip of the solid and gaseous phases.

The fraction of all the material that has stayed for a time *t* between $t = 0$ and $t = \infty$ in the reactor is 1:

$$\int_0^\infty E(t)dt = 1 \qquad (1.\ 4)$$

The cumulative distribution $F(t)$ can be determined directly from a step input since the RTD function $E(t)$ can be determined directly from a pulse input.

$$\left[\frac{C_{out}}{C_0}\right]_{step} = \int_0^t E(t')dt' = F(t) \qquad (1.\ 5)$$

Equation (1. 6) was defined by Danckwerts [30] as a cumulative distribution function *F(t).* The relationship between *F(t)* and *E(t)* is:

$$F(t) = \int_0^t E(t)dt \qquad (1.\ 6)$$

The *F* curve has been defined as the normalized response to a particular input. Therefore, the *F* curve can be used in the same way as the RTD in the chemical reactors modeling [34].

Mean residence time (t_m), which corresponds to the average of the residence times, is given by the first moment of the distribution:

$$t_m = \int_0^\infty tE(t)dt \qquad (1.\ 7)$$

The precise reactor volume is determined from the equation (1. 1):

$$V = vt_m \qquad (1.\ 8)$$

When there is no relative velocity of gas and solid phase.

To compare RTDs, their moments are usually compared instead of their entire distribution. Three moments are normally used in order to compare RTDs: mean residence time, variance and Skewness [34].

The variance or square of the standard deviation is defined by:

$$\sigma^2 = \int_0^\infty (t - t_m)^2 E(t)dt \qquad (1.\ 9)$$

The skewness is defined by:

$$S^3 = \frac{1}{\sigma^{3/2}} \int_0^\infty (t - t_m)^3 E(t)dt \qquad (1.\ 10)$$

The magnitude of variance is a sign of the "spread" of the distribution. Therefore, the greater the value of variance is the greater the spread of distribution. In the same manner, the magnitude of skewness shows the limit that a distribution is skewed in one direction or another compared to the mean. For a complete description of a distribution, all three moments should be determined:

Normalized RTD function, $E(\Theta)$:

A dimensionless function $E(\Theta)$ can be defined as:

$$E(\Theta) = \tau E(t) \qquad (1.\ 11)$$

when the parameter Θ is defined as:

$$\Theta = \frac{t}{\tau} \qquad (1.\ 12)$$

The quantity Θ shows the number of reactor volumes that have passed through the reactor in time t based on entrance conditions. With defining this normalized distribution function the performance of flow inside reactors of different sizes could be directly compared [34]. In this way, as an instance, all perfectly mixed CSTRs have numerically the same RTD.

In order to determine the residence time distribution, a tracer is introduced into the system according to a known function and the concentration as a function of time. The tracer must not modify the physical properties of the medium (same density, same viscosity) and the tracer introduction must not modify the hydrodynamic conditions.

Different experimental techniques have been used to measure the solid residence time distribution in unit operations. Following subsection reviews several techniques used for measuring particle RTD in solid unit operations, especially in fluidized beds.

1.3 Reported experimental RTD techniques

The experimental determination of RTD has been used to correct the knowledge of the solid particle behavior and also different phases present in pilot studies or industrial reactors. Depending on the operating conditions different methods can be used. The general principle of RTD determination consists of tracer injection into a system and measurement of concentration as a function of time [46]. The particles trajectories in any solid unit operations are different because of the various particle properties, gas velocity field, inter-particle shocks and reactor geometry which influences on the fluid flow. The different particle trajectories give rise to a distribution of residence times for the particles flowing through the reactor [35].

In fluidized beds research, many different tracer methods have been used for particle RTD purpose such as radioactive tracers, thermal particle tracers, chemically different tracers, ferromagnetic tracers, different sized particle tracers and phosphorescent particle tracers. All RTD techniques have limitations such as disruption to the internal flow pattern, long time of sampling, health risks, difference between tracer and bed material and injection and detection systems.

Harris et al. [20] complied a detailed review of the most suitable techniques used until now in the measurement of RTD of particles and mixing behavior in fluidized beds. They proposed a classification of techniques based on disruptive and non-disruptive effects on the hydrodynamic flow. In disruptive techniques, the internal flow pattern and RTD were disrupted with injection devices and sampling probes. But non-disruptive methods are techniques that do not add disruptive device to the flow in the vessel. Generally, the non-disruptive methods are preferred for the experimental determination of residence time distribution.

According to Levenspiel [47], any material can be used as a tracer if it can be detected without disturbing the flow pattern in the vessel. In addition to this, the tracer has to meet the following general characteristics:

- It should have physical properties identical to all bulk particles. If more than one phase is involved in the experiment, the tracer must stay in the phase of interest.
- It has to be non-reactive and also detectable in small concentrations.
- The tracer and the detection device must not be too expensive.

The goal of this section is the explanation of the tracing techniques used until now to choose the best techniques for particle residence time distribution measurement in our experimental work.

1.3.1 Radioactive tracers

A number of researchers have utilized radioactive tracers in fluidized bed reactors [1]–[7], [48], [49]. The principle of this method consists of a radioactive tracer's injection into a system at the inlet of a studied zone and the measurement of its radiation intensity as a function of time, using the sensors placed at one or more selected points. Radioactive tracers are characterized by their activity and their half-lives. Their activity must be strong enough for an accurate and rapid detection through the walls; but not too much to avoid the risk of contamination and irradiation.

For radiation intensity's measurement, a series of detectors are placed around and along the examined area. These are generally scintillation sensors which count the number of photons emitted in a very short period of time. These signals are continuously monitored and displayed in the form of curves, which give an immediate representation of the response, while simultaneously being recorded and processed for further analysis. The appearance of radioactivity was monitored in all of these studies and in different locations. With this way, RTD of fluidized beds can be measured.

Ambler et al.[2], Bhusarapu et al. [3] and Mostoufi et al. [48] carried out a series of solid RTD experimental studies using a radioactive pulse tracer technique. Bhusarapu et al.[3] used ^{46}Sc as tracer for measuring overall solid mass flux and solid RTD for the entire riser. The Scandium particles were coated with a layer of polymer (*Parylene N*) to have the same density as the solids used (Glass beads). Three detectors in different sections (at the base of the riser, above the solid entry zone into the riser and at the start of the down comer) used for tracking the particles were placed in the loop. The results showed that 59% of the solids traveled from the inlet to exit in a single pass without re-exiting at the inlet.

Mahmoudi et al.[5] investigated the overall solid residence time in the riser of a CFB. They used a PEPT (Positron Emission Particle Tracking) technique with ^{18}F as a tracer. The PEPT technique involves a labeled tracer particle, a positron camera and a location algorithm used for calculating the tracer location and speed [50]. The results showed that according to the operating mode of riser, the particle motion and mixing mode differs. Lin et al.[4] also conducted series of solid RTD experiments using a radioactive tracer (^{56}Mn) to investigate the hydrodynamic of a commercial-scale CFB boiler. The tracer is resistant to heat and attrition, also its density is close to the density of the bed material in the boiler. The radioactive tracer particles were conveyed to the test location before the experiments started, and then were dispensed in a portion of sand and injected into the apparatus with a probe. They used 12 detectors which were placed in different positions (Figure 1.3).

They also used combinations of cascade tanks to model the particle flow pattern in the standpipe and in the furnace of the CFB boiler. This study showed that there was a significant reduction to the particle recirculating rate when the load of the boiler is decreased.

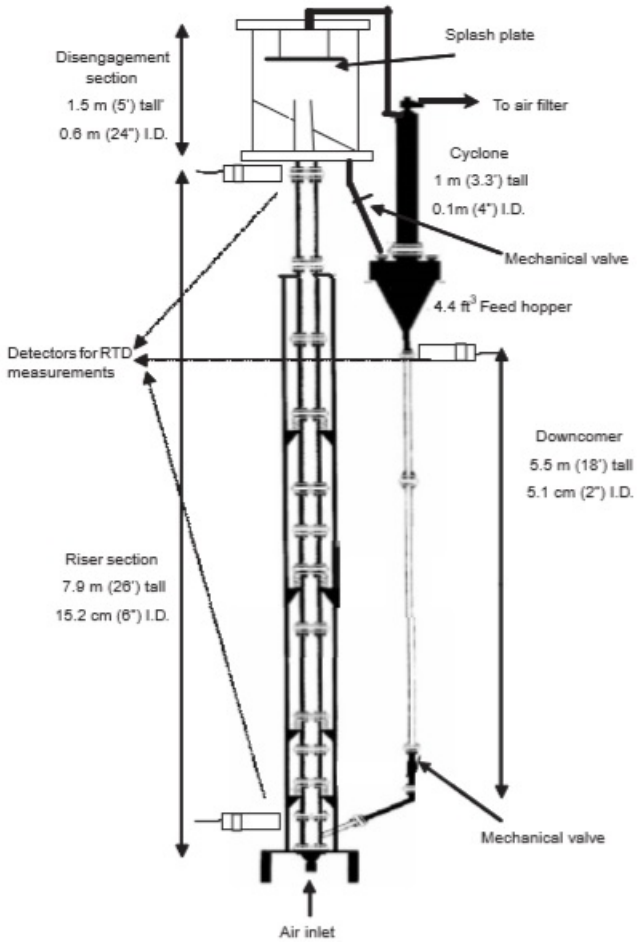

Figure 1.2: Schematic diagram of CFB setup used by Bhusarapu et al.[3].

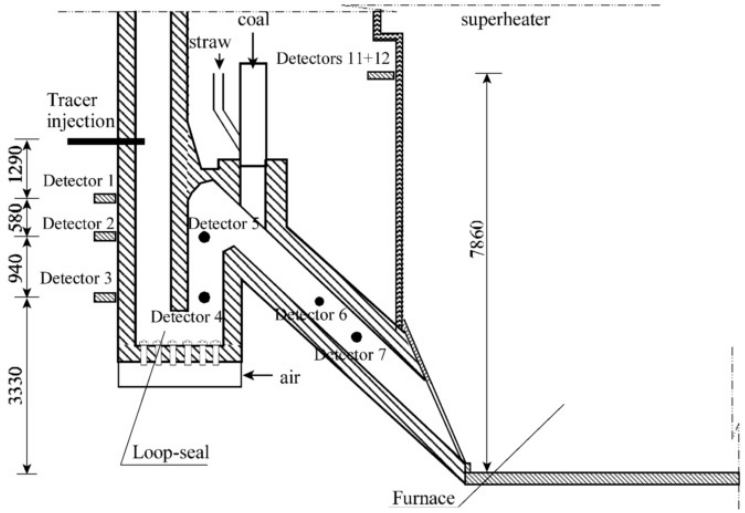

Figure 1.3: Detector locations used in the experimental set-up for particle RTD measurement [4].

Pant et al.[6] studied the influence of operating conditions on the residence time distribution of coal particles in a pilot-scale, gas-solid fluidized bed. *Gold-198* radioisotope was selected for labeling the coal particles and used as a radiotracer. The tracer was instantly introduced into the reactor after it achieved steady state condition. They used three detectors in different sections (inlet, bottom and top outlet) of the reactor to record tracer concentration. The results of this study indicated poor radial mixing and non-uniformity in the fluidized bed, but good axial mixing of the solid phase was observed.

Generally, the advantages and disadvantages of the radioactive tracer technique are listed below:

Advantages:

- This technique is a one of the non-intrusive techniques and it does not disturb the flow.
- It can often be applied by irradiating some of the solids already present in the medium. In addition, it generally requires only a small amount of tracer.
- Since the radiation is not even stopped by thick metal walls, the method can be used in industrial context, even under high temperatures and pressures.
- The measurement gives immediate information and, if necessary, simultaneously at different points.
- Several tests can be carried out consecutively, even in a looped system, by a simple correlation on the background noise, if the tracer is diluted quite rapidly.

Disadvantages:

- One of the most important constraints is the supply and handling of radioactive solids, which are subject to very strict regulations. Testing can only be done by companies and authorized persons. By observing these rules and putting in place the corresponding precautions, the risks of irradiation or contamination are low.
- Due to these constraints, the flexibility of use is reduced, since the tests must generally be programmed sufficiently in advance in a concise and concentrated manner over time.
- The signals are sensitive to certain external disturbances (echoes, distortions, parasitic absorptions due to the presence of various metallic masses) due to interference with other beam emitters, as is often found in certain industrial sites (Level measurements, welding controls, etc.). The measurements are therefore preferably evaluated in a relative scale.

In conclusion, this method is particularly well adapted to evaluate the stability or the evolution of a system by repeating measurements periodically on a well-identified system, but it has some negative points such as health risk.

1.3.2 Chemically different tracers

The present technique consists of injecting the tracer particle and sampling the particles as a function of time. The tracer must be distinguished by its chemical composition while keeping all its physical characteristics identical into the system. Under the experimental conditions the tracer must neither change phase nor react with the other elements or fluids present in the system. The sampling techniques have a direct influence on the response accuracy. Therefore, they must be chosen and applied with great care.

The chemically different tracers technique have been used extensively for fluidized bed and CFB studies [12]–[15], [51]. Bader et al. [52] obtained the solid residence time distribution in a fluidized bed cracking catalyst (FCC) riser from pulse injection of sodium chloride (*NaCl*) tracer. Later, Rhodes et al.[14] studied the effect of superficial gas velocity, mean solid flux and riser diameter on the longitudinal solid mixing in the CFB riser. A sodium chloride was used as a tracer along with the experimental techniques based on that of Bader and coworkers [52]. Tracer sampling was performed simultaneously at three locations in the riser. The samples were collected in containers and each sample was weighted before being washed with *100mL* of deionized water. They observed that the degree of longitudinal mixing of solids in the riser of a circulating fluidized bed decreases with increasing riser diameter.

Smolders and Baeyens [15] also investigated the influence of operating conditions on RTD of solids in CFB reactors with NaCl tracer. After sampling, the salt concentration is then derived from the electrical conductivity of the solution (sample and *100ml* water) by using a calibration curve. Figure 1.4 shows the sampling probe.

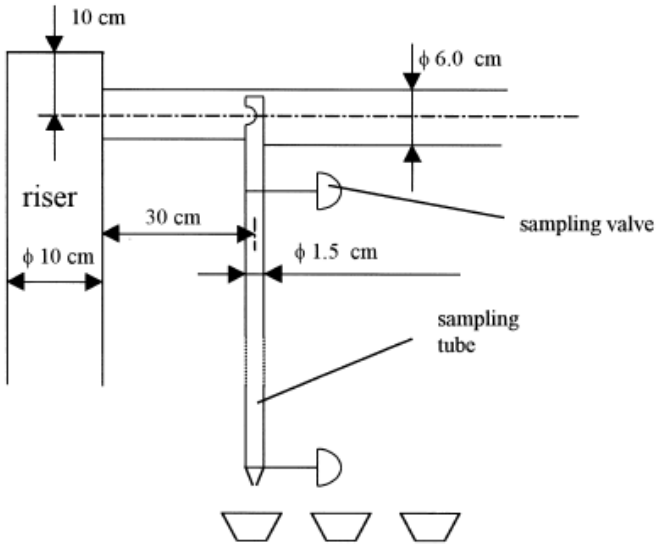

Figure 1.4: Sampling probe for determination of the solids RTD [15]**.**

Andreux et al. [12] investigated solid motion and particle RTD inside the riser of a CFB. *NaCl* was injected as a tracer in the connecting point between the L-valve and the riser and then sampled at the top of the riser. For prediction of the solid phase mixing in the riser, 3D transient CFB simulations were performed to conclude on the usability of the Eulerion-Eulerion approach. The axial dispersion of the solid phase (Geldart B particles) is found to decrease when increasing the solid flux rate.

Finally, the advantages and disadvantages of this technique are as follows:

Advantages:

- This method can be used in pilot or industrial installations and especially when operating conditions are difficult (high temperature or toxic atmosphere), at least until the tracer reacts.

- Since analyzes can often be fine, this method may be of a great interest when particularly when high sensitivity is required.

Disadvantages:

- This method disrupts the internal flow pattern because of the sampling probes and injection devices and then will have some effect on the RTD measurement.
- Analysis of data and determination of a relationship between the concentrations of tracer particles takes too much time and the measurement is rarely possible on-line.
- This method is limited to systems that evolve relatively slowly flow.

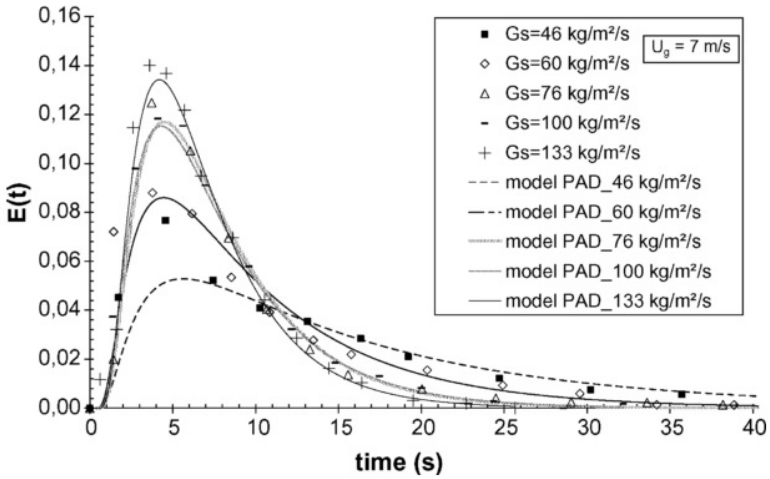

Figure 1.5: RTD modeling with plug flow model with axial dispersion for various mass fluxes [12].

1.3.3 Magnetic tracers

Particle RTD can also be determined with ferromagnetic tracers. The principle of this method is measuring the changes of magnetic permeability in different parts of reactor. Euzen and Fortin [53] studied solid mixing using a layer of magnetic tracer particles placed on top of the bed, and detecting the tracer concentrations at three bed locations. To know the concentration of ferromagnetic particles, coils were wound directly around the tubes on the sensing points (Figure 1.6).

An independent signal acquisition system is connected to each coil. The correlation between concentration of the ferromagnetic particles and the signals strength from the coil is needed for residence time distribution measurements [9].

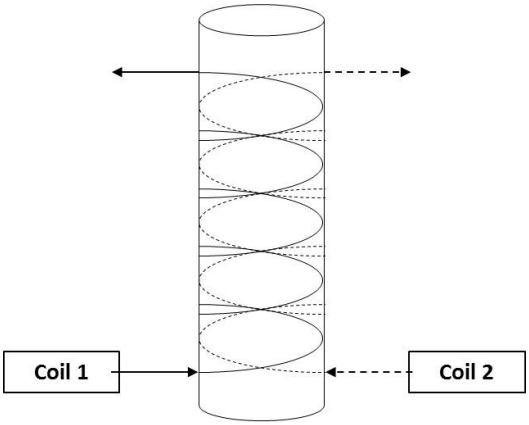

Figure 1.6 : Magnetic tracer technique [54].

The earliest article about the application of magnetic tracers in fluidized beds was published by Heertjes et al.[55]. The tracer was obtained by impregnation of the porous material used in colloidal Fe_2O_3. Then, a strong magnetic field was used for the tracer separation. They claimed that their tracer is an excellent tracer and the separation technique gives fast and accurate results.

Avidanand Yerushalmi.[8] investigated the solid mixing of group A powders with a ferromagnetic tracer in an expanded top fluidized bed. Results showed that the axial dispersion coefficients increased with gas velocity. Guio-Pérez et al.[9], [10] also studied the influence of global circulation rate, reactor inventory and reactor fluidization velocity on the solid residence time distribution. They used steel particles as tracers in a dual circulating fluidized bed (DCFB) system shown in Figure 1.7.

In another study, a simple coil was used as a measurement system for quantitative detection of ferromagnetic particles [31]. They observed that the mean residence time in the global loop is inversely proportional to the global circulation rate while the mean residence time in the internal loop appeared inversely proportional to the reactor fluidization velocity.

Sette et al. [56] used a magnetic tracer particle (NdFeB-based) in a bubbling fluidized bed in order to evaluate the influences of different parameters on the lateral dispersion coefficients of the bed material. This work showed that the lateral dispersion coefficient increases with bed height and gas velocity. However, the low-pressure drop distributor was found to be less sensitive to change in the bed height and gas velocity.

Some advantages of magnetic tracer technique for measuring the mixing behavior of solids are:

- This technique does not require special handling and the tracers are not toxic.
- The density and size can be modified to fit fluid dynamic requirements by forming a composite with a polymer.
- The magnetic properties of the material do not deteriorate with time or use.
- Temperature has only a slight influence on the magnetic tracers until it is kept below certain limits.
- The particles can be easily separated from bulk particles by means of magnets so the tracer can be re-used.

- A simple coil inductor can be used for the detection of tracer particles.

Ferromagnetic tracers exhibit also a number of disadvantages:

- The size of the coils is geometrically limited; the maximum diameter is currently about *15 cm*. Nevertheless, the construction of larger/thinner coils may be possible.
- Finding a suitable tracer can be quite difficult especially if the tracer must be manufactured.

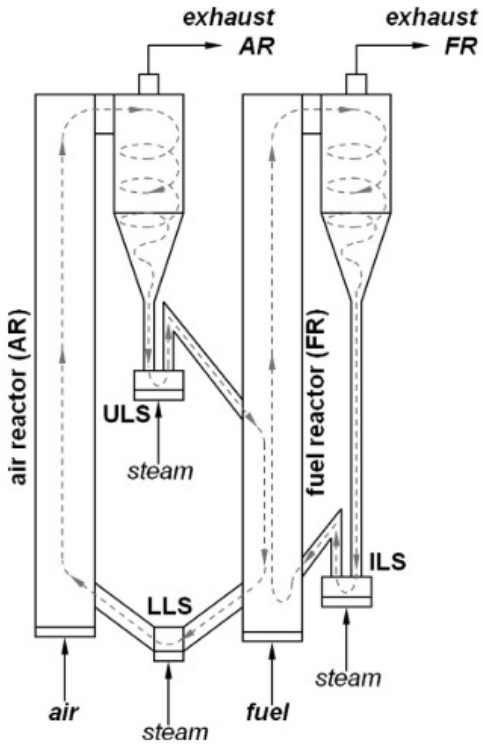

Figure 1.7: Dual circulating fluidized bed used by Guio-Pérez [10].

1.3.4 Thermal particle tracers

Thermal particle tracer is another technique developed by Thiel and Potter [57] and used in fluidized beds for particle RTD measurement. This technique uses bed temperature for RTD measurement. The bed was simultaneously heated and cooled at different locations until steady state conditions were reached. Afterward, the bed temperature was recorded at different sections. Valenzuela [58] also used heated particles as a tracer and a thermocouple as a recording device. He found that vertical particle transport in bubbling beds is asymmetrical. A thermal technique for lateral solid mixing in CFB was developed by Westphalen and Glicksman [59]. They demonstrated that the particle radial diffusion coefficient was in the order of magnitude of *10 cm^2/s*.

The main problem with thermal methods is in linking temperature to RTD, because it requires complicated assumptions. This technique imposes a complete thermal insulation of systems in order to be able to detect the temperature gradient between the heated particles (tracer) and the system.

Advantage:

- The technique can be carried out without contamination risk.
- The technique can employ high-tech sensors (thermal/infrared camera).
- This technique has the advantage of being easy to implement which facilitates the repeatability of the measurement with the same tracer.

1.3.5 Phosphorescent particle tracers

One of the non-disruptive techniques to determine the particle residence time distribution is the optical/phosphorescent particle tracer method. This technique utilizes the characteristics of the phosphorescent material which becomes fluorescent for a short period of time after being exited [24]. The phosphorescent particle tracer technique was developed by Wei et al.[23]. Phosphorescent material has a unique characteristic: sometimes it is excited by a light source, it emits light instantly and the light emission can be produced during a last few minutes depending on the phosphorescent properties; the strength of the emission decays with time [23]. It is an ideal material for a solid tracer. The phosphorescent particle tracers have a number of advantages such as [60]:

- Tracer injection is easy and immediate by using a light impulse.
- Detection of the tracer is easy and can be done on-line by using a light detector.
- The tracer particle is identical to the rest of the bed particles.
- There is no tracer accumulation in the bed within a few minutes after injection.

The principle of the phosphorescent tracer technique is demonstrated in Figure 1.8.

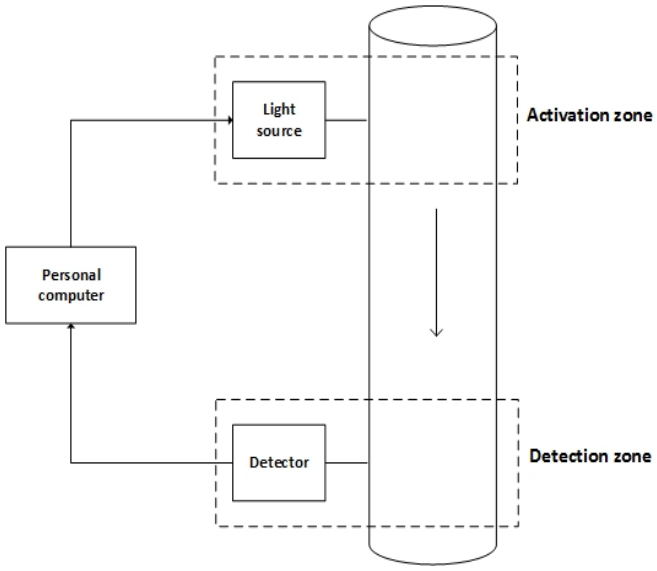

Figure 1.8: Schematic of phosphorescent tracer technique [23].

The phosphorescent tracer system consists of three parts: tracer injection, tracer detection and computer system acquisition. During experiments, the phosphorescent particles are injected into the system and excited by a strong light source. Only the portion of the phosphorescent particles surrounding the light source become excited and starts to emit light. Therefore, the excited phosphorescent particles take the role of tracer particles.

When the tracer particles pass by the detector, their emission light is captured by a photomultiplier detector and collected by a computer data acquisition subsystem as a function of time. Hence, the tracer concentration can be quantified. The higher the light intensity, the greater its concentration is.

Since the emission light from the phosphorescent particles decays with time, the light decay must be considered in the calculation of tracer concentration [16], [23]. Therefore, the light decay characteristics of the phosphorescent particles with time must first be calibrated.

Wei et al. [23], [61] and Ran et al. [62] developed a phosphorescent tracer technique to measure lateral and axial solid dispersion and solid mixing in different CFB units. They used alumina powder coated with a phosphorescent compound as a tracer particle. Chen et al.[25] also chose the method of light transmission, using fluorescence to study the RTD in extruders. A He/Ne laser was used as a light source and a photomultiplier was used to detect the particle concentration. From the experimental results they concluded that the method of transmission of light works well and gives good RTD curves with an uncertainty of 6% on average residence time.

The phosphorescent particle tracer technique was perfected by Harris et al. [17]–[21]. They measured the particle RTD in a circulating fluidized bed riser under experimental closed boundary conditions. In their experiments, both the bed material and the tracer particle are the same phosphorescent particles. Consequently, large amounts of the expensive phosphorescent particles would be necessary in experiments especially in large-scale apparatus. Then, a small quantity of phosphorescent particles was illuminated at the injection location of the fluidized bed and used as tracer particles. Consequently, the usage efficiency of the phosphorescent tracer particle is quite low.

In order to improve the phosphorescent tracer method, Huang et al. [22] proposed a pneumatic injection phosphor tracer technique (PIPTT) based on the phosphorescent tracer technique developed by Wei et al. [23], [60], Harris et al. [17]–[21] and Ran et al. [62]. In this approach, small amount of phosphorescent tracer particles with similar property to the bed material were injected into the fluidized bed resulting in the reduction of the amounts of used phosphorescent tracer particles.

A major disadvantage of the pneumatic injection phosphorescent tracer technique (PIPTT) method is that the light emitted from the tracer is shielded by the bulk particles and cannot be properly detected. For example, close to the wall region in fluidized bed riser the concentration of bulk particles is higher than that in the core region, so the shielding effect is also intense.

Figure 1.9 shows the typical experimental RTD curves obtained by Huang et al. [22] at the same axial but different lateral positions.

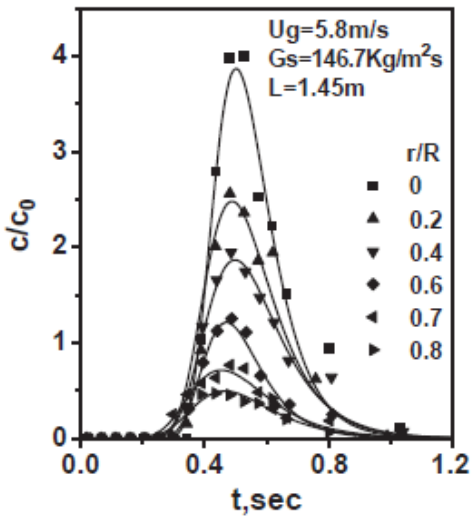

Figure 1.9 :Typical RTD curves at different lateral positions in fluidized bed downer reported by Huang et al. [22].

The advantages and disadvantages of this technique for measuring the mixing behavior of solids are:

Advantage:

- The measurements can be carried out without disturbance.
- The implementation of the technique is not costly.
- The technique can be used for systems where the average residence time is very short.

Disadvantage:

- The upper limit residence time of the method is short (about 3 minutes) due to the decay of the emission of the activated particles.
- The method requires the prior characterization of the decay of phosphorescence.
- It is generally difficult to deduce a flow of solid at the exit.

In order to provide a better comparison between different experimental particle trace methods a summary of their advantages and disadvantages is given in Table 1.1.

Table 1.1: Summary of particle trace methods for fluidization mixing studies.

Method	Advantages	Disadvantages
Radioactive tracers	non-intrusive requires only a small amount of tracer	Constraint of the supply and handling of radioactive solids Not flexible in use

	Can be used in industrial context, even under high temperatures and pressures. immediate information	Sensitive to certain external disturbances (echoes, distortions, parasitic absorptions due to the presence of various metallic masses)
Chemically different tracers	can be used in pilot or industrial installations and high temperature or toxic atmosphere high sensitivity Very practical in some systems Ability of sampling in particular areas Possibility of determination an extremely precise map of the areas	disrupts the internal flow pattern Long analysis time Off-line measurement Limited to systems that evolve relatively slowly
Magnetic tracers	Not requiring the special handling Non-toxic Not deteriorate of the magnetic properties of the material with time or use Ability of modification of density and size of tracer particles to fit fluid dynamic requirements by forming a composite with a polymer Separating the particles easily from bed material by means of magnets so the tracer can be re-used. Using a simple coil inductor for the detection of tracer particles.	Limited geometrically of the coils Finding a suitable tracer can be quite tedious especially if the tracer must be manufactured.

Thermal particle tracers	The technique can be carried out without contamination risk. Employing high-tech sensors (infrared camera) easy to implement and promotes the repeatability of the measurement with the same tracer	Difficulty of linking temperature to RTD because it requires complicated assumptions. Imposing a complete thermal insulation of the system
Phosphorescent particle tracers	Measuring without disturbance of system Low costly implementation Useful for systems with the very short average residence time	requiring the prior characterization of the decay of phosphorescence Finding a suitable tracer

1.3.6 RTD measurement using coated particles as a tracer

As mentioned before, the tracer particles should have similar physical properties as the bulk particles, other than being identifiable as a tracer. The conformability of the tracer particles with the bulk particles is the key ensuring the RTD experiments accuracy. However, it is actually very difficult to find a tracer agent having exactly the same physical properties as bulk particles. Therefore, bulk particles are often marked with a distinct color or coated with a radioactive material or any other material with properties that can easily be detected.

A number of researchers have attempted to coat the bed particles with the tracer compound in order to ensure that the tracer particles present the same flow behaviors as the bed material in the vessels and also to reduce the consumption of the tracer particles. Kang et al. [63] used potassium chloride (KCL) coated particles to measure the solids residence time in a cyclone and used titration method (Volumetric analysis) to measure tracer concentration. In their set-up they replaced the solids collection hopper at the dust outlet with a sampling tube of *10mm* ID. The column of sampled solids was then sectioned into small slices. The tracer particles in each slice were then dissolved in water for an hour and the tracer concentration determined by measuring the electrical conductivity of the solution.

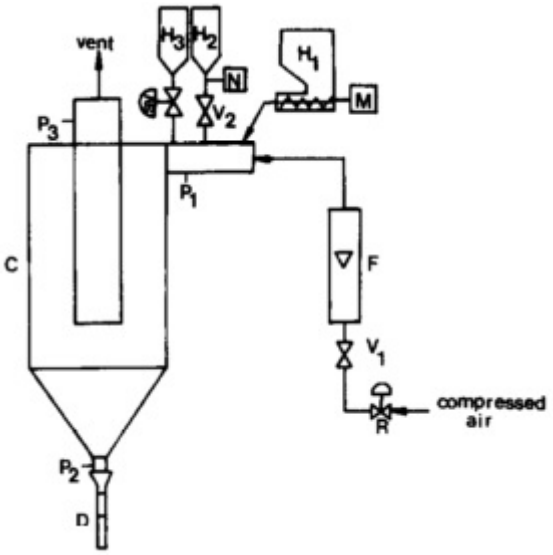

Figure 1.10: Schematic diagram of experimental apparatus used by Kang et al. [63].

The compound of alumina powder coated with pure phosphorescent material is also used as a tracer agent in order to find the particle RTD measurement in a fluidized bed riser [24]. A summary of the different coated particles used as a tracer for the particle residence time distribution studies is given in Table 1.2.

Table 1.2: Summary of coated particles used as a tracer.

Method	Author	System	Details of method
Phosphorescent tracer	Kulah et al. [26]	Riser of CFB	Phosphorescent-coated FCC particles used as a tracer
Phosphorescent tracer	Wei et al. [60]	Gas-solid concurrent upflow and downflow system	The phosphorescent material was blended with alumina powders to form tracer particles of similar size and density as typical FCC particles
Phosphorescent tracer	Yan et al.[24]	Riser of a fluidized bed petroleum coke combustor	The compound of alumina powder coated with pure phosphorescent material is used as the tracer agent in
Phosphorescent tracer	Du et Wei. [16]	Riser	The tracer particles are made by coating of fine phosphor particles on the surface of different property particles (Glass beads, silicone gel, paper chip, plastic chip) with nitryl varnish as the band.

Chemically different tracer	Kang et al. [63]	Cyclone reactor	Solid residence time in a cyclone was carried out using KCl coated tracer particles. The tracer particles in each slice were dissolved in water for an hour and the tracer concentration determined by measuring the electrical conductivity of the solution.
Radioactive tracer	Bhusarapu et al. [3]	Riser of CFB	A single radioactive particle (^{46}Sc) was used as a tracer. It was tailored by coating a layer of polymer (Parylene N) on the Scandium particle to achieve the same density as the solids used (glass beads) and the same diameter (150µm) as the mean particle size of glass beads.
Phosphorescent tracer	Ran et al. [62]	Riser of CFB	Alumina particles containing small amount of very fine phosphor particles (less than 10µm) were used as a tracer.
Radioactive tracer	Weinell et al. [64]	CFB combustor	The porous SiO_2 particles were coated with gold-198 and the trajectory of a single radioactive particle is monitored along the unit using scintillation detectors.

Fluidized bed coating:

Fluidized bed coating is a process that takes place inside a fluidized bed by which a layer is introduced to cover the desired object in order to protect it or modify its behavior [65]. In the fluidized bed coating process, a layer is deposited onto the surface of fluidized bulk particles by spraying a coating solution. The fluidizing gas is also used to dry the deposited solution to form a layer on the surface of the particle. The gas normally preheated before it is pumped to the bed to dry the coating solution. During the fluidized bed coating, number of processes can also take place inside the fluidized bed such as agglomeration or dry defluidization. These processes depend on the fluidized bed conditions, particle characteristics and the coating materials. Figure 1.11 summarizes the possible mechanisms that occur during the fluidized bed coating process suggested by Nienow [66].

The important point in a successful coating process is that the coating solution must be coated on the surface of bulk particles without excessive wetting. Furthermore, the liquid bridges formed by the collision of wet particles must break during drying, thus allowing the coating material to remain on the surface of particles.

In order to study the long RTD in solid unit operations using the phosphorescent tracer method, an experimental technique is required that should have a fast response and can measure very low tracer concentration.

It should be noted that the developed technique until now do not allow to detect the true tracer flow as a function of time due to the fact that the velocity of solid in not generally known. In the present thesis, a novel technique with fast response for RTD measurement has been developed based on the optical method which detects only the tracer concentration in the exit zone and not the concentration of flow at the outlet. It was necessary to consider while using this technique, which detects very low concentration, that the tracer consumption will be reduced, and the hydrodynamic patterns of the unit operation will be changed as little as possible.

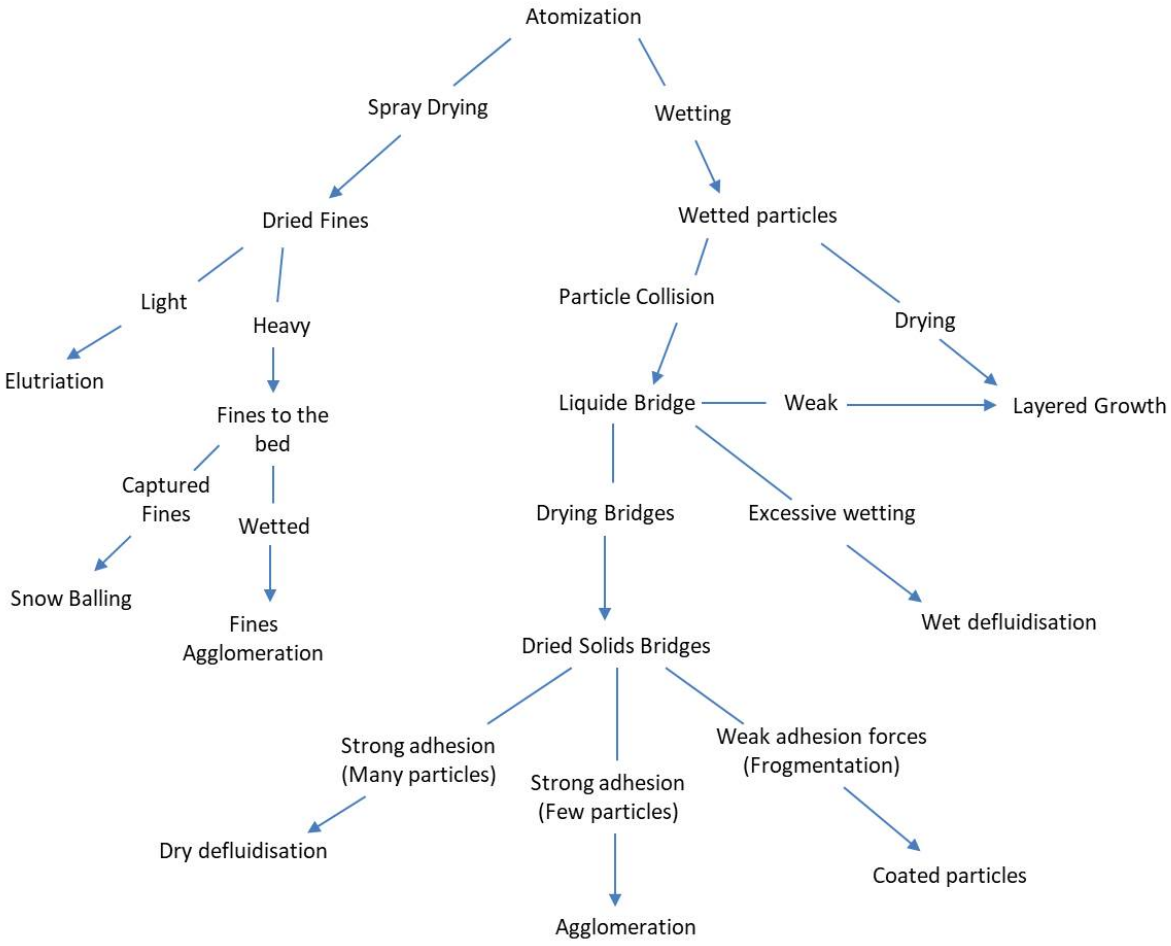

Figure 1.11: Possible phenomena that occur during fluidized bed coating process [66].

1.4 Residence time distribution models

Modeling a flow from experimental RTD data means to show the experimental RTD curve by a known theoretical function. In a flow model, the hydrodynamic characteristics of the transport material are quantitatively described. The model helps to understand a process and also to predict it for other conditions.

In order to have a proper model with a response close to the tracer experimental data, the arrangement of basic flow elements is used. This approach is mostly called as system (or systematic) analysis [49]. Then, it needs:

- A collection of elementary flow models describing the basic phenomena of fluid flow,
- A collection of rules combining these elementary models,
- An optimization method that makes model response fit with experimental data [49].

It must be noted that, some experiments are also required besides the purely mathematical or numerical tools.

1.4.1 Ideal reactors (Perfect mixer and plug flow)

The RTD of the ideal piston (plug flow reactor-PFR) and CSTR reactors can be easily determined using the passage time parameter τ. Mathematical expression of these reactors are illustrated in Table 1.3.

Plug flow and perfect mixing flow can be considered as two extreme cases, where mixing is either non-existent or completed instantaneously.

Table 1.3: Mathematical expression of the ideal reactors [67].

	PFR	**CSTR**
	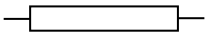	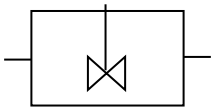
RTD *E(t)*	$\delta(t-\tau)$	$\frac{1}{\tau}e^{\frac{-t}{\tau}}$

1.4.2 Models for non-ideal flows

Modern RTD theory was originally developed from continuous fluid systems [30]. First models of fluid reactors supposed to be plug flow reactor (PFR) with tubular shape or continuous stirred-tank reactor (CSTR). These concepts demonstrate two extreme RTD profiles in the reactor. In continuous flow systems, experimental RTD profiles are usually between the two extremes.

Figure 1.12 illustrates the results of typical RTDs from different non-ideal reactors. Figure 1.12(a) and (b) correspond to almost ideal plug flow and mixed flow, respectively. Figure 1.12(d) shows the RTD for non-ideal CSTR shown in Figure 1.12(c), which has two flow effects (dead zones and bypassing). The dead zone reduces the effective reactor volume. Therefore, the active reactor volume is smaller than the reactor volume and consequently the average residence time is lower than expected.

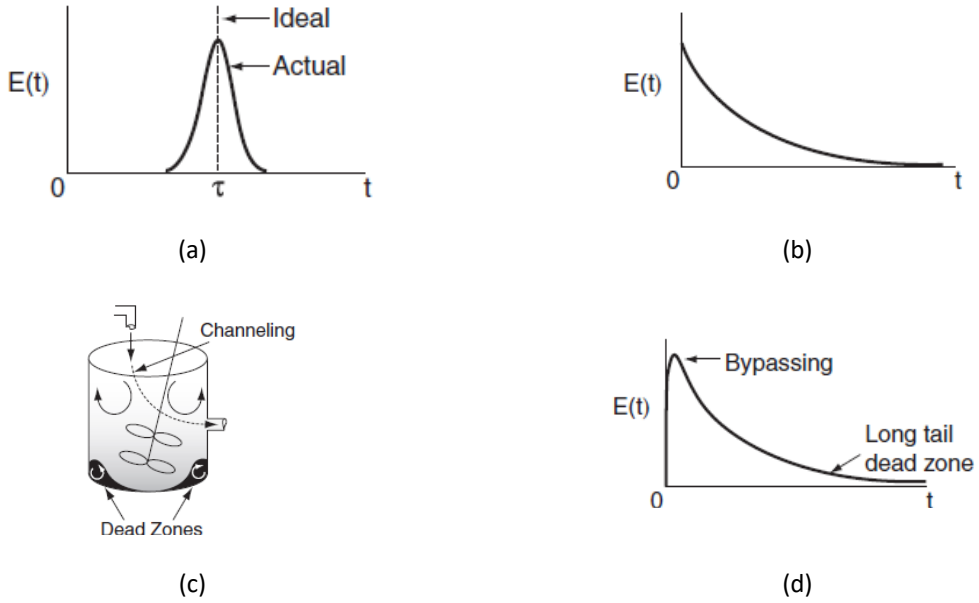

Figure 1.12 : (a) RTD for almost plug flow reactor; (b) RTD for perfectly mixed CSTR; (c) tank reactor with dead zones and channeling; (d) RTD for tank reactor with bypassing (Channeling or short circuiting) and a dead zone [34].

To predict conversions and product distributions for non-ideal systems, different approaches are possible:

- Axial dispersion model or axial plug flow model,
- Reactor network model or modeling reactors with combinations of ideal reactors (CSTR and PFR series).

1.4.2.1 Axial dispersion model

The axial dispersion (or axially dispersed plug flow) model is an efficient and simplest way to generalize the concepts of the RTD in most non-ideal reactors.

The flow in solid unit operations is normally a combination of convection (bulk movement of the fluid) and some amount of dispersion. Therefore, tracer concentration *C* is given by the equation (1. 13) in one dimension and providing that dispersion can be expressed by a Fickian law [68].

$$\frac{\partial C}{\partial t} + U\frac{\partial C}{\partial x} = D\frac{\partial^2 C}{\partial x^2} \qquad (1.\ 13)$$

where *U* and *D* are fluid velocity and axial dispersion coefficient respectively.

By expressing equation (1. 13) in non-dimensional form, two parameters appeared [49]:

- $\tau = L/U$, where L is the length of the system and U is the fluid velocity.

- Péclet number *Pe = (U.L)/D*, that shows the ratio of the convective to dispersive effects. Therefore, when *Pe* is low, dispersion is predominant and when *Pe* is large, dispersion is negligible.

Based on previous literature [47], [69], Fickian equation (eq.(1. 13)) can be solved for different initial and boundary conditions (Table 1.4). The initial condition, before tracer injection, the tracer concentration is evidently zero (*C=0*).

Depending on whether dispersion is allowed or not at the boundaries of the system, there are lots of boundary conditions possibilities. Table 1.4 gives the different boundary conditions for each case, considering that the variables t and z represent time and axial distance from the tracer injection point. The tracer is injected at *x= 0* and its output concentration considered at *x = L*.

Table 1.4: Possible boundary conditions at the inlet and outlet of a reactor subjected to a piston flow with axial dispersion [67].

Open input of the diffusion 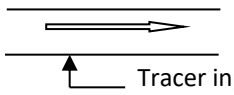 Tracer input $UC = D\left(\frac{\partial C}{\partial x}\right)_{x\to 0^-} - D\left(\frac{\partial C}{\partial x}\right)_{x\to 0^+}$	Close input of the diffusion 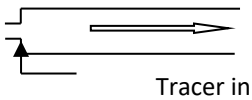 Tracer input $UC = UC_{x\to 0^+} - D\left(\frac{\partial C}{\partial x}\right)_{x\to 0^+}$
Open output of the diffusion 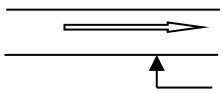 Tracer measurement $C = C_{x=L}$	Close output of the diffusion 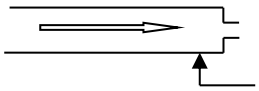 Tracer measurement $\left(\frac{\partial C}{\partial x}\right)_{x=L} = 0$

Taylor [70] developed The most widely used solution of the RTD with open–open boundaries. In open–open boundaries, N_0 moles of tracer are injected as a Dirac pulse at (*t=0, x=0*) and dispersion is allowed at both ends of the domain [49].

$$C\ (t,x) = \frac{N}{\sqrt{4\pi Dt}} exp\left(-\frac{(x-Ut)^2}{4Dt}\right) \qquad (1.\ 14)$$

The RTD at the outlet of mentioned system (at *x=L*) is easily deduced from equation (1. 15):

$$E(t) = \frac{1}{2}\left(-\frac{Pe}{\pi\tau t}\right)^{1/2} exp\left(-\frac{Pe(\tau - t)^2}{4\tau t}\right) \quad (1.\ 15)$$

Table 1.5: Axially dispersed plug flow model, depending on boundary conditions [67].

Type of reactor	Transfer function (F)	Mean residence time (t_m)	Variance (σ^2)
Open at both ends	$\frac{exp\left[Pe\ \frac{1-\beta}{2}\right]UL}{\beta}$	$\tau\left(1+\frac{2}{Pe}\right)$	$\tau^2\left(\frac{2Pe+8}{Pe^2}\right)$
Open at one end, close at the other	$\frac{2exp\left[Pe\ \frac{1-\beta}{2}\right]UL}{(1+\beta)}$	$\tau\left(1+\frac{1}{Pe}\right)$	$\tau^2\left(\frac{2Pe+3}{Pe^2}\right)$
Close at both ends	$\frac{4exp\left[Pe\ \frac{1-\beta}{2}\right]U}{(1+\beta)^2-(1+\beta)^2}$	τ	$\tau^2\left(\frac{2Pe-2+2e^{-Pe}}{Pe^2}\right)$

$\beta = \sqrt{1+4sD/U^2}\ and\ \tau = \frac{L}{U}$

The advantage of the axial dispersion model is the clear physical meaning of its parameters [27]. Many researchers have used axial dispersion model in their studies [12], [15], [33], [71]–[73]. Ran et al.[62] investigated the lateral mixing of solids in a high density riser by measuring the solids RTD at different radii and comparing with results of dispersion model. A sensitivity analysis of the model demonstrates that the *Pe* is sensitive to the shape of RTD curves at different radii.

1.4.2.2 Modeling reactors with combinations of ideal reactors (CSTR and PFR series)

To describe the non-ideal behavior of the RTD profile using this model, different combinations of CSTR and PFR were introduced. Tanks in a series model (*T-I-S*) is one generally used model [4], [74]–[79]. As illustrated by its name, the tank in series model is composed of perfect mixing cells connected in series (Figure 1.13).

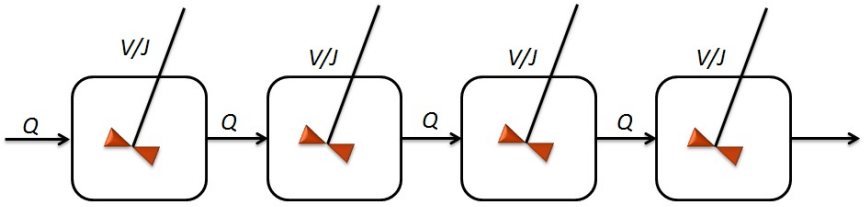

Figure 1.13: Tank in series model

For *N* multistage CSTR reactors in series, the equation for single CSTR reactor ($\frac{1}{\tau}e^{\frac{-t}{\tau}}$) is generalized to:

$$E(t) = \frac{1}{(N-1)!\,\tau_j}\left(\frac{t}{\tau_j}\right)^{N-1}.e^{-t/\tau_i} \qquad (1.16)$$

where, $\tau_i = \tau/N$ is the average residence time per reactor and τ is the total residence time. A large number of tanks (N approaches infinity) indicates a PFR-like reactor, and a small number of tank leads to a CSTR-like reactor (*N=1*). Equation (1. 16) is plotted in Figure 1.14 as a function of t/τ for different values of *N* [27].

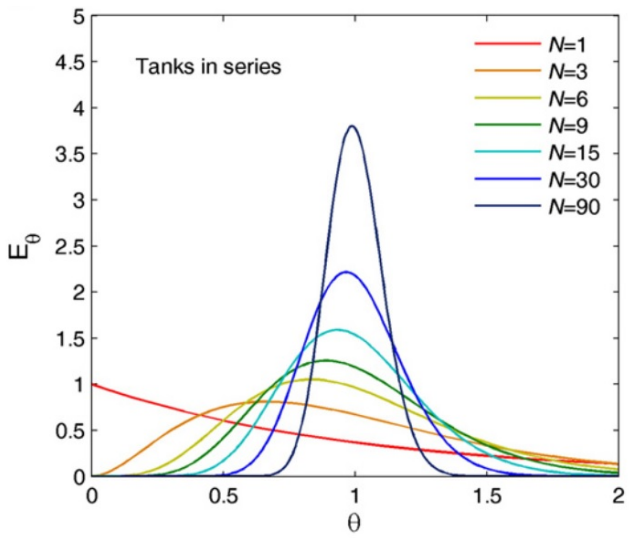

Figure 1.14: The residence time distribution of equation (1. 16), plotted for a set of different *N*. When *N* approaches infinity, the residence time distribution approaches that of plug flow [27].

Experience has shown that the easiest model to handle is the tank in series, it is therefore recommended to use this model initially for the simulation of experimental data.

Two modifications to this model were reported:

- The tanks in series were followed by a PFR when axial dispersion is significantly limited in case of the partial delay of RTD [80],
- Backward flux was presented in the CSTR tanks to capture the long tail in the RTD profiles [48], [49].

According to the second modification, large backward flux shows fast material exchange between adjacent tanks. The RTD profiles with the long tail can also be modeled by a dead zone volume cross-flowing with the CSTR element [79], [82]. It should be noted that the degree of non-idealness of the continuous flow system can be presented by the fraction of the dead zone element.

This type of modeling with simple ideal reactors has been used by several researchers [9], [81], [83] due to its flexibility and good results. Guio et al. [9] proposed a model in a dual circulating fluidized bed system which consists of a combination of ideal plug flow and stirred tank reactors. Results showed an excellent fitting between the simulated output and the experimental output with errors of about *5%*.

1.4.2.3 Stochastic model and Markov chain

Stochastic model is a one widely used RTD model that considers the particle movement as a stochastic process. The axial motion of the any particle within a continuous system is considered as a two-dimensional probabilistic process. Therefore, the RTD of system can be calculated by the accumulation of the random axial motions of particles. This type of model is suitable for a process where there is no RTD prediction model for example in case of complicate system geometry [27]. Stochastic model defines the flux exchange ratio between supposed elements connected in a network and the next state of the system. In a Markov chain model, the flux exchange among different elements is well modeled while the mixing inside each element is not considered. As a result, Markov chain model is very useful in the flow regions within a the system which can be easily separated into different elements [17].

1.4.2.4 RTD constructed by velocity profile

Different CFD software and velocity sensors were used to give velocity profiles and to construct RTD profiles in the fluid systems [59], [60]. The equivalent tools in solid systems are the Discrete Element Method (DEM) and positron emission particle tracking (PEPT) [85]. Since the velocity profile has varied in lots of solid unit operations, the RTD is not commonly measured on the basis of practical velocity profile.

At present, the particle RTD determination using these models leads to reliable results only in very simple geometries using a limited number of particles. Therefore, the experimental determination of particle RTD seems to be much more accessible.

1.5 General description of fluidized bed reactors

The fluidized bed reactor, as a widely used solid unit operation, has been described in this section. The fluidized bed will be the subject of the application of the developed technique for determining the residence time distribution.

1.5.1 Fluidization basics

Fluidization is a process in which solid-fluid suspension behave like a fluid. The gas blows upward through the reactor filled with solids until the solid particle are suspended. Fluidization is widely used in two groups of physical and chemical operations. Physical operations such as transportation, mixing of powders, heating, adsorption and chemical operations such as solid catalysts reactions with gases or coal combustion.

The advantage of this type of contacting method is that particles are subject of very intense mixing that gives a rise to very low temperature gradients. Therefore, fluidized beds are suitable for both small- and large-scale operations. There are many well founded operations that employ this technology, such as cracking and reforming of hydrocarbons, coal carbonization and gasification, ore roasting, Fisher-Tropsch synthesis, coking, aluminum production, melamine production, and coating preparations [86]. Another application of fluidization is in nuclear engineering for example in uranium extraction, reprocessing of fuel and waste disposal [86].

1.5.2 Fluidization regimes

1.5.2.1 Fluidization phenomena

As shown in Figure 1.15, different fluidization regimes from homogenous fluidization or bubbling fluidization to pneumatic conveying can be observed according to the gas velocity and solid particles.

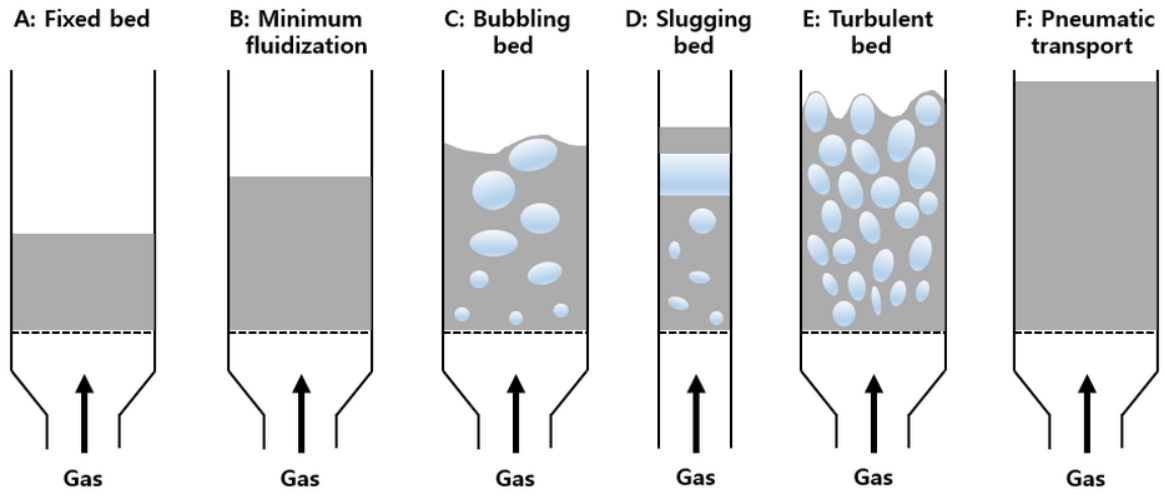

Figure 1.15: Different regimes of fluidized beds (Based on study of Kunii and Levenspiel [86]).

The fixed bed (Figure 1.15A) occurs when the flow of the gas passes through a bed of particles at a low velocity. With increasing the gas velocity, the drag force becomes equal to the apparent weight of the particles that are then suspended. This point is called minimum fluidization which is the beginning of fluidization (Figure 1.15B). It must be noted that with increasing the gas velocity the voidage of the bed increases slightly. By increasing the gas flow, fluidization bubbles were formed, and a bubbling fluidization occurs. On the other side, for solids of class B, homogeneous fluidization is not observed before bubbling fluidization. By increasing the gas flow, the size of bubbles becomes about the same as the bed diameter (in the bed with high enough height to diameter ratio) and the slugging fluidization occurs (Figure 1.15D).

Turbulent fluidization as shown in Figure 1.15E occurs when the velocity exceeds the terminal velocity of the particles. In this condition, the upper surface of the bed disappears and a turbulent motion of the solid clusters and voids of gas of various shapes and sizes is observed. By further increasing the gas velocity, the fluidization switches to pneumatic transport of solids.

1.5.3 Effect of physicochemical properties of particles on fluidization regimes

The size of the fluidized particles may vary from *15* to *6000* µm. It is clear that the fluidization velocity required for the fluidization of fine particles is much lower than that used for the fluidization of large particles. Moreover, the fluidization regime strongly depends on the nature of the particles. In order to classify particles of diverse nature according to their fluidization behavior, Geldart [87] propose an empirical diagram in which the solids are divided into four groups (A, B, C and D).

Figure 1.16 shows different particle classes, where ρ^* represents the difference between solid and fluid density.

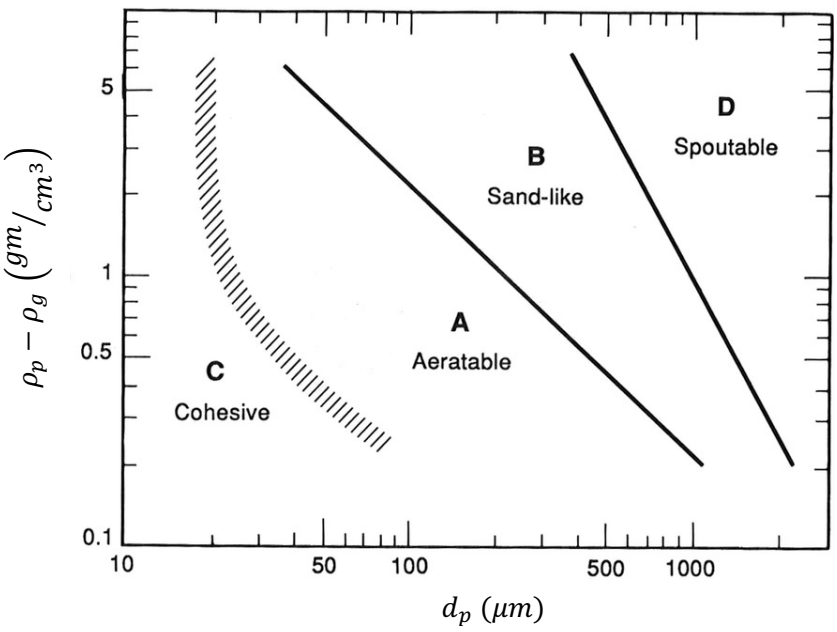

Figure 1.16: Powder classification according to Geldart classification [87].

According to Geldart, particles of group A are aeratable. These particles expand in homogenous fluidized bed until bubbles are created. For group B particles, when the superficial gas velocity is small above the minimum fluidization velocity, the formation of bubble occurs which causes a good mixing of the bed. This phenomenon can even occur at a low superficial gas velocity with a bed expansion less significant than that of group A particles.

Group C particles have cohesive characteristics which makes it difficult to establish "normal" fluidization of the bed. The particles are difficult to individualize by the gas flow which gives rise to channeling flow or short circuits. This class of particle is difficult to fluidize as it is difficult to convey by pneumatic transport. Particle of group D are spoutable. The mixing is not well enough, and the bubbles have the tendency to rise more slowly for this group even if the superficial gas velocities are high.

It has been given that Geldart's classification is efficient, clear and practical for fluidization at ambient conditions and for U less than about $10U_{mf}$ [88]. Geldart's classification could also be used to predict other properties of the fluidized bed like bubble size and velocity, the existence of slugs, etc.

1.5.4 Classification of fluidization regimes according to size particles and fluidization velocity

Reh [89] proposed a diagram with two dimensionless parameters. Thus, this diagram was divided into several zones, each correspond a specific fluidization regime (Figure 1. **17**).

The bubbling fluidization zone is represented under form of board band that cuts the diagonal diagram on low velocities / fine particles, high velocities/ large particles. This zone is delimited by two curves. The first corresponds to the terminal velocity of particles and the second corresponds to the minimum fluidization velocity of particles. The fast fluidization regime corresponds to the fluidization of relatively fine particles at velocity greater than U_t where the solid leaves the fluidized bed and therefore must be recovered and reintroduced into the bed (Circulating fluidized beds). This operation can be carried out by means of cyclones or standpipes.

There is another area above the fast fluidization regime which corresponds to higher velocities. This regime is that of transported bed/ Pneumatic transport, and it can occur in a petroleum riser of the FCC process. There are also some regimes in the diagram of Reh such as spouted bed regime. This regime is used for large particles with relatively difficult fluidization [90].

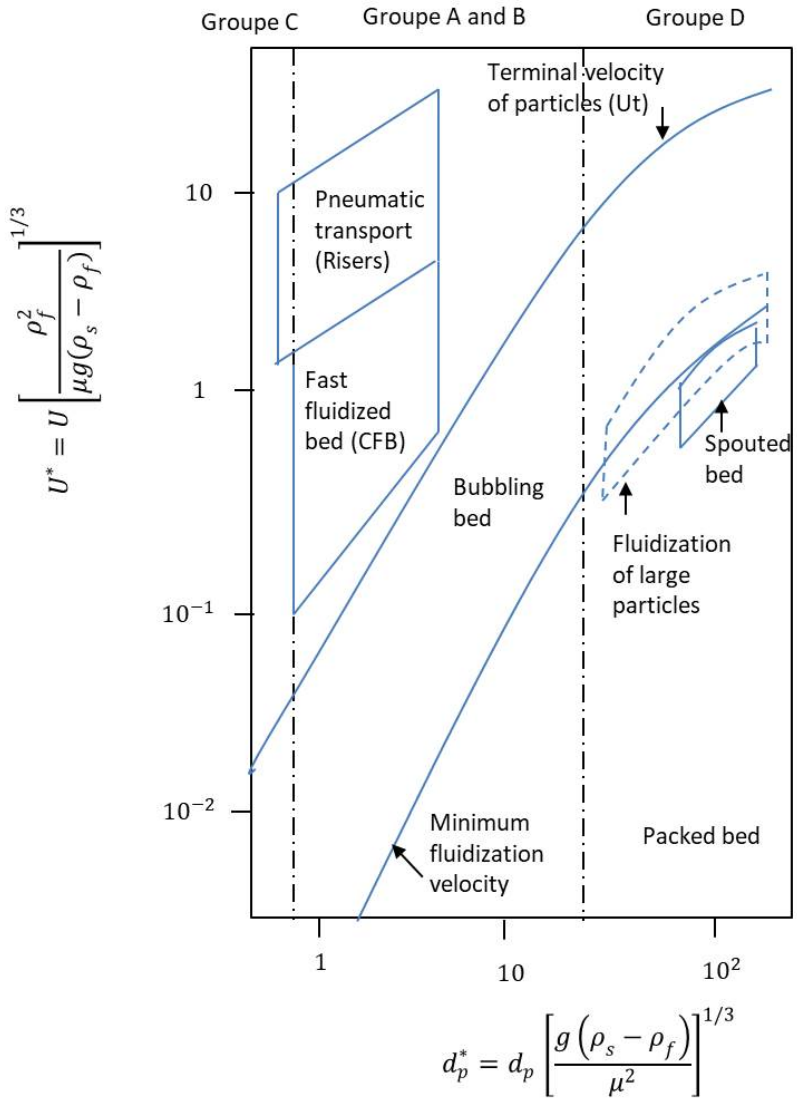

Figure 1. 17: Diagram of Reh [89].

1.5.5 Bubbling fluidized bed

Bubbling fluidization regime is the most common fluidization regime in the chemical industries. In this regime since the pressure drop across the bed equals the bed weight, the fluid drag is:

$$F_D = \Delta PA = AL(1-\varepsilon)(\rho_p - \rho_g)g \qquad (1.17)$$

where A is the cross section, ΔP is the pressure drop and L is the height of the bed.

For group B and D particles, a further increase in gas flow can cause the bubbles formation. The superficial gas velocity in this condition is called as bubbling velocity, U_{mb}. For group A particles, the bubbles are formed until the superficial gas velocity reaches to the minimum bubbling velocity.

The minimum bubbling velocity for group A particles given by [97]:

$$\frac{U_{mb}}{U_{mf}} = \frac{2300\mu^{0.523}\rho_g^{0.126}e^{0.716F}}{d_p^{0.8}g^{0.934}\left(\rho_p - \rho_g\right)^{0.934}} \quad (1.\ 18)$$

where *F* is the mass fraction of particles less than *45 μm*, d_p, is the mean diameter of particles (m), μ is the viscosity of gas (Pa.s) and ρ_g is the density of gas (kg/m^3). The dimensional constant (2300) in equation (1. 18) has unit of $Kg^{0.285}m^{-0.167}s^{-1.345}$. The bubble size increases along the bed and also increases with particle diameter and excess gas velocity [91].

A bubble also carries some solids and erupts at the surface of the bed. Therefore, the carried particles entrained into the space above the bubbling bed, called freeboard area. The entrained particles travel upward depending on their momentum and local gas-particle drag. Due to gravitational force, some particles may disengage from the gas and return to the dense bed. Along the height in the freeboard, the flux of the disengaged particles is reduced. In certain height, the flux of disengaged particles is negligible. This height is known as transported disengaging height (TDH).

Identifying the Minimum Fluidization Velocity

Minimum fluidization velocity (U_{mf}), is an important design parameter for fluidized beds. It is generally defined as the minimum superficial velocity at which the pressure drop through the bed is equal to the bed weight apparent per unit cross sectional area. Usually, the minimum fluidization velocity is obtained experimentally and there are several techniques reported in the literature to find the minimum fluidization velocity in a multiphase flow system. Gupta and Sathiyamoorthy [92] described three different methods to measure U_{mf}; (i) the pressure drop method, (ii) the voidage method and (iii) the heat transfer method. The first method measures the pressure drop across the bed as a function of the superficial gas velocity. The point of transition between a fixed bed regime and a bubbling regime is denoted by a constant pressure drop line in a plot of pressure versus superficial gas velocity. This point marked the minimum fluidization velocity. In the voidage method, the minimum fluidization velocity is determined when the voidage inside the bed starts to increase due to bed expansion as the superficial gas velocity is increased. However, this method is not commonly used because it is much more complicated to locate the point where bed expansion starts. Finally, in the heat transfer method, the variation of the wall heat transfer coefficient is measured as the gas velocity increases. The point where the heat transfer coefficient increases suddenly is the start of fluidization or the minimum fluidization velocity point. This method is too expensive and requires a good experimental setup to measure the heat transfer data under steady-state conditions.

The basic theory for the prediction of the minimum fluidization velocity is that the resultant pressure forces acting on either side of the bed should compensate the actual weight of particles.

This can be expressed mathematically by:

$$\Delta P = (\rho_p - \rho_g)(1 - \varepsilon_{mf}) g L_{mf} \quad (1.\ 19)$$

ΔP is the pressure drop, ρ_p and ρ_g are the densities of the particle and fluid respectively. ε_{mf} is the minimum fluidization porosity, and L_{mf} is the minimum bed height at the beginning of fluidization. Ergun [93] developed, for fixed beds, a pressure drop correlation at incipient fluidization based on drag force consideration as follows:

$$\frac{\Delta P}{L} = 150 \frac{(1 - \varepsilon_{mf})^2 \mu_g U_{mf}}{\varepsilon_{mf}^3 (\psi_s d_p)^2} + 1.75 \frac{(1 - \varepsilon_{mf}) \rho_g {U_{mf}}^2}{\varepsilon_{mf}^3 (\psi_s d_p)} \quad (1.\ 20)$$

The relationship between the pressure drop and U_{mf} is shown in Figure 1.18.

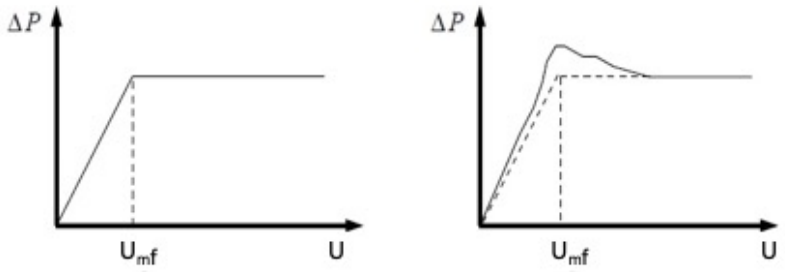

(a) (b)

Figure 1.18: Pressure drop versus fluidization velocity; a) idealized curve, b) real curve.

The determination of U_{mf} from Ergun's equation for pressure drop requires detailed knowledge of sphericity of the solid particles, $\boldsymbol{\psi_s}$, and bed voidage, $\boldsymbol{\varepsilon_{mf}}$, which cannot be perfectly determined in a given real system [94].

Wen and Yu. [95] developed an expression for the minimum fluidization velocity for a range of particle sizes and types by assuming the following approximations to hold based on experimental data:

$$\frac{1 - \varepsilon_{mf}}{\psi_s^2 \varepsilon_{mf}^3} \cong 11 \; and \; \frac{1}{\psi_s \varepsilon_{mf}^3} \cong 14 \quad (1.\ 21)$$

They combined these with Ergun equation and obtained the following relation:

$$U_{mf} = \frac{\mu_g}{\rho_g . d_p} \left(\sqrt{33.7^2 + 0.0408 \frac{d_p^3 . \rho_g . (\rho_s - \rho_g) . g}{\mu^2}} - 33.7 \right) \quad (1.\ 22)$$

Re_{mf} is the Reynolds number in minimum fluidization and Ar is the Archimede number:

$$Ar = \frac{d_p^3 . \rho_g . (\rho_p - \rho_g) . g}{\mu_g^2} \quad (1.\ 23)$$

Leva [96] empirically obtained another widely used expression:

$$U_{mf} = 7.90 \times 10^{-3} d_p^{1.82} (\rho_s - \rho_g)^{0.94} . {\mu_g}^{-0.88} \quad (1.\ 24)$$

This equation (1. 24) is valid for $Re_{mf} \leq 10$, whereas for higher values of Re_{mf} a correlation factor must be applied. The dimensional constant in equation (1. 24) has unit of $m^{0.12} kg^{-0.06} s^{-0.88}$.

Baeyens [97] evaluated the properties of a bed high-boiling dense fine powder (Group A) and proposed:

$$U_{mf} = 9 \times 10^{-4} d_p^{1.8} [(\rho_s - \rho_g) . g]^{0.934} . {\rho_g}^{-0.066} . {\mu_g}^{-0.87} \quad (1.\ 25)$$

Thonglimp's equation [98] also estimates the minimum particle fluidization velocity as follows:

$$Re_{mf} = \frac{U_{mf} . \rho_g . d_p}{\mu_g} = (31.6^2 + 0.0425 . Ar)^{1/2} - 31.6 \quad (1.\ 26)$$

Youjun et al.[99] correlated the minimum fluidization velocity in a fluidized bed with supercritical water:

$$U_{mf} = \frac{\mu_g}{\rho_g . d_p} \left(\sqrt{27.3^2 + 0.0434 Ar} - 27.3 \right) \quad (1.\ 27)$$

A wide variety of empirical correlations can be found which allow the estimation of the minimum fluidization velocity, but these correlations have a strong dependence on the physical properties of the particles and fluid and ε_{mf}. This dependence impose that the empirical equations are applicable only in specific cases and cannot be generalized.

The various correlations that have been developed by the different authors to predict minimum fluidization velocity are listed in Table 1. 6.

Table 1. 6: List of some of the available correlations to predict minimum fluidization velocity.

NO.	Researchers	Correlation
1	Wen and Yu. [95]	$U_{mf} = \frac{\mu_g}{\rho_g . d_p}\left(\sqrt{33.7^2 + 0.0408\frac{d_p^3 . \rho_g . (\rho_s - \rho_g) . g}{\mu^2}} - 33.7\right)$
2	Leva [96]	$U_{mf} = 7.90 \times 10^{-3} d_p^{1.82}(\rho_s - \rho_g)^{0.94} . \mu_g{}^{-0.88}$ (The dimensional constant has unit of $m^{0.12}kg^{-0.06}s^{-0.88}$)
3	Baeyens [97]	$U_{mf} = 9 \times 10^{-4} d_p^{1.8}\left[(\rho_s - \rho_g) . g\right]^{0.934} . \rho_g{}^{-0.066} . \mu_g{}^{-0.87}$
4	Thonglimp et al. [98]	$U_{mf} = \frac{\mu_g . ((31.6^2 + 0.0425 . Ar)^{1/2} - 31.6)}{\rho_g . d_p}$
5	Youjun et al. [99]	$U_{mf} = \frac{\mu_g}{\rho_g . d_p}\left(\sqrt{27.3^2 + 0.0434\, Ar} - 27.3\right)$

1.5.6 Entrainment and elutriation of solids from fluidized beds

The entrainment is defined as the flux of solids that is being carried out the fluidized bed by the gas in Kg per unit cross sectional area and second. It means that per unit time how much solids per unit cross sectional area carried out by the gas. The origin of the ejected particles is due to the following sources [100]:

- Bubble bursts at the bed surface and some of solids which have been lifted by the bubble wake are moved upwards
- Bubble breaks at the bed surface and some solids contained in the leading bulge of the bubble are detached.

It is essential for predicting the bed behavior in order to optimize the fluidized bed process. A fluidized bed can be divided into three different zones as shown in Figure 1.19 [100].

- Distributor zone or grid region
- Bubbling zone
- Freeboard zone.

The distributor zone is close to the bottom of the bed. Above the distributor zone is the bubbling zone in which bubbles grow by coalescence and rise to the surface of the bed. Then, bubbles break at the surface of the bed and particles are thrown up above the bed surface. The zone above the bed surface where particles are entrained by the upward flowing gas stream is the freeboard zone. The transport disengaging height (TDH) is defined as the height at which the entrainment rate becomes almost constant (See Figure 1.20) [100].

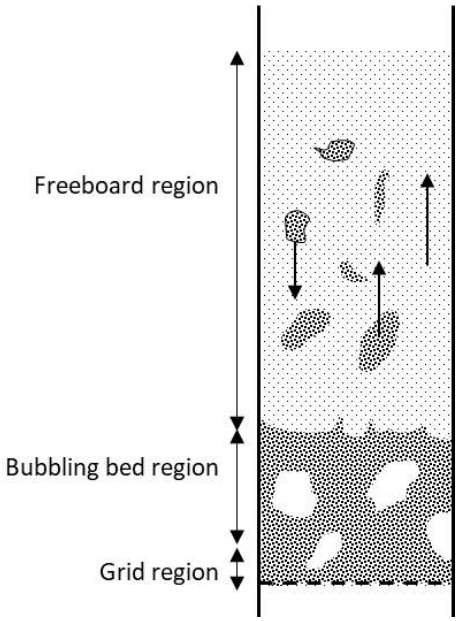

Figure 1.19: Particle entrainment from fluidized bed [100].

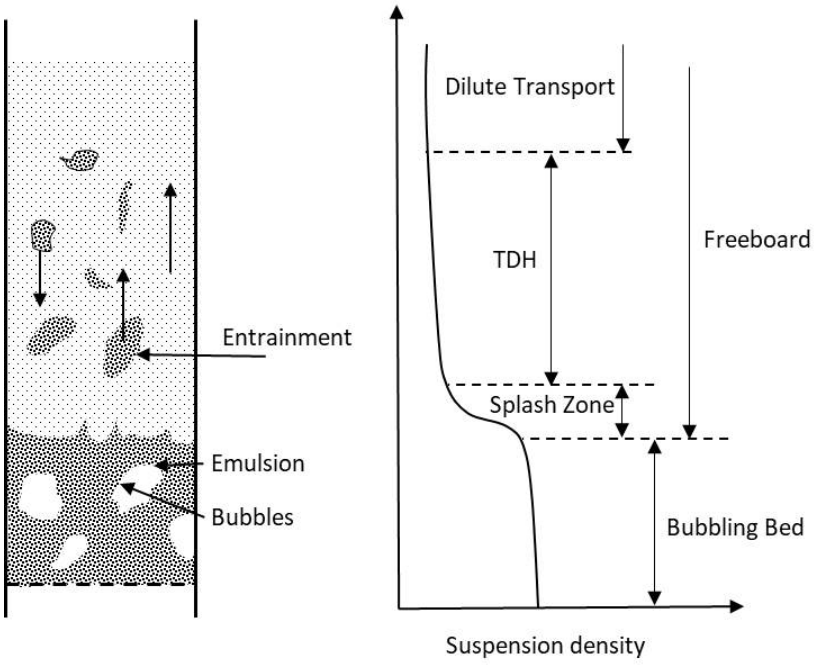

Figure 1.20: Different region above a bubbling bed. The solid concentration reduces along the bed height but remains unchanged beyond the TDH.

The disengagement height (TDH) is an important design parameter for a fluidized bed. TDH directly affects the height of column and is required for determination of the appropriate placement of the cyclone and the recovery of the elutriated materials.

The entrainment rate can be obtained experimentally by extrapolation of the entrainment data the freeboard to the bed surface. The correlation equation is given by [100]:

$$\frac{F_0}{AD_B} = 3.07 \times 10^{-9} \frac{\rho_g^{3.5} g^{0.5}}{\mu^{2.5}} \left(U - U_{mf}\right)^{2.5} \quad (1.28)$$

where F_0 is the entrainment rate of particles at the bed surface, *A* is the cross-sectional area of the column, D_B is the bubble diameter at the bed surface and $U_0 - U_{mf}$ is the excess gas velocity.

The amount of fine particles projected into the freeboard at the bed surface can be approximated by the equation below.

$$F_{i0} = F_0 . X_i \quad (1.29)$$

where, F_{i0} is the amount of fine particles in the freeboard and X_i is the weight fraction of fine particles present in the bed [100].

It was shown that only a small particle which has the terminal velocity less than the gas velocity will be carried out of the freeboard if the freeboard is tall enough. In fluidized bed, elutriation is defined as a loss of fines particles from the fluidized bed which is due to bursting of bubbles on the surface of fluidized bed. The flux of particles carried away beyond the TDH is known as the elutriation rate. The amount of the particles elutriated can be determined by following equation:

$$F_{i\infty} = E_{i\infty} \times X_i \quad (1.30)$$

where, $E_{i\infty}$ is the elutriation rate constant and X_i is the weight fraction of the fine particle present in the bed. The elutriation rate constant has been determined experimentally by different investigators in which it is limited to the employed experimental conditions. The total amount of particles elutriated is:

$$F_\infty = \sum_i F_{i\infty} \quad (1.31)$$

1.5.7 Hydrodynamics in fluidized beds

Numerous authors have shown that the fluidization pattern change progressively from one to the other by changes in fluid density or operating velocity. It is possible to observe different hydrodynamic flow regimes in a fluidized bed from bubbling to pneumatic conveying. The presence of these different regimes depends on the superficial gas velocity and particle size. Studying these different flow regimes

in a fluidized bed becomes more important when different flow regimes can provide widely different gas-solid mixing, and thus different chemical reaction rates as indicated by Yang [101]. Therefore, an efficient design, scaling, conception and even a good operation of a fluidized bed system depends on the flow regime and consequently the correct gas velocity to better transport the solids. Different attempts have been made to determine a criterion to discern between bubbling (aggregative, heterogeneous) and non-bubbling (particulate, homogeneous) fluidization. Some concepts are based on the inter-particle forces in the vicinity of bubbles and lead to dimensionless groups such as Froude number or combinations of *Fr* with *Re* and other groups [87].

Two different stages of fluidization are recognized depending on the ratio fluidization density to bed material density. For slightly different density, the bed is smoothly fluidized and raw flow instabilities are damped which is known as homogeneous fluidization. In contrast, for a large difference in density, the bed is more turbulent, bubbles and channels are formed and the bed is not stable which is known as heterogeneous fluidization [103].

It has been shown by Monazam et al. [104] that a classic fluidized bed regime is formed immediately above the gas distributor when the gas velocity exceeds minimum fluidization velocity in conventional gas-solid fluidization of Geldart's group B particles. When the gas velocity approaches the terminal velocity of a single particle, U_t, turbulent fluidization occurs which is accompanied by the high particle elutriation rates. Figure 1. 21 shows the interrelationship of regimes in dense phase fluidization and lean-phase fluidization, which converse fast fluidization and dilute transport.

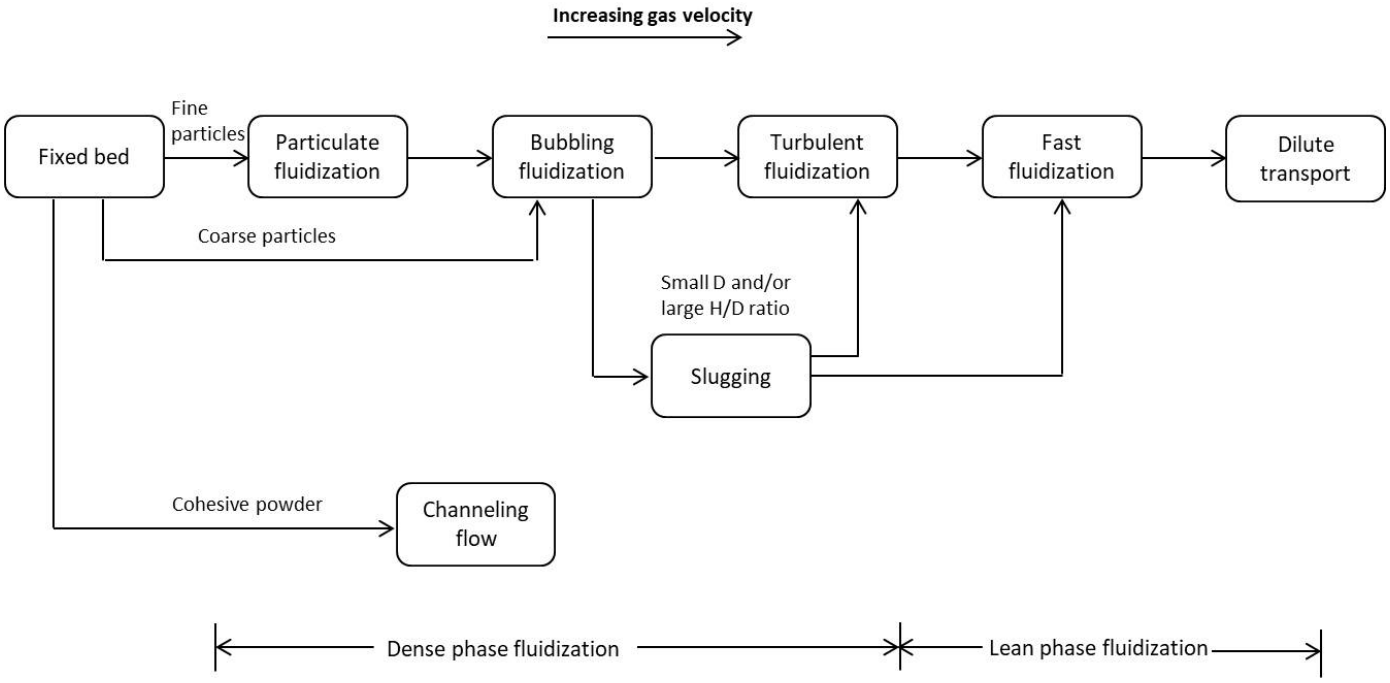

Figure 1. 21: Interrelationship of different regimes including fixed bed, dense phase fluidization and lean-phase fluidization [105].

Dense-fluidization regimes include particulate fluidization, bubbling fluidization and turbulent fluidization [106]. In a broad sense, dense-phase fluidization also consists of the slugging, spouting and channeling regimes which depend on the operating conditions. Lean-phase fluidization consists of two flow regimes; the fast fluidization regime and the dilute transport regime.

For the gas flow in the riser, energy in the gas phase is partially transferred into the solids phase through gas-particle interactions and is partially dissipated as a result of friction [105]. Numerous studies on circulating fluidized bed riser regimes are available in the literature e.g., [107]–[110].

The other important aspect to understand in fluidized beds is the effect of bubbling and local and global holdup or concentration. The bed mixing and the reaction efficiency are influenced by the bubble size and the rise velocity. Bubbles form in the heterogeneous bed for superficial velocities greater than the bubbling fluidization velocity. When the superficial velocity increases bubbles form more frequently and rise more rapidly. Many researchers concluded that bubble size and rise velocity are mainly influenced by the size of bed particle, the superficial velocity and the type of distributor [5], [6]. Nienow et al. [113] found that bubbles have the main influence for the mixing in fluidized beds. They also found that the mixing occurs when particles move upward by being caught in the wake of bubbles and later move downward by being released by the bubbles that explode at the fluidized bed surface. Bubbles can also coalesce and form larger bubbles as they move upward depending on the superficial velocity. This phenomenon influences the local holdup because neighboring regions are not fluidized enough. In order to have a fluidized bed with high efficiency with the best mixing, big bubbles should be avoided [103].

As suggested in the literature about the various flow regimes in fluidized beds, a uniform void fraction along the riser belongs to the dilute transport regime [114]. A core-annular flow is produced when the solids tend to fall in denser cluster along the wall. By increasing solids flux at the same velocity, the solids rise in more dilute concentration towards the center and a core-annular flow occurs [114]. The fast fluidization starts when the solids flux is increased to the saturation capacity point. At this time, in the upper part of the riser and below a dilute phase transport region, a dense phase transport region is formed. In the following, the fully developed fast fluidized bed regime shows a progressive transition between the lower dense bed and the upper dilute bed.

Bi and Grace [108] defined two regimes (fast fluidization and dense phase conveying) for the circulating fluidized beds. They founded the transition velocities by plotting pressure gradient against the superficial gas velocity in dense and dilute phases. They also suggested flow regime maps including homogeneous dilute-phase flow, core-annular dilute-phase flow and fast fluidization.

The fast fluidization regime is divided into the two sub-regions; fast transition and the fully developed fast fluidization region [115].

The average voidage is obtained using the pressure difference across the bed through the following expression assuming negligible acceleration effect, shear stress at the wall and the weight of the gas [116], [5], [114]:

$$\frac{\Delta P}{\Delta z} = \rho_p . (1 - \varepsilon) . g \qquad (1.\ 32)$$

where, Δ*z* is the distance between the pressure sensors along the riser, *z* is the longitudinal abscissa of the flow oriented from top to bottom, ρ_p is the density of solid particles and P is the pressure along the riser. Louge and Chang [116] declared that this calculation is erroneous when momentum losses due to the wall fraction or solid acceleration cannot be neglected.

Many operating variables such as the rate of solids circulation, superficial gas velocity, bed diameter, riser exit structure, total solids inventory and particle properties (density, size distribution) affect the axial voidage or holdup profile [117]. With increasing the solids flux, the transition region between the dense bed and dilute phase move higher in the riser and a denser bed could be observed. Similarly, with decreasing solids flux the solids holdup decreases. The axial voidage and holdup profile can also be affected by the superficial gas velocity. With increasing the superficial gas velocity, the solids holdup decreases or the axial voidage increases. An increase in bed diameter could result in a high and more uniformly voidage in the bed.

When the system is in a fast fluidization, there are several acceleration zones (the initial acceleration zone and the second acceleration zone). The initial acceleration zone is in the bottom of the dense phase before the particles move somewhat constant. The second acceleration zone displays when the particles arrive in the dilute regime. Bai et al. [117] have shown that this second acceleration region is not very short but can extend into the riser, while some particles can still be accelerating at the top of the riser when forced out.

According to Yin and Wei. [118] solid particles in fast fluidized beds are still accelerating through most of the bed height, especially at high solid circulation rate and low gas flow rate. Since in the dense phase particle velocity is very low versus the dilute region, this acceleration region becomes the guideline to determine the transition between dense and dilute phases. Bai et al. [119], [120] indicated that this acceleration zone may occupy from *1/3* to *2/3* of the riser height.

1.6 Conclusion

The present chapter gave an overview of the research currently being carried out on the various aspects relating to the characterization of gas/solid flows in solid unit operations using the RTD approach. In the first section the RTD theory in solid unit operations (RTD definition, RTD function as well as RTD models) was described. Then, numerous residence time distribution measurement techniques, which have been studied until now, were reported.

Our own contribution is the development of an experimental technique for particle residence time determination using a phosphorescent tracer. The phosphorescent tracer technique has many advantages and in particular that of being a non-intrusive method. Its disadvantage is due to the decay of pigment luminosity which limits the possibilities of application in lots of solid unit operations. For measuring particle RTD in solid unit operations with long residence time a more effective and accurate technique is needed to be developed. For this purpose, it would be necessary to realize a system which can determine very low pigment concentration. Due to the low consumption of the tracer, RTD experiments can be conducted without separating the tracer particles and bulk particles. Besides, to go further in the understanding, a model will be developed and compared with the experimental results. The combination of RTD results using the developed technique with a theoretical model will

allow formulating the modifications and obtaining more information about the flow pattern inside a solid unit operation.

Chapter 2

Methodology validation

2.1 Introduction

The main objective of this chapter is to present a novel technique to measure the phosphorescent tracer concentrations for experimental RTD studies. The role of the tracer concentration measurement system is to measure the concentration of tracers in samples taken from solid unit operations for instance, fluidized bed reactors. Using this system, the RTD study can be performed on any solid unit operations where samples can be taken with an adequate concentration. This technique can accurately detect very low tracer concentrations as well as high tracer concentrations.

This chapter is divided into three major sections. The first section describes the experimental setup, technique employed in the tracer concentration measurement system as a novel measurement technique. The second section presents particle RTD measurement of a simple bubbling fluidized bed in order to validate our measurement methodology. And, section 3 provides a full discussion of the significance of the results.

The tracer concentration measurement system is based on the optical method that was developed by Harris et al. [20]. Experiments were carried out with two powders, Silicon Carbide (SiC) and the phosphorescent pigment (Lumilux® Green SN-F50 WS). The SiC/pigment mixtures in different proportions were injected continuously at the top of a vertical tube where the tracer (phosphorescent pigment) was activated by a UV light and detected at the bottom of the tube. The calibration procedure was performed to provide the empirical relationship between the integral of the detected signals and the pigment concentration.

Subsequently, a simple fluidized bed reactor was employed as a solid unit operation in this study in order to validate this measurement methodology. Harris et al. [18]–[21], used the phosphorescent tracer to measure the particle RTD in a circulating fluidized bed riser. In these phosphorescent tracer experiments, both the bed material and the tracer particles were the same phosphorescent particles. Thus, large amount of the expensive phosphorescent particles was needed in these experiments especially for large-scale solid unit operations. In comparison, during our phosphorescent tracer experiment, just a small quantity of phosphorescent particle was illuminated and used as tracer particle. Therefore, the consumption efficiency of the phosphorescent tracer particle is quite low and RTD measurements can be performed with different bulk solids in different solid unit operations. Furthermore, its ability to detect very low tracer concentrations allowing experimental RTD studies with extended residence times can be carried out without perturbing the hydrodynamics of the studied system.

2.2 Materials and method

2.2.1 Materials

In the present study, two different particles were used:

- SiC (Silicon Carbide) as a bulk particle; SiC was selected due to its mechanical resistance to attrition and volumetric heat capacity that is essential in wide range applications. For instance,

a PhD thesis was performed at "Institut National Polytechnique (INP)" Toulouse which used SiC particles in a fluidized bed reactor as a solar receiver [121].

- Pigment particle (Lumilux® Green SN-F50 WS) as a tracer particle; composed mainly of Zinc sulfide enriched with copper (chemical formula: ZnS; Cu+): ZnS is the oldest known phosphorescent material, it is a solid of very low toxicity, low flammability but soluble in acid. This pigment absorbs and emits photons in the visible range. The spectrum of absorption and emission light are shown in
- Figure 2.1.

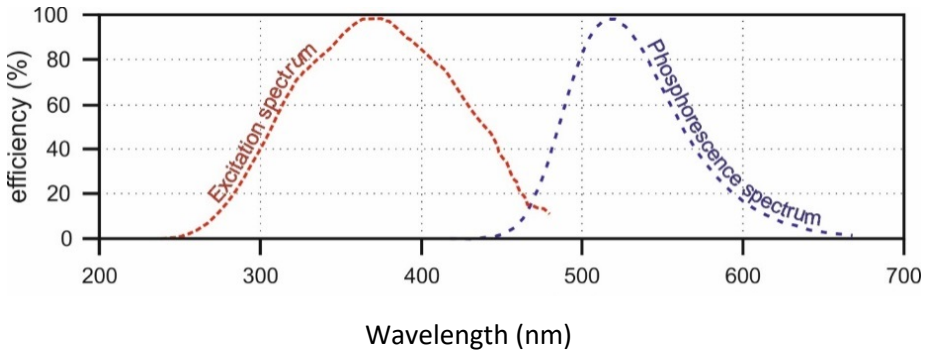

Figure 2.1: Absorption and emission wavelength of Lumilux® Green SN-F50 WS

The emission spectrum has an increased wavelength size compared to the excitation spectrum due to the loss of vibrational energy of the electrons. Therefore, there is usually an overlap between the excitation and the emission spectrum, known as the Stokes law or Stokes shift [122]. In order to ease the excitation light separation from emission light, this overlap must be eliminated by using an appropriate filter. To achieve the best detection and excitation efficiency, the pigment particles are usually excited by the wavelength at the peak of the excitation curve and the emission detection is selected at the peak wavelength of the emission curve.

Pigment selection:

The tracer particle (Lumilux® Green SN-F50 WS) was chosen in this study to have similar fluidization properties to the SiC particles which were needed for the methodology validation in the second part of this chapter. The densities and particle size distribution were studied using a laser granulometer Mastersizer 2000 (Malvern Instruments) and a helium pycnometer Accupyc 1330 (Micrometrices) respectively. The properties of the SiC and pigment particles are summarized in Table 2.1.

Table 2.1: Physical properties of SiC and phosphorescent tracer powders.

Particle	D10 (µm)	D50 (µm)	D90 (µm)	Sauter mean diameter D[3,2] (µm)	Density [g/cm^3]	Geldart Classification
Silicon Carbide (SiC)	41.4	72.7	122.2	58.3	3.22	B
Phosphorescent Tracer (Lumilux® Green SN-F50 WS)	40.9	70.4	120.3	64.5	3.63	B

In order to choose the correct phosphorescent tracer it was necessary to find a material with a notable difference between the excitation and emission wavelength peaks (great Stokes shift), as mentioned in section 2.2.1. This difference allows the photomultiplier to detect the intensity of the excited tracers without being influenced by the intensity of the light source which emits the same wavelength of the pigment excitation. Based on this argument, slight difference in the density and particle sizes of the bulk particles and tracer particles were considered negligible. Therefore, the Lumilux® Green SN-F50 WS was chosen as a tracer. It had practically similar hydrodynamic proprieties and a great Stokes shift. The peak of the excitation spectrum is in the UV zone (*360-380nm*), whereas the emission peak is in the visible light (*520nm*), having a yellowish-green light (see Figure 2.1).

(a) (b)

Figure 2.2: PigmentLumilux® Green SN-F50; a) in ambient light, b) in dark room.

2.2.2 Phosphorescent particle tracer technique

The phosphorescent particle tracer technique is one of the non-disruptive techniques that can be used to determine the particle residence time distribution in solid unit operations. This technique is based on the characteristics of the phosphorescence of certain compounds or solid particles. The phosphorescent material can emit light immediately and continuously, for a short period with

decreasing intensity, after being excited by a strong light source (Figure 2.3). Therefore, it is an ideal material for use as a solid's tracer.

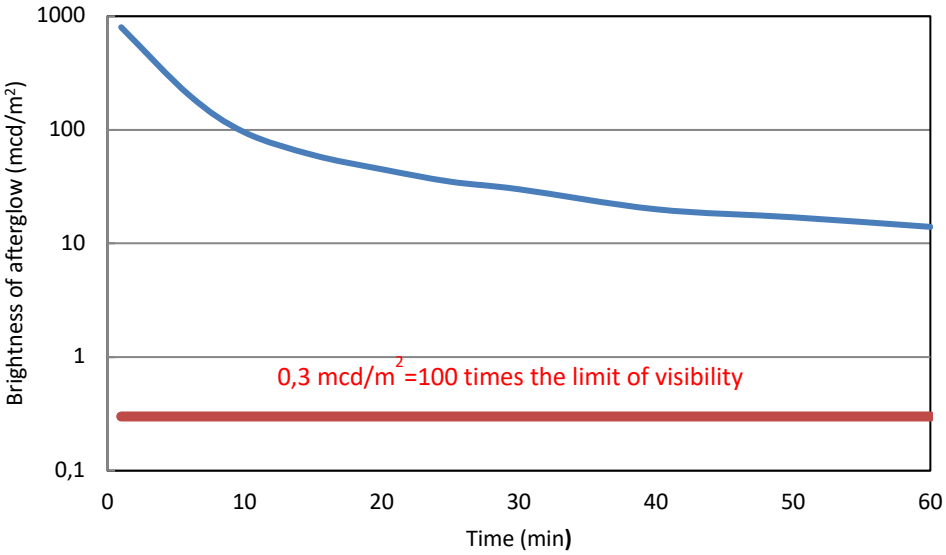

Figure 2.3 : Typical decay curve of pigment phosphorescent Lumilux® Green SN-F50 WS from pigment technical sheet.

A disadvantage of this technique appears in concentrated flows when detection is not accurate due to the superposition of particles [67]. In this study, a high-speed camera of i-SPEED3 with maximum speed of *50 000 photos/sec* and a resolution of *528x396* pixel was used in our experimental setup to illuminate the particles at the detection part. The solid dispersion shown in Figure 2.4 indicates that the particle concentration in front of the light source is fairly low. Therefore, we assumed that there was no particle superposition in our system with considered operating conditions and mass flow rate (*6+/-1g/min*).

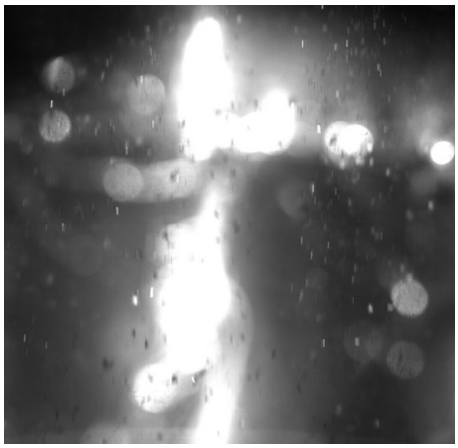

Figure 2.4: Flow concentration of SiC-Pigment particles in activation part.

2.3 General description of the system of tracer concentration measurement

The system of tracer concentration measurement used in the experiments is originally designed, constructed and operated at the University of Technology of Compiègne. This system meets the following requirements:

- Have a minimum length to allow minimum intensity reduction and maximum sensibility.
- Be flexible in order to couple with different solid unit operations.
- Be opaque to limit the detection just from excited tracer particles in front of the detector.

The tracer concentration measurement system is composed of a vertical tube (PVC; ID=*38mm*, h=*300mm*) with two transparent sections for activation of the tracer particles and detection of their intensities. The lower section of the tube is equipped with a storage bin to collect the particles. This system is used under ambient temperature and in a darkroom. The tracer concentration measurement system can be divided into three principal parts:

- The activation zone
- The vertical PVC tube
- The detection zone

A schematic diagram of the setup is presented in Figure 2.5 where the feeding system, activation zone, vertical tube and detection zone are identified. A photograph of the setup was also provided for more details.

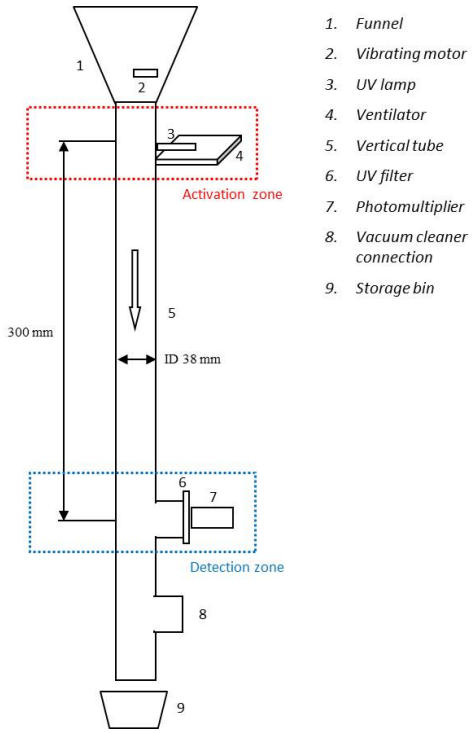

Figure 2.5: Schematic diagram of the concentration measurement system

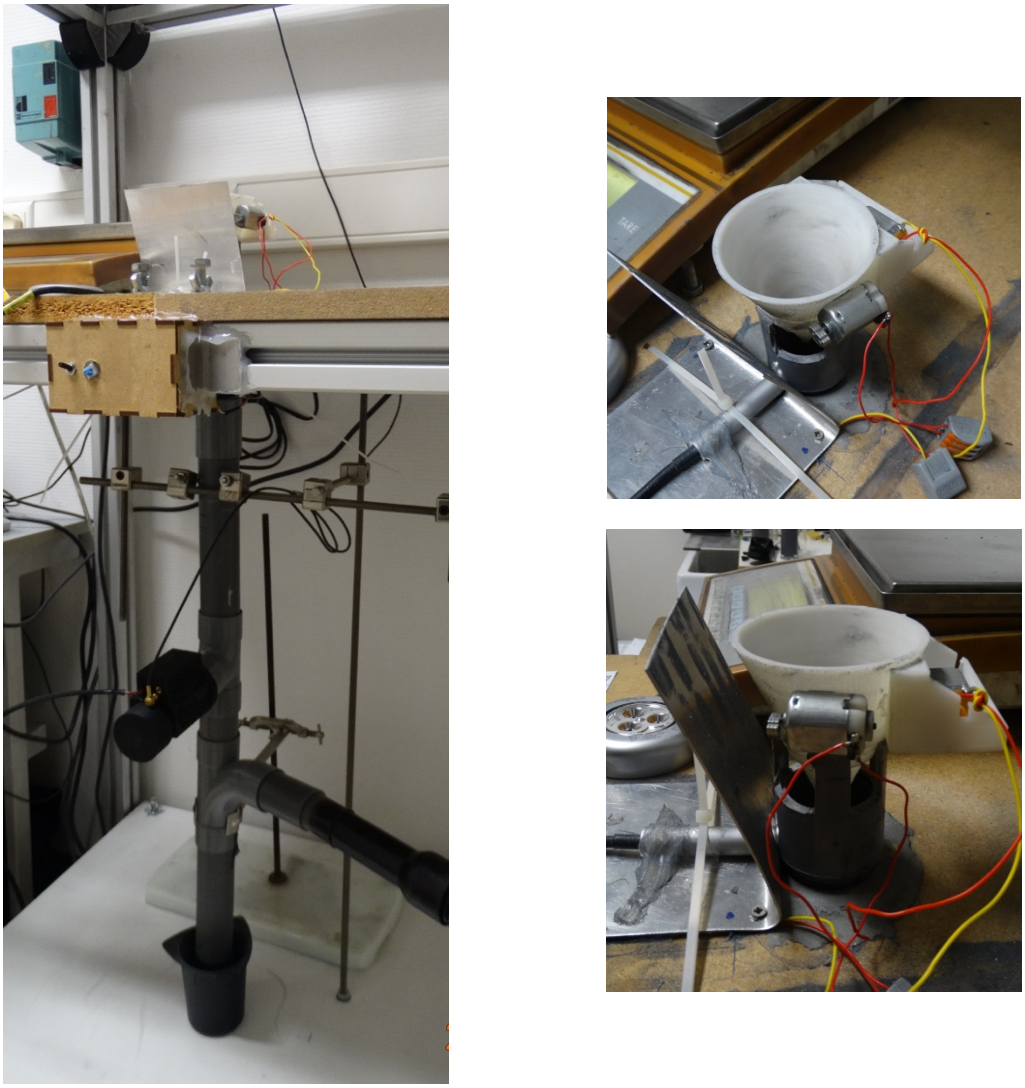

(a) (b)

Figure 2.6: (a) Photograph of the concentration measurement system; (b) Photograph of UV light position.

2.4 Detailed description of setup

2.4.1 Activation part

In the activation zone, the sample goes through a funnel with an exit orifice of *1.5mm*, using a vibrating motor attached to the funnel to ensure a steady and low particle mass flow rate (*≈6+/-1g/min*). A *25W* UV-LED spot light source with an LED controller from Hamamatsu L11921-415, is directed right at the exit of the funnel. As shown in Figure 2.7, the emission spectrum of the UV light (*365nm +/- 5nm*) fits around the maximum of the excitation spectrum of the tracer. It is so important that the light source chosen for the pigment excitation has sufficient brightness especially for very low pigment

concentration. Therefore, the relatively weak emission light can be maximized, and detection efficiency can be increased.
A ventilator was used under the UV-LED light in order to prevent overheating of the lamp during the experiment. The interior portion of the tube in the activation zone was covered by a reflective aluminum film in order to reflect the UV light toward the pigment particles and increase the activation efficiency of the system. As a consequence, all the particles had a proper excitation after leaving the activation zone.

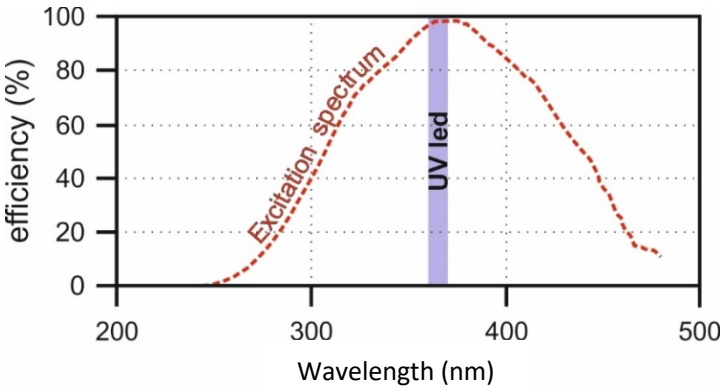

Figure 2.7: Absorption wavelength of Lumilux® Green SN-F50 WS with the wavelength of the UV LED used in the device

(a) (b)

Figure 2.8: The activation system in this study: a) UV-LED spot light source and LED controller (Hamamatsu) and b) Transparent section in activation zone

2.4.2 Vertical tube part

A vertical tube with *300mm* height and *38mm* of interior diameter was modified such that two portions of the pipe were transparent (at the bottom and at the top of the tube). The solid particles fall down in the tube due to gravitational force. The tube length was determined by a) determining the minimum detectable tracer concentration (sensibility of detection) and b) the signal/noise values. The following subsection illustrates the results obtained with two different tube lengths.

Effect of the tube length on the pigment detection:

The tube length which corresponds to the distance between the activation part (UV light) and detection part plays an important role in the detection efficiency and overall system performance. The effect of the tube length was evaluated using two different tube lengths (*300* and *600mm*). The emitted light of pigment particles was measured at the tube outlet and the effect of the tube length was determined by comparing the signal to noise values and minimum detectable tracer concentration. The noise of the measured signals corresponds to the signals measured at the tube outlet while there is no tracer in the mixture. The experiments were performed with different concentrations of SiC/pigment mixtures, with sample size of *4g*. Figure 2.9 shows the raw signals detected by the apparatus with a SiC/pigment mixture of *1wt.%*.

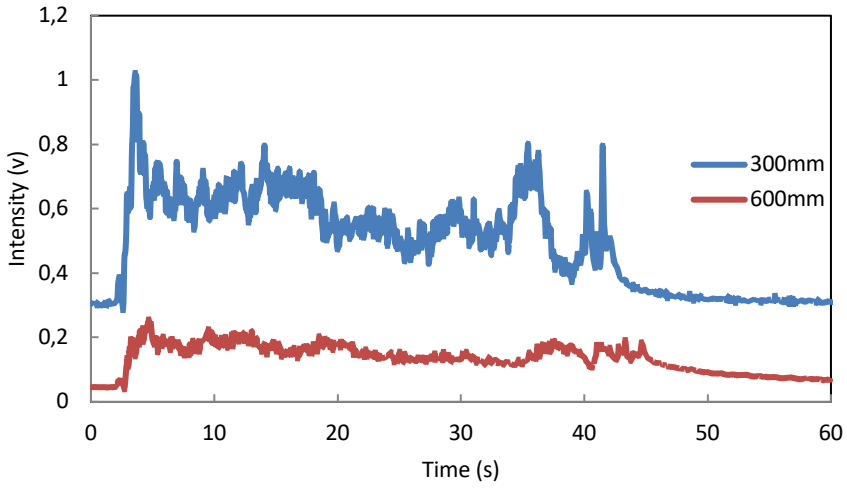

Figure 2.9: Effect of tube length on the detection performance using 6gr of SiC/pigment mixture of 1%wt. (without optical filter).

By varying the tube length, the noise signal and the raw signals were changed due to the increased length of the tube and decay time of the pigment particles (Figure 2.3), respectively. It can also be mentioned that the dilution of particles as a result of particle acceleration can change the noise signals and the raw signals. For a better understanding of the tube length effect, the signals to noise ratios were also compared.

Figure 2.10 shows the signal to noise ratio for different pigment concentrations and the tube lengths of *300* and *600mm*. Signal to noise ratios are the average signal intensities of each sample divided by the noise intensity. As shown in Figure 2.10 the maximum signal to noise ratio corresponds to the tube length of *600mm*. These ratios also increase with the increase of pigment concentration for both tube lengths.

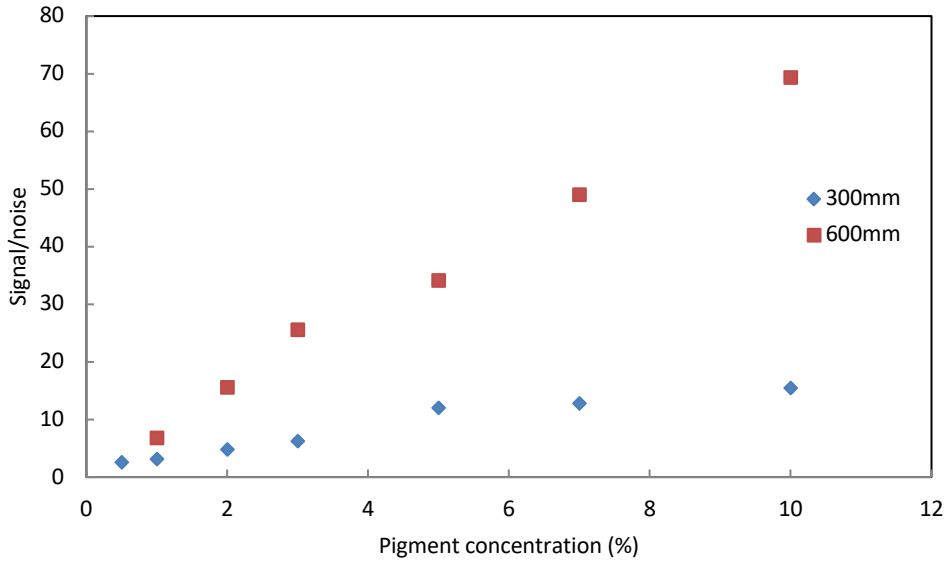

Figure 2.10: Signal to noise ratio for tube of *300mm* and *600mm* in different pigment concentration

The main problem in tube length of *600mm* relates to the detection of the very low pigment concentration. In tube length of *600mm* the pigment concentration below *1wt.%* cannot be detected despite the high signal to noise ratio. Consequently, in order to have a maximum signal to noise ratio the tube length of *600mm* must be used but to have a maximum sensibility the tube length of *300mm* must be used. Because the emphasis on high results sensibility for residence time distribution measurements and minimum pigment consumption, the tube with *300mm* length was chosen for all experiments. Tube lengths shorter than *300mm* present a high risk of disturbance of the results by UV light due to a high noise to signal value, therefore they were not considered for use.

2.4.3 Detection part

The detection part is composed of four elements, a photomultiplier, a supply system, an acquisition system and a UV filter. The photomultiplier (or PMT), Lynx Silicon Photomultiplier Module LynX-A-33-W50-T1-X, utilizes a 3×3mm^2 active area Silicon Photomultiplier (SiPM) (Technical data sheet in annex. II).

The choice of this type of PMT is justified by the compatibility with the selected pigment because of its precision in the wavelength range from *350-950nm*, and peak of detection at *510nm*, which allows it to be the most efficient in measuring the pigment emission light (Technical data sheet in annex. I). The PMT was installed at the tube outlet at a distance of about *50mm* from the tube wall. This distance is close enough for detection of the pigment intensities and at the same time far enough from the wall such that it is not overwhelmed by the particles closest to the PMT, therefore detecting all particles in flow. The detection efficiency according to the wavelength is presented in Figure 2.11.

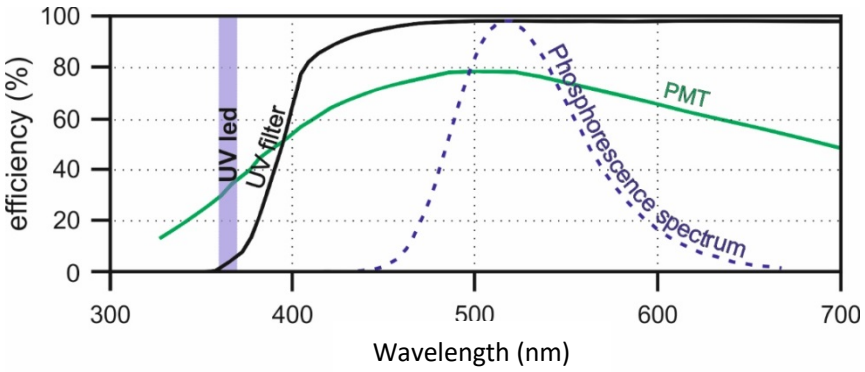

Figure 2.11: Lumilux® Green SN-F50 WS, PMT, UV filter and UV LED efficiency variation in the spectra. The efficiency of the UV filter is defined as the quantity of the luminance it is going to let pass.

The supply system shown in Figure 2.12 developed by electronic service at UTC is used as a PMT supply system in order to change the sensibility of detection.

Figure 2.12: Supply system and PMT.

The acquisition system shown in Figure 2.13 was used in our experiments to collect the signals detected by the PMT. The data is retrieved by the computer using a USB connector and processed using software developed by UTC, which allows communication with the PMT via the acquisition system. The software sampling period is adjustable between *10* and *40ms*.
The UV filter, HOYA UV(0) L39, was used in front of the PMT to reduce the signal of the UV-LED detected by the PMT. This UV filter only eliminates the wavelength of the UV light so it increases the sensitivity of the detection system and allowing lower tracer concentrations to be measured, without being masked by the UV light [20].
The separation of excitation and emission wavelengths is achieved by proper selection of filters to block or pass specific wavelengths of the light spectrum, as presented in Figure 2.1. The detection efficiency is based on control of excitation light and emission light by readily changeable filter insertions into the light path.

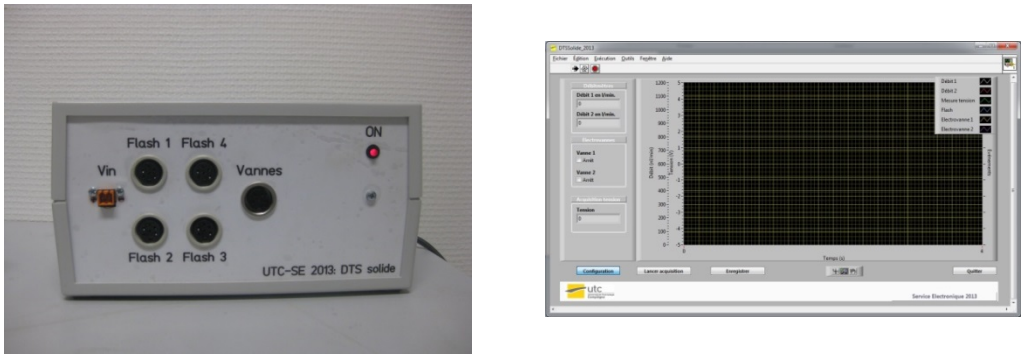

(a) (b)

Figure 2.13: a) Acquisition system; and b) Software of detection

2.5 Protocol of experiments

The following experimental protocol was used for all our experiments:

- At the beginning, the laboratory light was turned off and the perfect insulation was made in the detection part. The darkroom allowed us to measure only the emission light of the excited tracers without disturbance from the ambient light.
- The UV light (the UV-LED light) was turned on. The activation of pigment particles was carried out by the UV-LED light which excited them as they passed under the transparent slit at the entrance.
- The photomultiplier was turned on which detects the emitted light of the pigment particles as they pass in front of the PMT and towards the outlet of the vertical tube.
- Detection software was launched. The sampling period was fixed at *40ms*.
- Then, the feeding system (vibrator of funnel) was started.
- Twenty grams of each sample were poured (injected) into the funnel vibrating at a low mass flow rate (*≈6±1g/min*). This low mass flow rate and the flow dilution ensure that the particle superposition in front of photomultiplier can be neglected.
- Data was recorded. Each sample took approximately *200* seconds to pass through the system. In order to measure the intensities of tracer particles for very low concentrations, all the experiments were carried out using the maximum sensitivity of the PMT.
- After each measurement the equipment was cleaned with the vacuum cleaner in order to remove any remaining particles, so they do not influence the subsequent measurements.

2.6 Calibration procedure

A calibration of the concentration measurement system was carried out which provided the empirical relationship between the integral of the detected signals and the pigment concentration. To make the calibration curve, SiC/pigment mixtures with different compositions (ranging from *0.25%wt.* to *6.25%wt.*) were prepared. The upper limit of sample concentration was set to 6.25%wt. In order to have a low consumption of the tracer particles in the experiments, the measurements were carried out with high sensibility of the PMT and very low pigment concentration. In the calibration curve method, twenty grams of different samples (SiC/Pigment mixtures) with known composition were injected into the concentration measurement system according to the experimental protocol described in section 2.5. It must be highlighted that this calibration curve focuses mainly on very low pigment concentration since this method is devoted to particle RTD measurement in solid unit operations with long residence time. The measurement was repeated seven times for each tracer concentration in order to ensure that there was no drifting in the measurement and that it was reliable overtime. The integral of the emitted light from each sample was related to the pigment concentration after eliminating the background noise from the integral results of the sample data.

The operating parameters of the calibration procedure are reported in Table 2.2.

Table 2.2: Operating conditions used for the calibration procedure.

Operating parameters	Values
Mass of sample (g)	20
Pigment concentration (wt.%)	0-6.25
Mass flow rate (g/min)	6±1
Tube inner diameter (mm)	38
Tube length (mm)	300

2.7 Calibration results

The present section describes the influence of the pigment concentrations in the SiC/pigment mixtures on the integral of the detected signals.

As mentioned in section 2.6, more than *40* experiments were conducted with the concentration measurement system using different SiC/pigment mixtures in order to establish a relationship between the integral of the detected signal from the PMT and the pigment concentration.

The calibration curve was determined on the following criteria:

- The increasing of pigment concentration in samples leads to an increased intensity of the measured signals.

- Since the relationship between the signals measured by PMT and pigment concentration is not accurate, the integration method was used to generate the measured signals of each sample. Consequently, a graphical integration for the intensity-time diagram is applied to calculate the pigment concentration.
- It was assumed that the sample without pigment (Pure SiC) has the measured value (an integral value) of zero.
- Note that it is necessary to calculate the error bars for the integral values.

Figure 2.14 represents the measured raw signals of SiC/pigment mixtures as a function of time. The operating conditions are reported in Table 2.2.

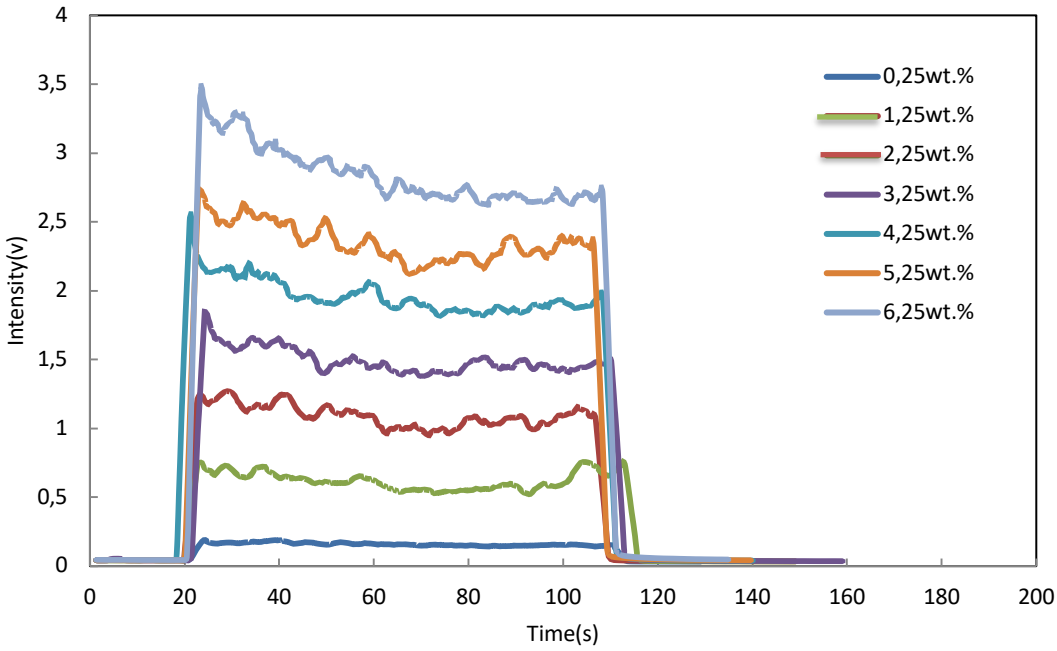

Figure 2.14 : Measured raw signal curves of the twenty grams of SiC/pigment mixtures.

Calculating the area under the measured signal intensity curves in terms of time and plotting it as a function of pigment concentration gives a linear relationship, as seen in Figure 2.15.
Figure 2.15 plots the integral values of samples as a function of the pigment concentration. The errors introduced by sample dividing process were estimated in a separate series of tests. The linear fitting of the integral with the concentration of tracer in the mixture gives the correlation (2. 1).

$$I = 38.62 \times C_{Pigment} \qquad (2.\ 1)$$

where *I* is the integral of the detected signal and $C_{Pigment}$ is pigment concentration (wt.%) in a SiC/pigment mixture. It is clear that by increasing the pigment concentration, the detected signal integral will be increased. It should be noted that the mentioned equation is only obtained for very low concentrations and is not suitable for very high concentrations.

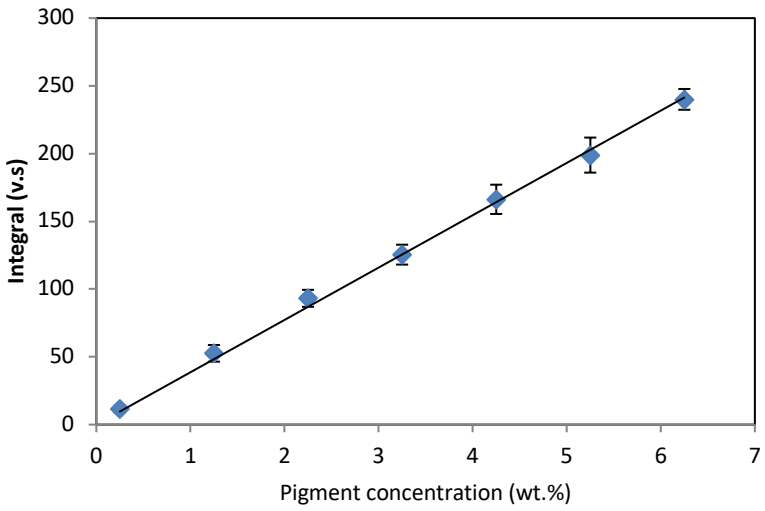

Figure 2.15 : Calibration curve (Tracer concentration (%) vs Integral of the PMT measure), the measurement was repeated seven times for each tracer concentration.

Table 2.3 provides a summary of the numerical values presented in Figure 2.15.

Table 2.3: Integrals of detected signals as a function of pigment concentrations.

Number	Concentration (wt.%)	Mean Integrals of detected signals (v.s)	Standard Deviation (v.s)
1	0.25	11.50	2.4
2	1.25	52.60	6.1
3	2.25	93.20	6.2
4	3.25	125.45	7.3
5	4.25	166.26	10.8
6	5.25	198.91	12.9
7	6.25	240.03	7.6

2.8 Methodology validation using a simple fluidized bed

In the present section, a simple bubbling fluidized bed was used to study its particle RTD experimentally and compare it with theoretical results in order to validate our RTD measurement methodology. To determine the RTD of particles within the fluidized bed reactor, SiC particles were used as a bulk particle and phosphorescent tracer particles (Lumilux® Green SN-F50 WS) were used as a tracer particle. The tracer particles were premixed with bulk particles in the fluidized bed reactor, using the gas fluidization flow before starting the experiment. Therefore, the behavior of SiC/pigment mixture inside the reactor would be similar to a simple continuous stirred tank reactor. Validation of this

particle RTD measurement technique will be investigated comparing the theoretical and experimental RTD curves. Sampling was performed with a sample tube of *4mm* ID located at the exit of the fluidized bed. Particle RTD curves were obtained at the same operating conditions but different height to diameter (H/D) values. Three RTD curves were determined by varying H/D (*1, 1.5* and *2*) with the same operating conditions. These measurements serve as a validation process for the concentration measurement system. It should be noted that the trajectories of the particles during their displacement in the reactor depend on the inter-particle collisions, the particle-wall collisions and the nature of the laminar or turbulent flow. Similarly, the residence time distribution is a direct consequence of the trajectories which differ for all particles, the velocity field of the fluid volume and the laminar or turbulent character of the flow [123].

2.8.1 Fluidized bed reactor

The fluidized bed reactor used in the present study is shown in Figure 2.16. This fluidized bed consists of six main parts: fluidization column, air distributor, air flow meter, feeder, acquisition system and exit of the fluidized bed. The fluidization column is a Pyrex cylinder of *100mm* inner diameter and *480mm* height. A transparent column was used in experimental setup to allow the solid flow visualization at global scale.

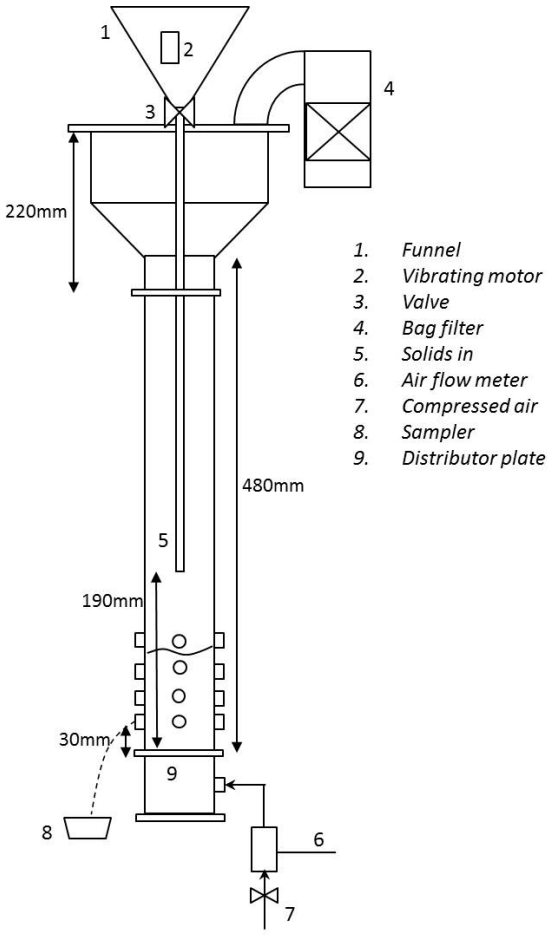

Figure 2.16: Schematic diagram of bubbling fluidized bed reactor.

The solid feed control system (feeding system), which consists of a funnel with a vibrating motor and a soft tube with a valve, serves two primary objectives:

- To provide the stable mass flow rate of particles to the fluidized bed.
- To provide varying mass flow rates that allow to have a precise entrance flow control

At the bottom of the fluidized bed, a solid exit channel was created with a *4mm* tube connected to the lower exit port of the fluidized bed, by a quick coupling connector. The air distributor is made of a perforated plate (*2mm* 176* holes, *7%* open area). The fluidization gas (air at ambient temperature) is supplied from the high-pressure air system available in the laboratory. Before entering into the spouting vessel, the compressed air passes through a filter, pressure regulator and a calibrated mass flow meter.
A photograph of the experimental setup (Figure 2.17) is also provided for more details.

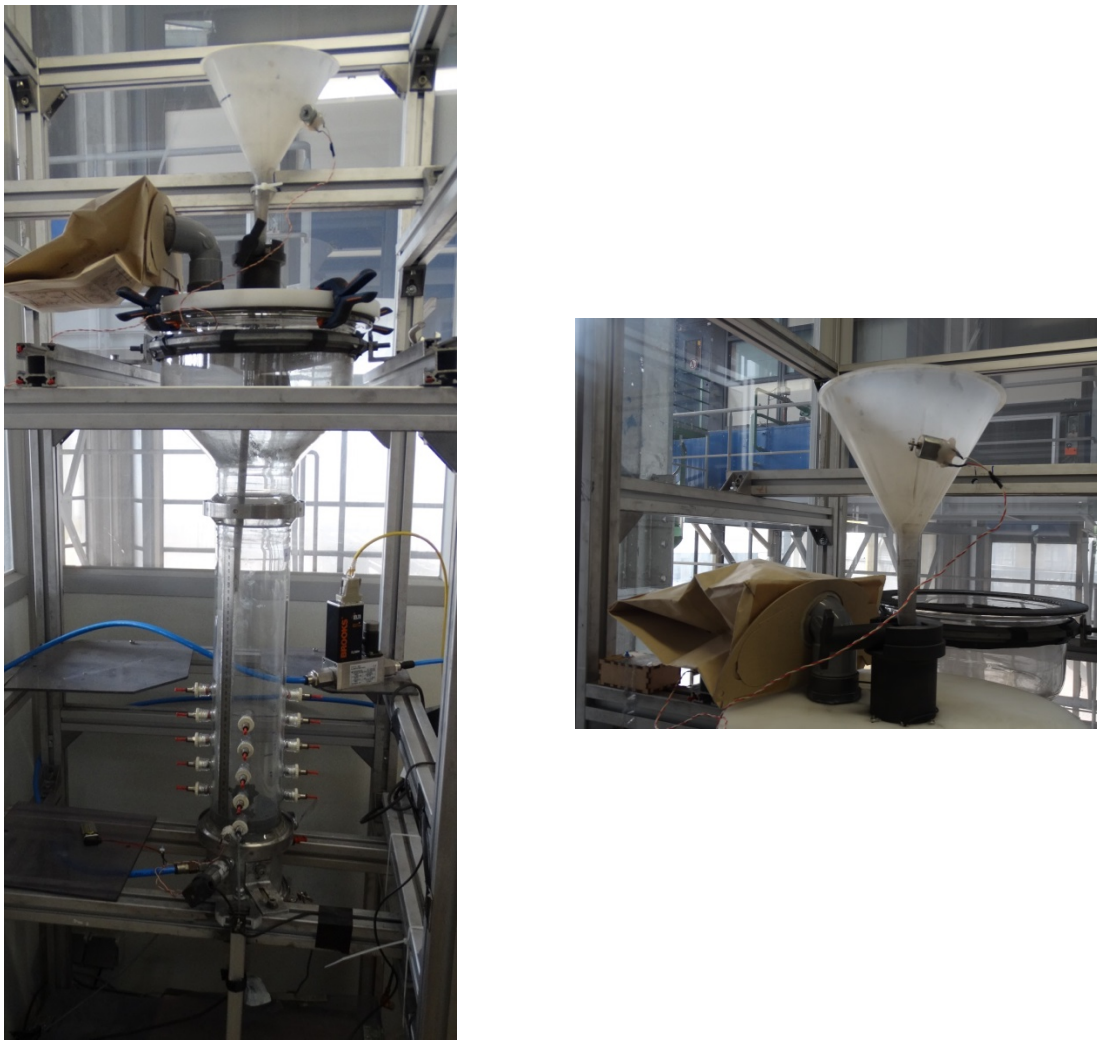

(a) (b)

Figure 2.17: Photograph of: a) Fluidized bed, b) Feeder.

2.8.2 Experimental procedures

In the present study, the pressure drop method was used for the minimum fluidization velocity measurement of the SiC particles. Figure 2.18 shows the pressure drop diagram as a function of superficial gas velocity. The minimum fluidization velocity was determined experimentally using the standard method proposed by Richardson [124]. This author defines the minimum fluidization velocity as the abscissa of the intersection point between the tangents of the pressure drop portion of the curve and the steady pressure portion of the curve obtained during the decreasing velocity analysis. The minimum fluidization velocity of the SiC particles measured is *6.3 mm/s*.

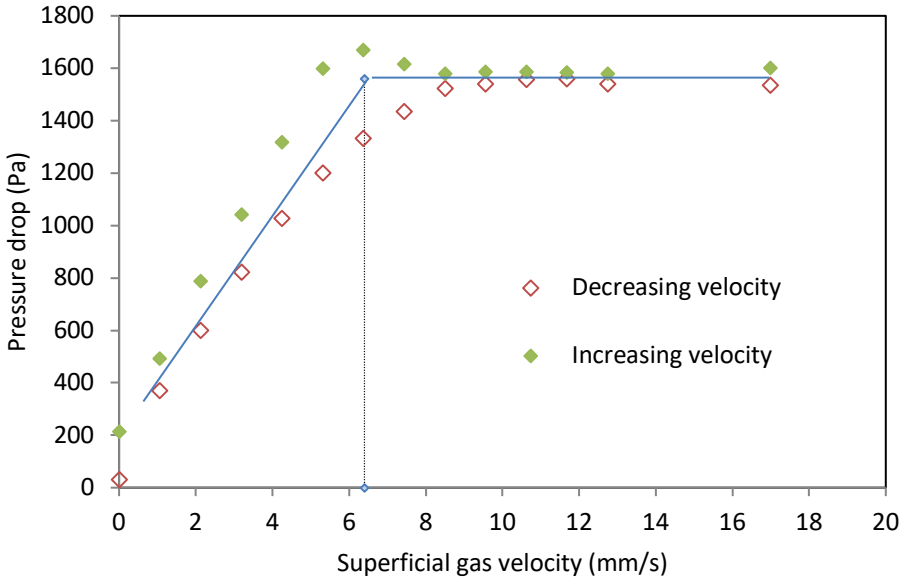

Figure 2.18: Pressure drop versus superficial velocity (H/D=1; SiC mass=1422gr).

Table 2.4 compares the calculated minimum fluidization velocity using different experimental correlations with the experimental data.

Table 2.4 : Calculated minimum fluidization velocity using different correlations.

Number	Researchers	U_{mf} (mm/s)	Relative error (%)
1	Wen and Yu. [95]	5.6	11.08
2	Leva [96]	6.8	9.00
3	Baeyens [97]	6.7	6.45
4	Thonglimp et al. [98]	6.2	1.22
5	Youjun et al. [99]	7.3	16.72

It can be seen from Table 2.4 that the average error of the minimum fluidization velocity predicted by Thonglimp et al. [98] is about *1%*. Therefore, the experimental value is comparable to that predicted from the Thonglimp correlation [98].

Running the RTD experiments:

In order to measure the particle RTD in the fluidized bed, some amount of SiC particles was introduced to the system such that the column had a height to diameter ratio (H/D) between 1 and 2 depending on the experiment; where *H* represents the height of the particles in the fluidized bed (SiC and tracer particles) and *D* the diameter of the fluidized bed column.

The tracer was premixed with the bulk powder (SiC) for *5* minutes to ensure a homogenous mixture, with a total concentration of *6.25wt.%*. The initial concentration was selected to be as low as possible in order to have the lowest consumption of the tracer without the loss of detection sensibility using the concentration measurement system. It should be noted that the low concentration of the tracer was necessary, since high concentrations would generate alterations in the fluidization and the high price of it would be a constraint for the implementation of the technique in larger equipment.

The pressure sensor placed at the wind-box measures the variation of the mass inside the fluidized bed through the experiment. After the premixing, both the exit and entrance tubes were opened such that the system maintained at steady state regime. The entrance flow was composed only by SiC, and samples at the exit flow were recovered during varying periods of time, such that the concentration between each measure could be considered constant in each sample. The experiment lasted for four times the theoretical residence time, based on the mass and flow rate of the bed material. When this time was achieved, the entrance flow was stopped, and the remaining powder was recovered from the equipment to determine the remaining tracer quantity. All the samples were analyzed in the developed system to measure the tracer concentration, in order to find the experimental RTD.

The study of the particle RTD was performed under the same operating conditions but in different height to diameter ratios ($1 \leq H/D \leq 2$).

2.9 Results and discussions

The reproducibility of the developed pigment concentration measurement technique was evaluated by varying the operating conditions of the fluidized bed during the RTD experiments.

The present section describes and discusses the results obtained from the particle RTD measurement of the fluidized bed reactor presented in section 2.8.1. The RTD curves were determined experimentally by adding the tracer particles and measuring the variation in time of the pigment concentration in the outflow.

The operating conditions of three different experiments with different residence times are shown in Table 2.5. For each experiment, the measured RTD curve was compared with the theoretical RTD curve of a perfect mixed reactor.

Table 2.5: Experimental conditions used for particle RTD measurement in the fluidized bed.

Number	H/D	Solid mass flow rate (gr/s)	SiC total (gr)	Initial pigment concentration (wt.%)
1	1	2.5±0.2	948	6.25
2	1.5	2.5±0.2	1422	6.25
3	2	2.5±0.2	1896	6.25

Figure 2.19 shows the C-curves and F-curves as a function of time for various values of the parameter *H/D*.

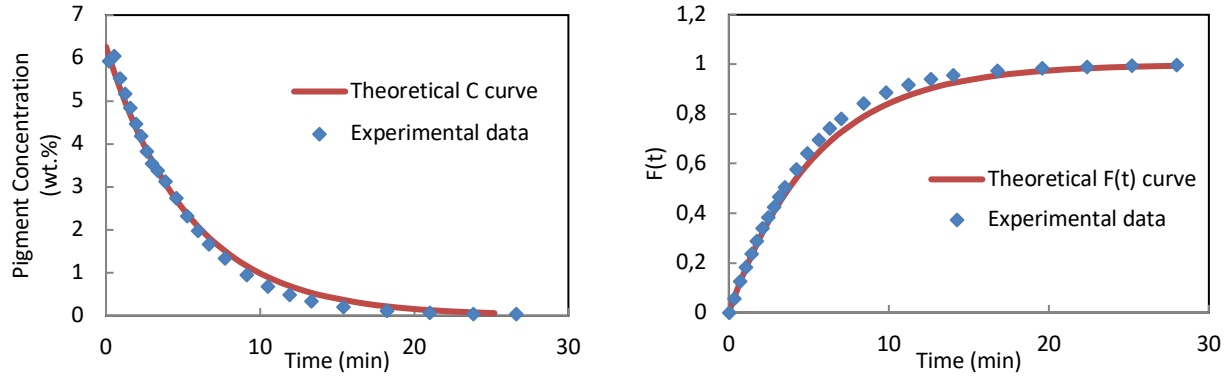

(a)

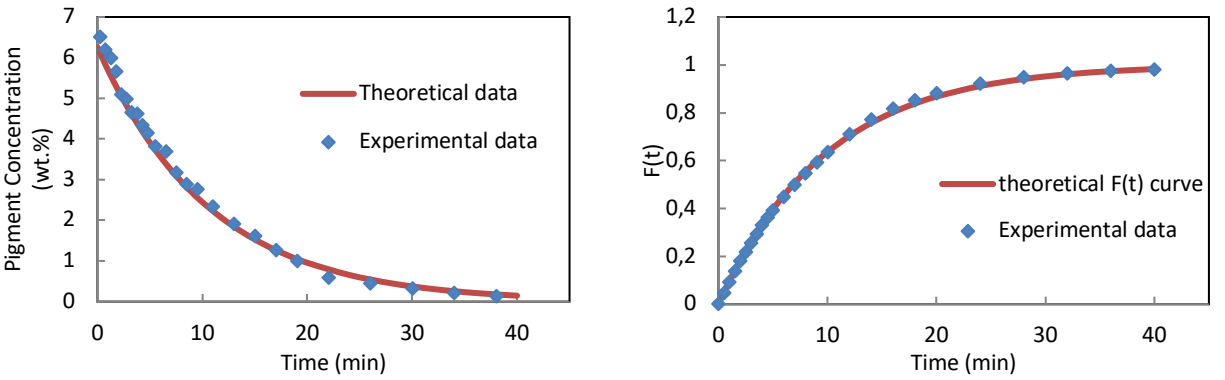

(b)

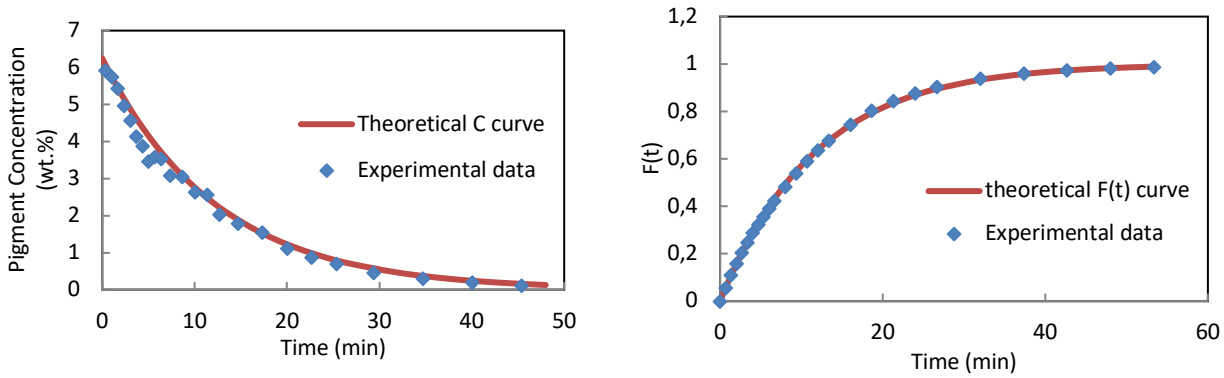

(c)

Figure 2.19: C (t) and F (t) of the fluidized bed as a function of time comparing with theoretical results for three different H/D: a) 1 b) 1.5 and c) 2.

Usually the first two RTD moments are used to compare RTDs, instead of trying to compare the entire distribution [46]. For this purpose, the mean residence time (t_m) and the variance (σ^2) were determined as follows:

$$t_m = \int_0^\infty tE(t)dt \qquad (2.\ 2)$$

$$\sigma^2 = \int_0^\infty (t - t_m)^2 E(t)dt \qquad (2.\ 3)$$

where, $E(t)$, is:

$$E(t) = \frac{C(t)}{\int_0^\infty C(t)dt} \qquad (2.\ 4)$$

The outcome of RTD analysis in terms of mean residence time and the variance is given in Table 2.6. As shown in Table 2.6, the experimental values of the mean residence time are close enough to the theoretical mean residence time values with negligible relative errors (less than 7%). The results confirmed the robustness of the methodology as a novel method for measurement of particle residence time distribution in solid unit operations especially with long residence time.

Table 2.6: Effect of height to diameter (H/D) of fluidized bed on the mean residence time.

Height to diameter (H/D)	Mean residence time (t_m) (min)		*Relative error (%)*	*Variance (σ^2)*
	Experimental	*Theoretical*		
1	5.07 ± 0.4	5.4	6.07	17.12
1.5	10.13 ± 0.4	10.15	0.18	58.24
2	12.44 ± 0.4	12.26	1.44	92.18

Figure 2.20 provides a summary of the mean residence time values presented in Table 2.6.

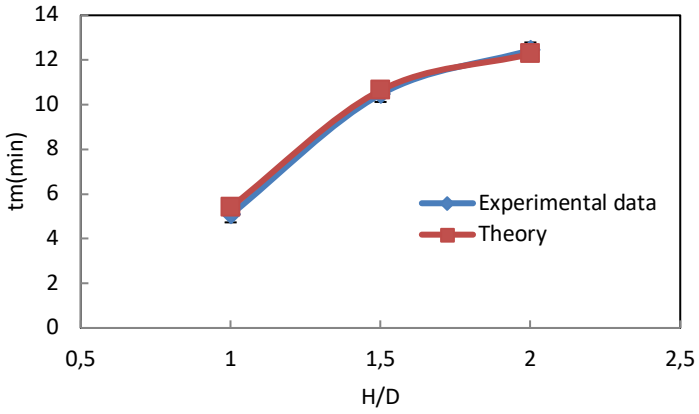

Figure 2.20: Theoretical and experimental mean residence time measured in different operating conditions (H/D=1, 1.5 and 2).

It should be noted that the mentioned mean residence time value for *H/D=1* in Table 2.6 was obtained by repeating the RTD experiment for three times and the lowest relative error was obtained.
Figure 2.21 gives the F-curves as a function of time for three experiments which were carried out under identical condition (*H/D=1.5).*

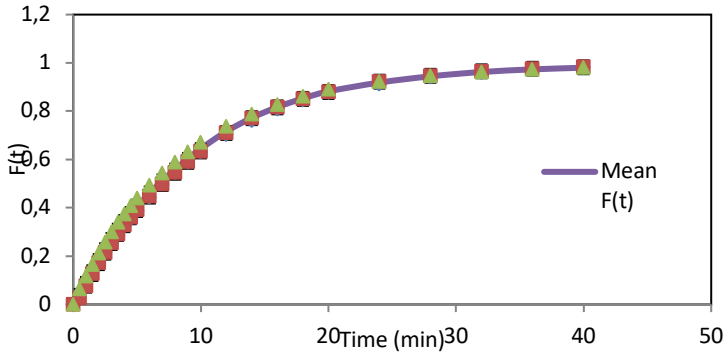

Figure 2.21 : F(t) curves for identical conditions (H/D=1.5).

The error bars refer to the 95% confidence intervals based on repeated determinations.

$$Confidence\ interval\ (95\%) = \bar{F} \pm Z\alpha_{/2} \frac{SD}{\sqrt{n}} = 10.13 \pm 0.42 \text{ min}$$

where, $\bar{F}$ is the mean values of *F*, $Z\alpha_{/2}$ is the confidence coefficient, SD is the standard deviation and n is the sample size.

The results of comparison between introduced pigment and measured pigment (detected by PMT) for different operating conditions can be seen in Figure 2.22.To illustrate it better, Table 2.7 provides the introduced and measured pigment values presented in Figure 2.22.

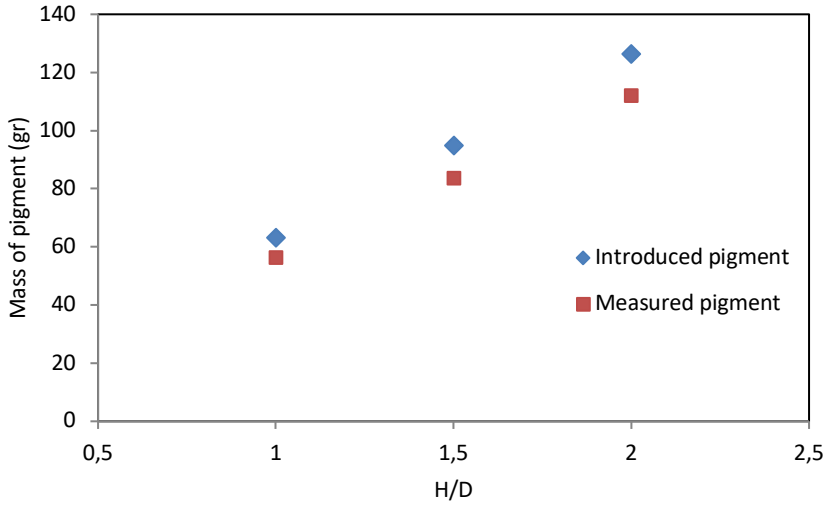

Figure 2.22: Masse of measured and introduced pigment for different operating conditions (H/D=1, 1.5 and 2).

Table 2.7: Introduced and measured pigment values presented in Figure 2.22.

H/D	Introduced pigment (g)	Measured pigment (g)	Relative error (%)
1	63.3	56.47	10.82
1.5	95	83.63	11.96
2	126.4	112.08	11.32

It must be added that in this study:

- The pigment concentrations were obtained by measuring only twenty grams of samples (According to the calibration curve method described in section 2.6).
- The mass flow rate in the fluidized bed outlet was changed overtime (*2.3g/s* to *2.7 g/s*).

The results discussed above indicate that the novel technique developed in the present study is capable to obtaining reliable measurements of the tracer concentration in SiC/pigment mixture with very high accuracy and residence time of different solid unit operations with long residence time. These results prove the validation of pigment concentration measurement technique.

2.10 Conclusion

A new concentration measurement technique is developed in this study for the determination of the particle residence time distribution in different solid unit operations. The pigment particles (Lumilux® Green SN-F50 WS) and SiC particles (Silicon Carbide) were used as a tracer and bulk particles respectively. Twenty grams of SiC/pigment mixtures with different concentrations were fed into the concentration measurement system using a vibrating funnel in order to establish a relationship between the integral of the detected signal from the PMT and the pigment concentration. A simple bubbling fluidized bed was used to study its particle RTD experimentally and compare it with theoretical results to validate the concentration measurement technique.
The following conclusions can be drawn based on the results obtained in this study:

- According to the obtained results, this system of tracer concentration measurement has the ability of the tracer detection with very low pigment concentration (even less than *0.5%wt.*). It is necessary to measure the RTD of solid unit operation with long residence time with minimum consumption of tracer particles which allows the RTD experiments to be conducted without separating the tracer particles and bulk particles.

- The linear relationship between the integral of the detected intensities and pigment concentration was found and was proven to be reliable.

- The experimental C-curves and F-curves of the fluidized bed reactor measured by the concentration measurement system fit well with the theoretical results.
- The experimental values of the mean residence time were close enough to the theoretical mean residence time values with negligible relative errors (less than 7%).
- The fundamental advantage of the presented measurement technique compared to the on-line measurement techniques is that this technique eliminates the knowledge of the particle concentration and velocity profiles in the outlet of solid unit operations.
- This technique can be used in solid unit operations with the residence time greater than *3* minutes corresponding to the decay of the light signal after the excitation of the particles.
- Sampling at the outlet can be very difficult for high velocity flows such as pneumatic conveying.
- It is possible to coat the outside of the bulk particles using the pigment. In this way, any particles that can be coated may be used for the RTD experiments.

Chapter 3

RTD measurement in a deep fluidized bed

3.1 Introduction

In the following chapter, the developed technique of the concentration measurement (Described in Chapter 2) was applied to measure the residence time distribution of a deep fluidized bed in order to present an application of the developed technique.

The experiments were carried out using SiC particles as a bulk solid and the pigment phosphorescent (Lumilux® Green SN-F50 WS) as tracer particles in a Plexiglas fluidized bed with an inner diameter of *63mm* and height of *2m*. Eight pressure gauges were used to measure differential pressure along the deep fluidized bed from a point immediately above the air distributor to the freeboard of the bed. In the present study, pulse injection of a tracer was performed using solid feeding system with a constant mass flow rate at the inlet of a continuous system where steady state of bulk flow was reached. Then, the response of the tracer profile at the outlet was measured using the developed system of the concentration measurement.

Fluidized beds promote highly efficient contact between gas and particles (*e.g*., a catalyst), resulting in high heat transfer, chemical reaction rates and product yields. The objective of the present work is to apply the technique of tracer concentration measurement in a real fluidized bed as an extensively used solid unit operation in order to present an application of the developed technique of tracer concentration measurement.

The following subsection describes the general description of the experimental setup used in the present study including the deep fluidized bed, the solid flow systems and the instrumentation used to measure pressure.

3.2 General description of the experimental setup

The fluidized bed setup used in the experiments is designed, constructed and operated in our laboratory. A schematic diagram and photograph of the experimental setup used in the present study are shown in Figure 3.1.

The system major components include a deep fluidized bed with an inner diameter of *63mm* and *2m* in height, solid feeding system, acquisition system, and pressure sensors for pressure profiles measurements.

The particulate materials used for this study were SiC (Silicon Carbide) particles as a bulk and Pigment particle (Lumilux® Green SN-F50 WS) as a tracer particle (See Table 2.1).

By following the solid path, the components of the setup are:

- The solid feeding system which consists of a funnel with a vibrating motor to provide the stable mass flow rate of particles and a soft tube with a valve to provide varying mass flow rates
- The deep fluidized bed column (*63mm* of inner diameter and *2m* of height) made of Plexiglas for visual observation
- The air distributor which is made of a perforated plate (*2mm* 176* holes, *7%* open area)

- Air flow meter
- Acquisition system
- The fluidized bed exit was located at the bottom of the fluidized bed with the inner diameter of *3mm*
- The bag filter.

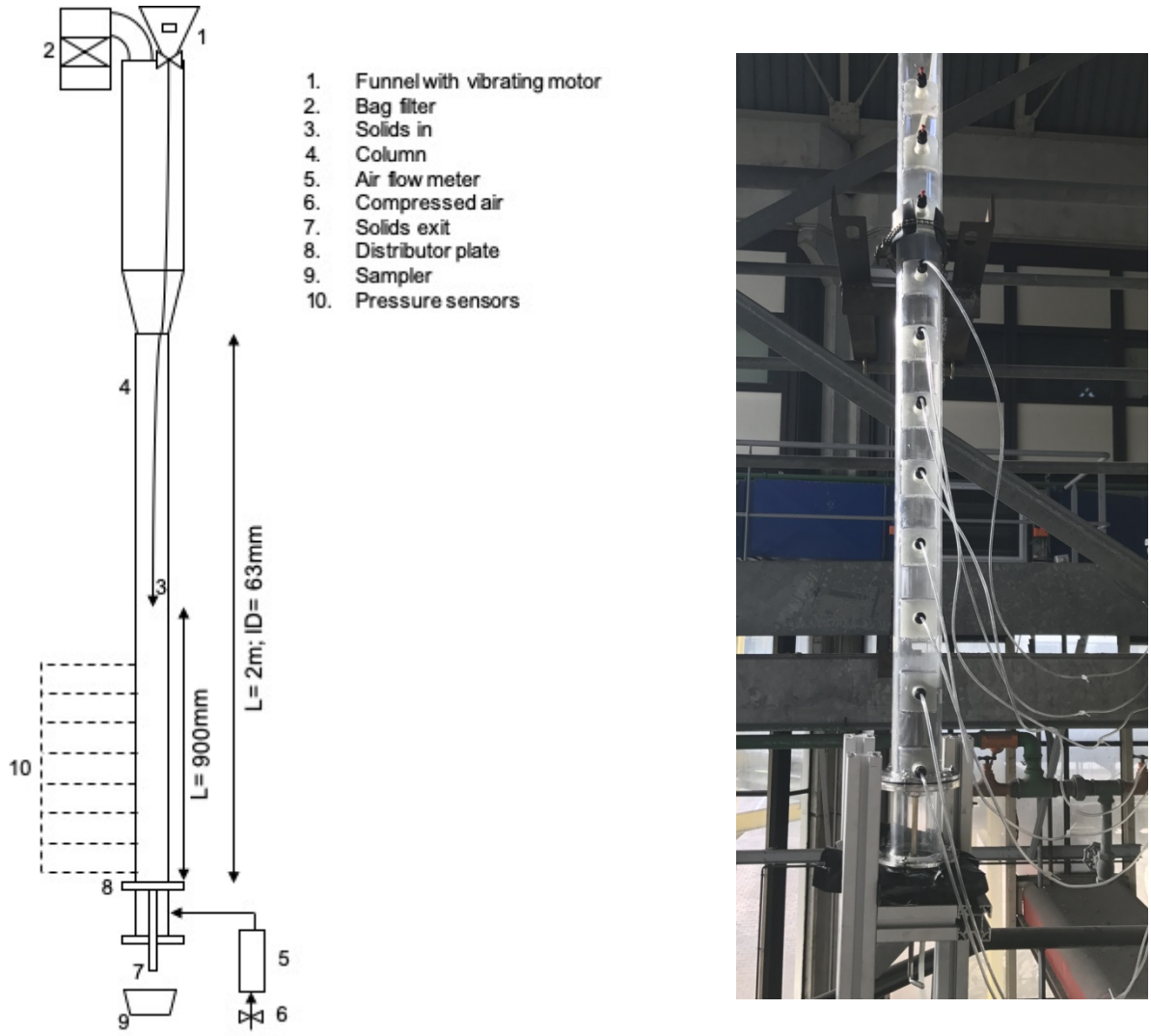

Figure 3.1 : Schematic diagram and photograph of the experimental setup used in the present study.

Solid particles are first injected from top of the fluidized bed column using solid feeding system. Then, the particles in the fluidized bed column obtain momentum from the air passing through the gas distributor made of perforated plate and are fluidizing along the column. At the top of the fluidized bed, particles and gas are separated by bag filter. Eight pressure sensors are installed along the fluidized bed column to measure the pressure fluctuations during the experiments. In order to adjust the operating conditions, an acquisition system is also used. By regulating the solid exit diameter, the solids holdup can be maintained at the desired level during each experiment.

3.3 Detailed description of the experimental setup

3.3.1 Solid feeding system

The solid feeding system used in the present study is the same as that used in section 2.8 (Methodology validation). It is composed of a funnel, a vibrating motor, a valve and a soft tube. The feeding system is located at the top of the fluidized bed where the SiC and pigment particles are fed. The solid feeding system is pictured in Figure 3.2. By adjusting the valve installed in the vibrating solids feeder, various solids mass flow rates can be achieved to provide different solids holdups in the fluidized bed.

Figure 3.2 : Schematic of the solid feeding system.

3.3.2 Pressure sensors

To obtain pressure profile along the fluidized bed column, *8* differential pressure sensors from AMSYS (AMSYS AMS 4711-0050-D) are installed. Excitation voltage required for these sensors is *8-36V*, giving a voltage output of *0-5V* over their respective pressure ranges.

One end of the sensor is connected to the fluidized bed column at high pressure and the other end is open to surrounding air. Differential pressure data are acquired with an on-line computer.

Table 3.1 represents a summary of the pressure sensors and their characteristics.

Table 3.1 : Summary of pressure sensors and their characteristics.

PRESSURE SENSOR	PARAMETERS	MEASURING RANGE
AMSYS AMS 4711-0050-D	Pressure type	Differential/relative
	Pressure range	0-50 mbar
	Operating and storage temperature	-25/+85 °C
	Supply voltage range	8-36 V
	Output voltage	0-5 V

3.3.3 Recording device

The acquisition system developed by electronic service at UTC is used in the present study in order to collect the signals and allow the monitoring of the pressure evaluation in the time. For all experiments, signals delivered by pressure sensors are displayed by the computer using a USB connector and processed using fluidization software developed by UTC. The software sampling period is adjustable between *100ms* and *10s*. The acquisition frequency of pressure fluctuation was selected at *1s* and 900 samples were collected for each experimental condition.

3.4 Protocol of experiments

The first tests demonstrated the ability to perform a steady solid flow rate in the system from the hopper to the fluidized bed exit. From a general point of view, the solids flow rates in the fluidized bed have well responded to the tests. Then, experiments were conducted under three different operating conditions in ambient temperature. Experimental protocol consists of the following steps:

- At the beginning, a particle mass was introduced to the system such that the bed height had a height to diameter ratio (*H/D*) between *5* and *7* depending on the experiment.
- The pressure profile was measured using the pressure sensors placed along the fluidized bed column through the experiment. The distance between the pressure sensors is fixed at *10cm*.
- The entrance and exit tubes were opened simultaneously such that the system is maintained in steady state condition. The entrance flow composed of only SiC particles with the mass flow rates between *7.3±0.2* and *8.8±0.2gr/s* depending on the operating conditions.

- The instantaneous injection of tracer was applied at the entrance flow. Once the tracer particles are finished, a solid feeding flow rate composed of only SiC particles is applied by the solid feeding system. The tracer was injected as quickly as possible to obtain as closely as practical a δ-pulse of tracer at the inlet. The injection time of the tracer particles has been measured for each experiment.
- The samples at the exit flow were recovered every *15s* during the first four minutes to record fast processes, and then measuring interval was kept *30* seconds. It took *10-12*minutes from the injection to collect the whole tracer particles.
- All the samples were analyzed in the developed system of concentration measurement in order to obtain experimental RTD. In the concentration measurement system, the pigment particles are activated by the UV-LED light and the light intensity of the pigment particles is detected and converted into voltage signals and the voltage signals are further amplified and fed into a PC (as described in details in Chapter 2). The voltage signal obtained by the probe is then converted into solids concentration using a calibration equation. During the tracer concentration measurement, the whole experimental apparatus is in dark to avoid the interference of the ambient light with the afterglow emitted by the phosphorescent tracer particles.

3.5 Results and discussion

The present section reports experimental data obtained in a *63mm* ID fluidized bed, using SiC particles as bed material and the pigment phosphorescent (Lumilux® Green SN-F50 WS) as tracer particles. The particle RTD curves were determined experimentally in different operating conditions. In order to not perturb the flow by the injection, the amounts of tracer particles are minimized as low as possible (the system of tracer concentration measurement is however able to detect *0,25 wt.%* of the tracer concentration with good precision).

The operating conditions of the experiments are shown in Table 3.2.

Table 3.2: Experimental conditions used in the present study.

Experiment Number	H/D	Solid mass flow rate (gr/s)	U/U_{mf}	SiC total (gr)	Mass of pigment (gr)
1	5	7.3±0.2	5	1423	95
2	7	8.8±0.2	5	1993	132.8
3	5	7.3±0.2	3	1423	95

A reference case (*H/D=5*; $U/U_{mf}=5$) is compared with cases in which one of the operational parameters is changed: increased height to diameter (*H/D=7*) and decrease superficial gas velocity ($U/U_{mf}=3$).

3.5.1 Identification of fluidized bed regions

Experiments were conducted for static pressure profile in the velocity ranging from *2.01* to *3.35cm/s* and height to diameter ratio of *5 to 7*. A classical bubbling fluidized bed regime is then formed immediately above the gas distribution. The positioning of the sensors makes it possible to determine the vertical profile of the pressure of the present setup. Figure 3.3 represents the pressure profile along the bed for the reference case.

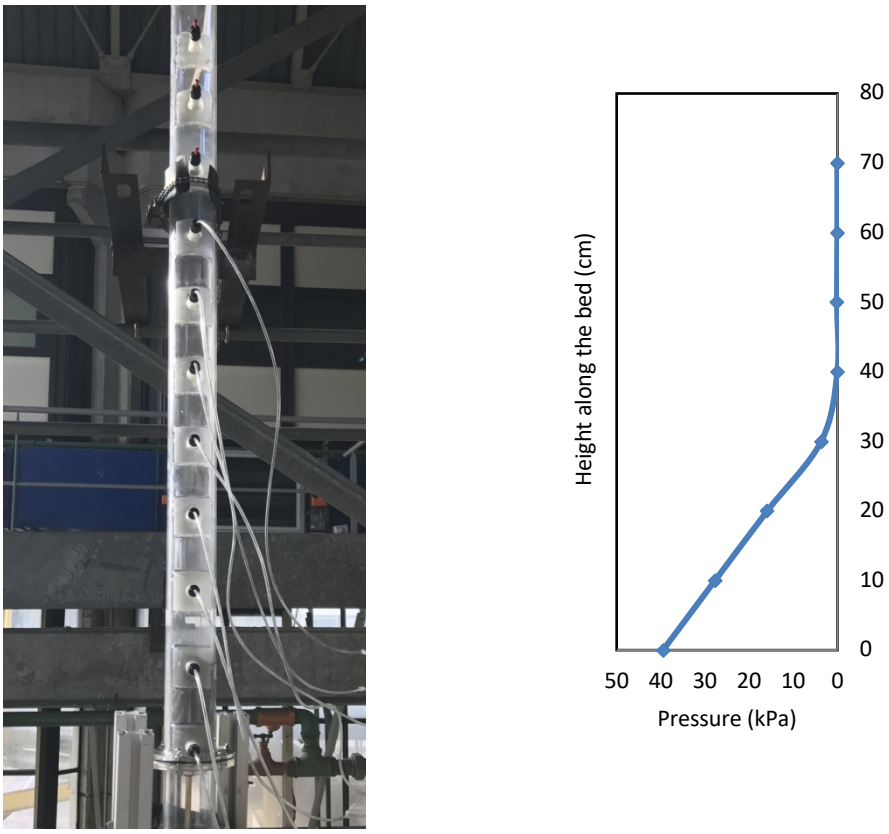

Figure 3.3: Pressure profile of bed for the reference case.

Based on the vertical pressure gradient, a distinct bed surface separating two regions:

- The dense region in the lower part of the bed (Bubbling bed), characterized by a big variation of the pressure gradient.
- The dilute zone in the upper part of the bed (freeboard), characterized by a pressure gradient practically independent from the height.

3.5.2 Particle residence times

The particle residence time distribution was determined by means of the tracer response technique. An approximated Dirac pulse of tracer particles was injected into the fluidized bed at a certain time (*t=0*) and the output signal was detected by the concentration measurement technique described in Chapter 2. The tracer was injected at *90cm* above the distributor plate as fast as possible to obtain as close as a δ-pulse of tracer at the inlet. When the tracer particles are introduced by δ-Dirac pulse into the system at time *t=0*, the recorded concentration *C(t)* describes also the residence time distribution. Before starting the RTD measurement, the pressure drop profile was measured. The injection time of the tracer particles has been also measured for each experiment.

Figure 3.4 shows the concentration curve and F-curve of the phosphor tracer particles changing with time, for the reference case.

The F-curve can be calculated from the experimentally tracer concentration as:

$$F(t) = \int_0^t E(t)dt \qquad (3.1)$$

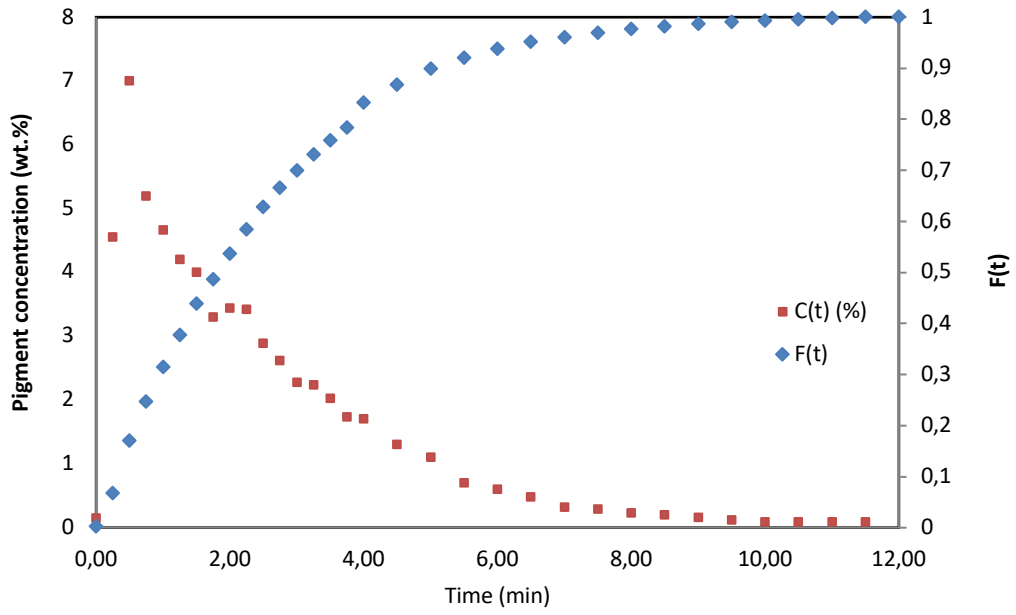

Figure 3.4 : C(t) curve and F(t) curve of the reference case.

The experimental RTD curve obtained (C-curve) indicates a sharp peak and long tail. It can be seen from this curve that 80% (F(t)) of the particles spend 4 minutes or less in the bed, and 20% of the particles spend more longer than 4 minutes in the bed.

Figure 3.5 also compares the F(t) curves for ideal CSTR reactor with the reference case. The results show that the F curve increases faster than that for perfect operation which could indicate the

presence of dead volume in the deep fluidized bed. Consequently, the particles pass through the fluidized bed column with the dead volume more quickly than that of perfect operation because there is smaller effective volume.

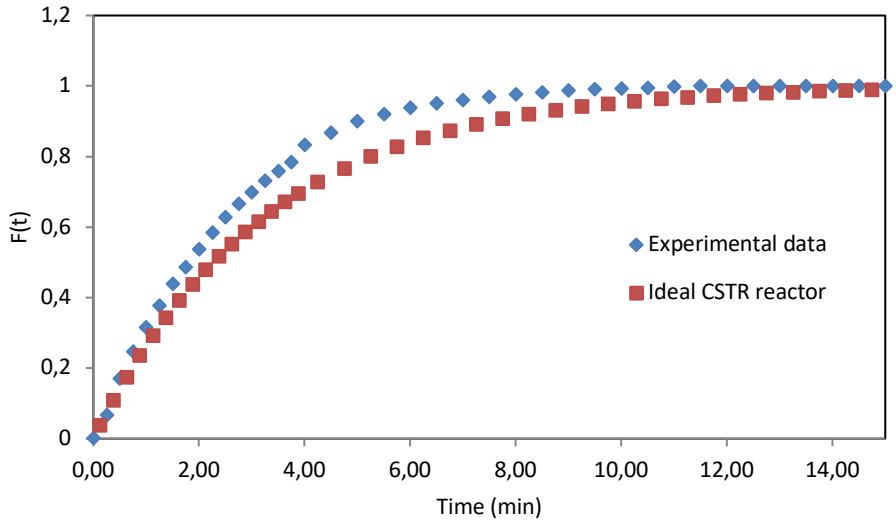

Figure 3.5: Comparison of F(t) curves for CSTR under perfect operation and experimental data.

Smolders and Baeyens [15] measured the residence time distribution in CFB reactor at different working conditions. They proposed that the injection time cannot be neglected and considered a block-function for the tracer injection. The injection was modeled as a block-function in the data treatment. Figure 3.6 shows the convolution principle of block-formed injection and system.

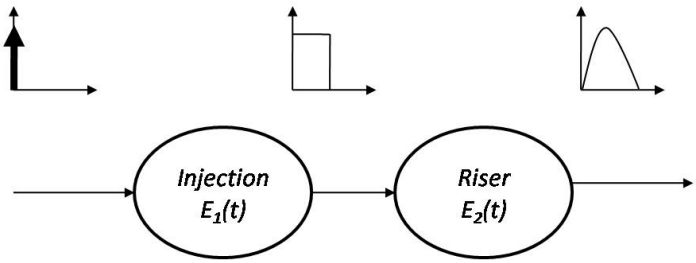

Figure 3.6: Principle of block-formed injection and riser system [15].

In addition, the global residence time of the bed is equal to the sum of the average residence time of the injection and the bed [46]:

$$E(t) = \int_0^t E_1(t^*)E_2(t - t^*)\, dt^* \qquad (3.\ 2)$$

where, E_1 is the RTD of the block-injection (dimensionless), E_2 is the RTD of the bed (dimensionless) and t^* is the dimensionless time. The residence time distribution of the block-function is [15]:

$$E_1(t) = \begin{cases} \dfrac{1}{2t_1}, & t < 2t_1 \\ 0, & t \gg 2t_1 \end{cases} \qquad (3.\ 3)$$

with t_1 equal to half the injection time.

Consequently, the average residence time for the bed is:

$$t_{m,bed} = t_m - \frac{t_{inj}}{2} \qquad (3.\ 4)$$

In this equation, t_{inj} is the injection time and t_m is the average residence time of the injection and the bed.

3.5.2.1 Effect of superficial gas velocity and solids inventory on RTD

The study of the fluidization flow rate effects on the particle residence time distribution is performed under the reference test case operating conditions and by varying the fluidization flow rate between *4* and *7.5lit/min*.

It is clear that U_g has an important effect on the maximum peak height, spread and general shape of the RTD depending on the increase of U_g. Increasing the superficial gas velocity decreases both the mean residence time (t_m) and the variance (σ^2) of the distribution (See Table 3.3). At the very high value of U_g, the RTD curve will be narrow and without a significant tail.

The solids axial mixing can be characterized by the profile of the RTD curve. Figure 3.4 shows that the RTD curves are composed of a single wave and a long tail. The width of the curves has a direct relation with the axial mixing of solids. The narrow peak of the RTD curve indicates that the mixing of the dispersed particles does not agglomerate.

The mean residence time (t_m) and the variance (σ^2) of data were calculated as follow:

$$t_m = \int_0^\infty tE(t)dt \qquad (3.\ 5)$$

(3. 6)

$$\sigma^2 = \int_0^\infty (t - t_m)^2 E(t) dt$$

Table 3.3: Effect of superficial gas velocity on the mean residence time and variance.

Experiment number	**U/U_{mf}**	**Mean residence time (t_m) (min)**	**Variance (σ^2) (min^2)**
3	3	2.76	2.15
1	5	2.64	2.07

The effect of the superficial gas velocity, U_g, and solids inventory are illustrated in Figure 3.7.

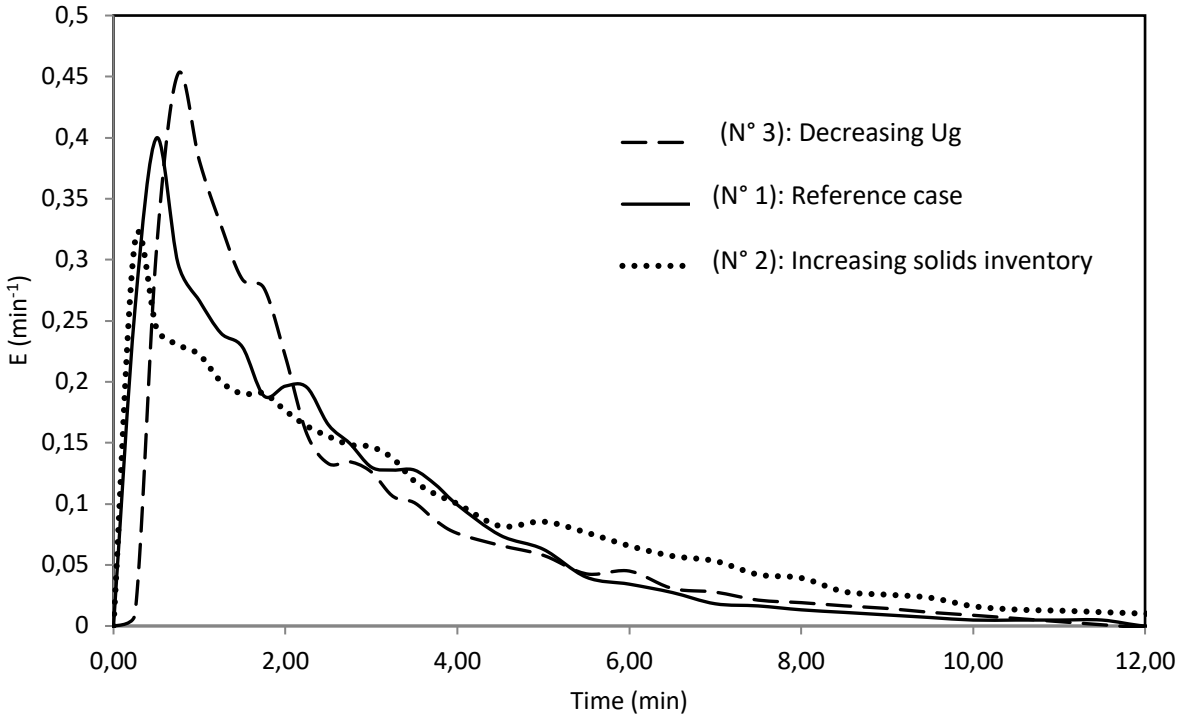

Figure 3.7 : Effect of solid inventory and superficial gas velocity on the RTD.

Figure 3.7 also shows the influence of the solids inventory on the global RTD. Two main variables are increased during the experiment: mass flow rate and the solids inventory which is proportional to the pressure difference in the bed. These two variables are directly related to the residence time distribution according to the equation below:

$$C(t) = \int_0^t C_0(t^*)E(t-t^*)\,dt^* \;\; or \;\; C(t) = E \times C_0 \qquad (3.\,7)$$

It was expected that with increasing of the solids inventory, both the mean residence time and the variance of the distribution increase therefore a more homogeneous distribution is reached. In contrast, increasing the mass flow rate decreases the mean residence time and the variance. In this case, the RTD data could not provide the correct comparison between two solids inventories while changing two factors having opposite effects on RTD.

3.5.2.2 Characteristics of the residence time distribution

As mentioned in Chapter2, the best manner of comparing RTDs is by using their moments (Equation (3. 5) and (3. 6)), instead of trying to compare the entire distribution. There are also combinations of moments (C_V) that are generally used to show the probability distributions. The coefficient of variation defined as [19]:

$$C_V = \frac{\sigma}{t_m} \qquad (3.\,8)$$

represents the ratio of the standard deviation to the mean residence time and provides a measure of the relative variation or diffusion of a distribution [21].

The results from the experiments are summarized in Table 3.4. Figure 3.8 also provides the parity plot comparing the mean residence time from RTD moments, t_m, and theoretical mean residence time, τ, presented in Table 3.4.

Table 3.4: influence of the operating conditions on the mean residence time and variance.

Experiment number	Height to diameter (H/D)	U/U_{mf}	Mean residence time (min)		*Variance* (σ^2)	C_V
			Experimental	*Time of passage*		
1	5	5	2.64± 0.1	3.2 ± 0.1	4.29	0.78
2	7	5	3.17± 0.1	3.8 ± 0.1	6.91	0.82
3	5	3	2.76± 0.1	3.2 ± 0.1	4.66	0.78

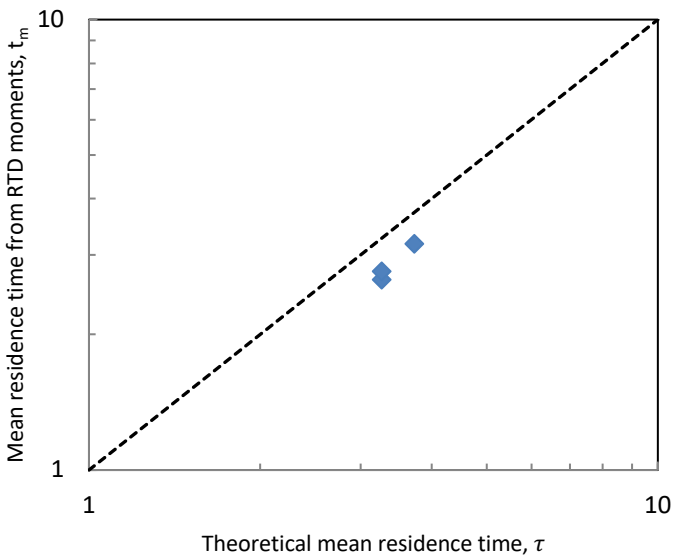

Figure 3.8: Parity plot comparing the mean residence time, t_m, calculated from the moments of the RTD, with the theoretical mean residence time, τ.

As shown in Table 3.4, the mean residence times calculated from RTD data were found lower than from the theoretical mean residence times. This could be related to the formation of dead regions at some locations inside the bed which was also be observed in Figure 3.5.
The "dead-volume tail" is a phenomenon caused by the angles and corners in the reactor, where fluidization can locally be deficient [74]. This effect slightly reduces the effective volume of the bed. The long tails observed in RTD curves also indicate the presence of dead zone inside the reactor.

The measured pigment detected by PMT was also compared with the introduced pigment for different operating conditions (See Table 3.5).

Table 3.5: Introduced pigment and measured pigment.

Number	Height to diameter (H/D)	U/U_{mf}	Introduced pigment (gr)	Measured pigment (gr)
1	5	5	95	87.4
2	7	5	132.8	127.6
3	5	3	95	79.4

The difference between detected pigment and injected pigment can be caused by:

- Pigment particles exiting from top of the bed,
- Changing the mass flow rate in the bed outlet overtime,
- Measuring only twenty grams of samples according to the calibration method.

3.6 Conclusion

In the present study, the novel concentration measurement technique described in Chapter 2 has been shown to be suitable for measuring the particle residence time distribution in a real and deep fluidized bed. The principle of this technique is measuring the intensities of tracer particles which excited by the UV-LED light. The pigment particles (Lumilux® Green SN-F50 WS) and SiC particles (Silicon Carbide) were used as a tracer and bulk particles respectively. The influence of the fluidization velocity and solids inventory on residence time distribution was analyzed based on a number of diagrams.

The following conclusions can be drawn based on the results obtained in this study:

- Experiments were conducted to determine the influence of the superficial gas velocity and height to diameter ratio (H/D) upon the particle RTD. The RTD curves demonstrated that the tracer particles are already detected shortly after its injection (*t=0*) even at low superficial gas velocity.
- An increase in the superficial gas velocity leads to a reduction in the mean residence time. This result is expected; the superficial gas velocity in the bed is closely related to the average particle velocity. An increase in average particle velocity corresponds to a decrease in the mean residence time.
- The RTD data obtained from the solids inventory effect cannot provide the correct comparison between two solids inventories while changing the mass flow rate and superficial gas velocity during the experiment.
- The mean residence time calculated from RTD data was found lower than from the theoretical mean residence time which could be related to the formation of dead regions in the bed.

Chapter 4

Model development

4.1 Introduction

The present chapter is focused on modeling of particle residence time distribution in the experimental setup used in Chapter 3. Two different methods are actually available: the powerful but complex computational fluid dynamics (CFD) simulation and the simple phenomenological structural models. In order to carry out CFD simulation in gas-solid contactors, some complex phenomena such as particular bubbles break up or coalescence is required. Considering this point, new approach was proposed as follow for particle residence time modeling: the reactor is modeled as a reactor assembling a combination of region with ideal reactor such as plug flow reactor (PFR) and perfect mixed reactor (CSTR). This method has some advantages, such as handy and giving fast answers.

The following features are listed to have a simple and reliable RTD model:

- The model should be able to reflect real feature of the flow characteristics which is observed in the studied system.
- The model should be as simple as possible.
- The model should contain as few parameters as possible.
- The intricacy of the mathematical unit involved in determination of model parameters should be rationally as simple as possible.

It is very important to avoid model with unnecessary complexity. By using the complex models, additional parameters are inevitably introduced in the model that one is forced to have high resolution data. The objective of the present chapter is to propose a methodology based on the combination of ideal reactors. The parameters in the model are chosen so as to obtain the closest possible agreement between the model predictions and experimental data presented in Chapter 3.

4.2 Theoretical aspects

4.2.1 Choice of model

To describe the flow pattern in solids unit operations two types of models are usually employed. These models are based on the experimental results obtained by an impulse injection of tracer. In the first time, the primary analysis of velocity profile may be giving us the RTD values. In the second approach, the main features of the physical flow pattern are used to build a conceptual flow model.

In this approach the combination of plug flow reactor (PFR), continuous stirred tank reactor (CSTR), Tanks-in-series (TIS), CSTRs with a dead volume, laminar pipe flow are usually used [82].

A fluidized bed is generally modeled as tank in series model or combination of ideal plug flow and stirred tank reactors because the good mixing of solids [125]. Tank in series model (TIS) or combination of ideal plug flow and stirred tank reactors model consist of a combination of ideal reactor models which the residence time distribution functions are known. Another advantage of this model is that ability takes into account of the chemical reactions more easily.

From these considerations, this type of modeling with simple ideal reactors has been chosen in the present study due to their flexibility and good results reported in the literatures [6], [31], [126]. In order to establish a good model fitting, input the measurement of residence time distribution is required. Therefore, the simulated output is then compared with the experimental output obtained in Chapter 3.

4.2.2 Modeling real reactors with combinations of ideal reactors

In some fluidized bed reactors, there is highly agitated zone that can be modeled as a perfectly mixed CSTR. Particles may follow some labyrinthine path after or before the perfectly mixed zone. These labyrinthine paths can be modeled as a plug flow reactor. Therefore, it can be considered that this type of tank reactor could be modeled as a CSTR in series with a plug flow reactor [34].

From Kunii and Levenspiel [86], a model describing the residence time distribution in a single continuous stirred tank reactor and single plug flow reactor are provided as:

$$E(t) = \frac{1}{\tau} e^{-t/\tau} \quad for\ CSTR \tag{4. 1}$$

$$E(t) = \delta(t - \tau) \quad for\ PFR \tag{4. 2}$$

For the CSTR followed by the PFR (Figure 4.1), the mean residence time in the CSTR is noted by τ_s and the mean residence time in the PFR by τ_p. The concentration of the CSTR output as a function of time for a pulse of tracer injected into the entrance of the CSTR can be calculated as follow:

$$C = C_0 e^{-t/\tau_s} \tag{4. 3}$$

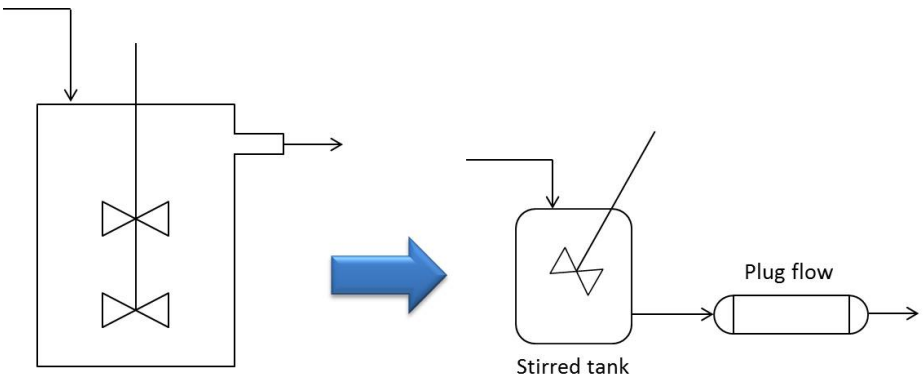

Figure 4.1: Real reactor modeled using a CSTR and PFR in series.

The output concentration decays by a time τ_p at the exit of the plug-flow section of the system (CSTR and PFR in series). Therefore, the mean residence time distribution of the system can be obtained by the following equation [34]:

$$E(t) = \begin{cases} 0 & t < \tau_p \\ \dfrac{e^{-(\frac{t-\tau_p}{\tau_s})}}{\tau_s}, & t \geq \tau_p \end{cases} \qquad (4.4)$$

Fogler [125] and Levenspiel [46] show that the sum of the mean residence time for the PFR and CSTR in series reactors is independent of the reactor arrangement. The RTD results for the CSTR in series with PFR or PFR in series with CSTR are the same.

4.3 Modeling

Figure 4.2 shows the concentration curve of the phosphorescent tracer particles obtained for the reference case (*H/D=5, U/U$_{mf}$=5*). *C*-curve displays a single peak with a long tail, which indicates that there might be backward flux or dead zones at some locations inside the bed.

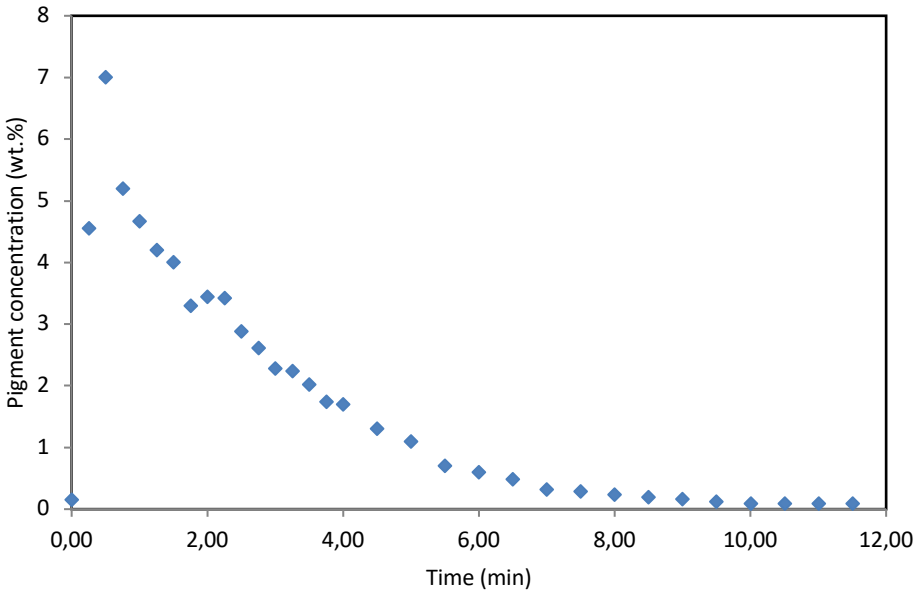

Figure 4.2: C(t) curve of the reference case (*H/D=5, U/U$_{mf}$=5*).

As shown in Figure 4.2, the shape of this curve suggests that the assumption of a "perfect solid mixing behavior (ideal CSTR)" is not quite correct for this case. There are various alternatives to explain what

is really happening in this situation. A real fluidized bed might be modeled by different combination of ideal reactors. Two types of ideal reactors are usually used: the PFR or the CSTR reactors. By comparing the *E(t)* experimental curves for the actual fluidized bed with the theoretical curves for the different combinations of ideal reactors, the best model can be found.

The first data point in Figure 4.2 is a zero-concentration value which can be modeled as a PFR reactor or maybe a large number of tanks in series. After this initial point, there is intensive mixing zone in the fluidized bed, which can be modeled as a CSTR reactor.

The intensive mixing zone followed by a tail indicating the part that has been back-mixed in the bed and it is detected with some delay. The long tail profile can also be modeled by a dead zone volume. It must be noted that the dead zone fraction represents the degree of non-idealness of the continuous flow system [79],[82].

According to Levenspiel [46], this dead volume can be attributed to the plug flow reactor or the CSTR reactor. Figure 4.3 shows the diagram of the experimental apparatus and the observed flow regions. In order to reduce the number of parameters in the model, the mixing occurs in the plug flow region is cumulated with mixed region (CSTR).

In a similar way, all plug flow regions can be cumulated in a single bigger plug flow reactor [46]. Consequently, the studied fluidized bed may be modeled as a PFR with dead volume in series with a CSTR. Figure 4.4 illustrates the schematic of the conceptual flow pattern.

The mean residence time can be written as:

$$\tau = \frac{V}{v} = \frac{V_p}{v} + \frac{V_s}{v} + \frac{V_d}{v} = \tau_p + \tau_s + \tau_d \qquad (4.\ 5)$$

where, v is the volumetric flow rate and *V* is the volume of the bed.

Since dead volume does not participate in the residence time distribution, one can write from a material balance of active volume of the bed:

$$v.C_{out}(t) = v.C_{in}(t).E_1(t).E_2(t) \qquad (4.\ 6)$$

The Laplace transform of equation (4. 6) is:

$$C_{out}(s) = C_{in}(s).E_1(s).E_2(s) \qquad (4.\ 7)$$

or

$$\frac{C_{out}(s)}{C_{in}(s)} = E_1(s).E_2(s) \qquad (4.\ 8)$$

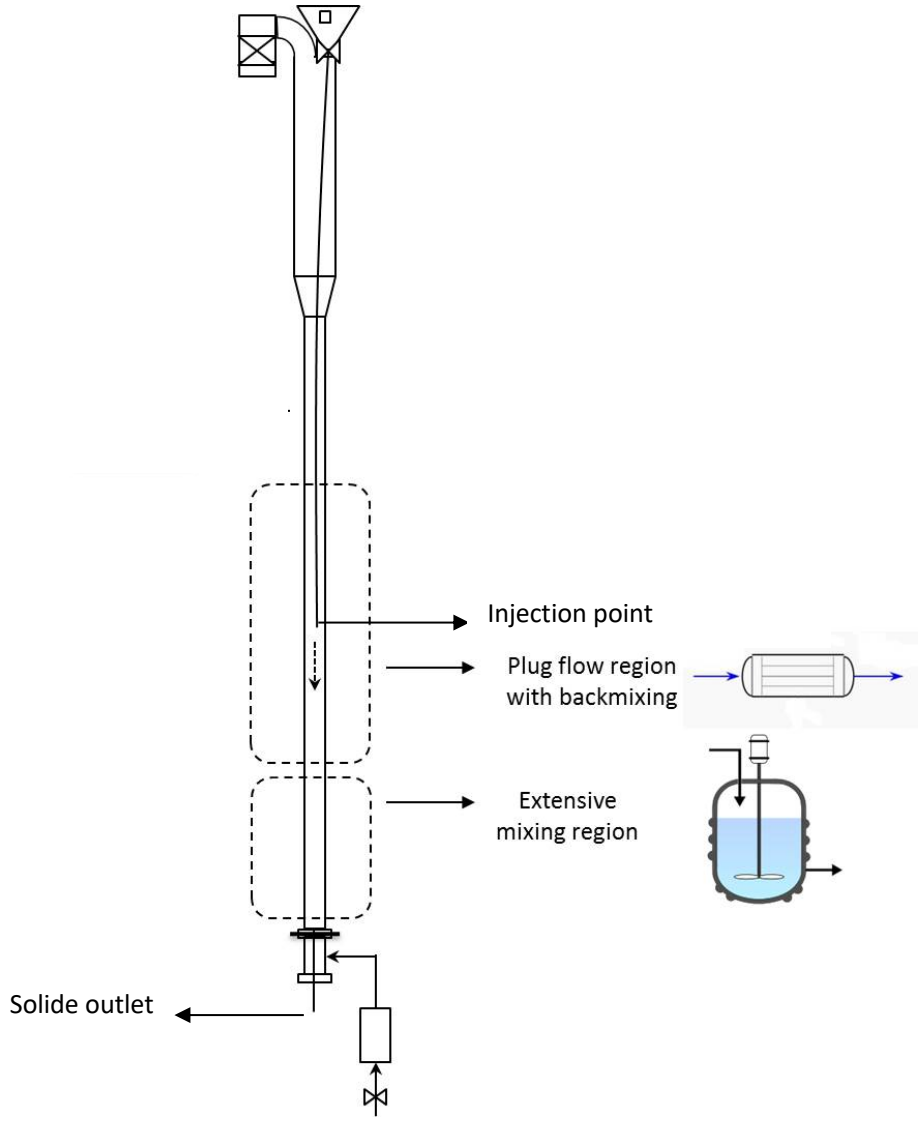

Figure 4.3 : Observed flow regions.

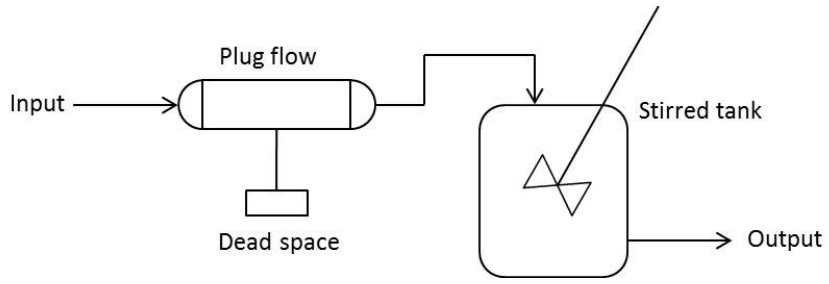

Figure 4.4: Flow diagram of CSTR cross-flowing with a dead volume in series with a plug flow reactor.

It can be shown that:

$$E_1(s) = -e^{s\tau_p} \tag{4. 9}$$

In a similar way:

$$E_2(s) = \frac{\frac{1}{\tau_s}}{s + \frac{1}{\tau_s}} \tag{4. 10}$$

The equation (4. 6) can be rewritten as:

$$\frac{C_{out}(s)}{C_{in}(s)} = \frac{1}{\tau_s}\left(\frac{-e^{s\tau_p}}{s + \frac{1}{\tau_s}}\right) \tag{4. 11}$$

The model equation is obtained after taking the inverse of the Laplace:

$$E(t) = \frac{C_{out}(t)}{C_{in}(t)} = \frac{e^{-\left(\frac{t-\tau_p}{\tau_s}\right)}}{\tau_s} \tag{4. 12}$$

When there are not dead zones in the system Equation (4. 5) reduces to:

$$\tau = \tau_p + \tau_s \tag{4. 13}$$

This is often the case when a powerful mix is provided [127]. This relation is based on the assumption that there is no influence of the dead zone on the mean residence time.

For this condition, it can be shown that:

$$E(t) = \begin{cases} 0 & t < \tau_p \\ \dfrac{e^{-\left(\frac{t-\tau_p}{\tau_s}\right)}}{\tau_s}, & t \geq \tau_p \end{cases} \tag{4. 14}$$

where, τ_p and τ_s represent the mean residence time of the plug flow and the ideal CSTR respectively.

The model parameters and the mean residence time in each reactor are determined by fitting the model with the experimental results. If the accordance is close enough, then the model is acceptable. To adapt the above discussed model to the experimentally measured RTD curves, the least squares curve-fitting technique is used. The fitting quality was studied by choosing the model parameters to minimize the sum of the squares of the differences between the data and model. This is known as root mean square (RMS) value. The model parameters values corresponding to the minimum RMS value are selected as the optimal set of parameters [128]. Thus:

$$RMS = \int_0^\infty [E(t) - E_m(t, parameters)]^2 \, dt = Minimum \qquad (4.\ 15)$$

In this equation E_m is the residence time distribution of model.

4.4 Results and discussion

In section 4.3, a model presented which describes the experimental situations depicted in Chapter 3. Visual observation of the apparatus obviously shows that the total volume of the bed contains of three different regions:

- Mixing region where particles are mixed together in the bed,
- Moving region where particles flow in the form of moving bed with negligible mixing,
- Dead zone where there is apparent no flow.

The *E(t)* equations for plug flow and mixed flow compartment give the *E(t)* equation (equation (4. 14)) that is used to represent the experimental data. The dead volume is an inactive volume of the bed. Therefore, it is not present in the overall residence time except for the shift in the observed mean residence time. The same analysis is also done in the work of Arriola [127].

The results of RTD simulation are given in Table 4.1. Apart from the proposed model, two model parameters τ_s and τ_p were obtained.

Table 4.1: Results of RTD analysis.

Run No.	Bed height (cm)	U/U_{mf}	Mass flow rate (gr/s)	Time of passage (min)	Experimental mean residence time (min)	Model predicted mean residence time (min)	τ_p (min)	τ_s (min)	$\frac{\tau_s}{\tau_p}$	Relative error%
1	31.5	5	7.3±0.2	3.2 ± 0.1	2.64±0.1	2.77	0.27	2.5	9.2	4.57
2	44	5	8.8±0.2	3.8 ± 0.1	3.17±0.1	3.43	0.26	3.17	12.2	7.55
3	31.5	3	7.3±0.2	3.2 ± 0.1	2.76±0.1	2.81	0.6	2.21	3.6	1.6

The representative comparison of experimental and model simulated RTD curves are shown in Figure 4.5.

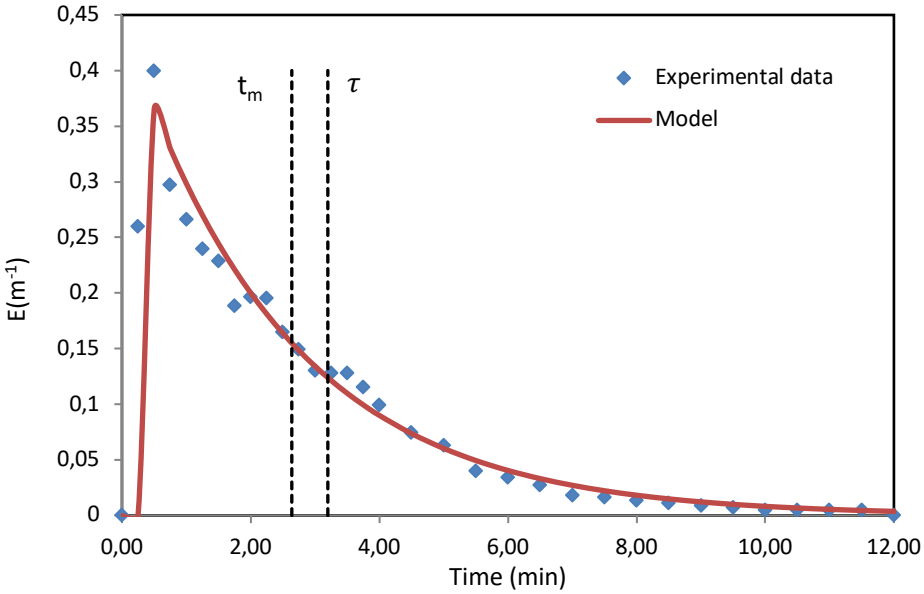

(a)

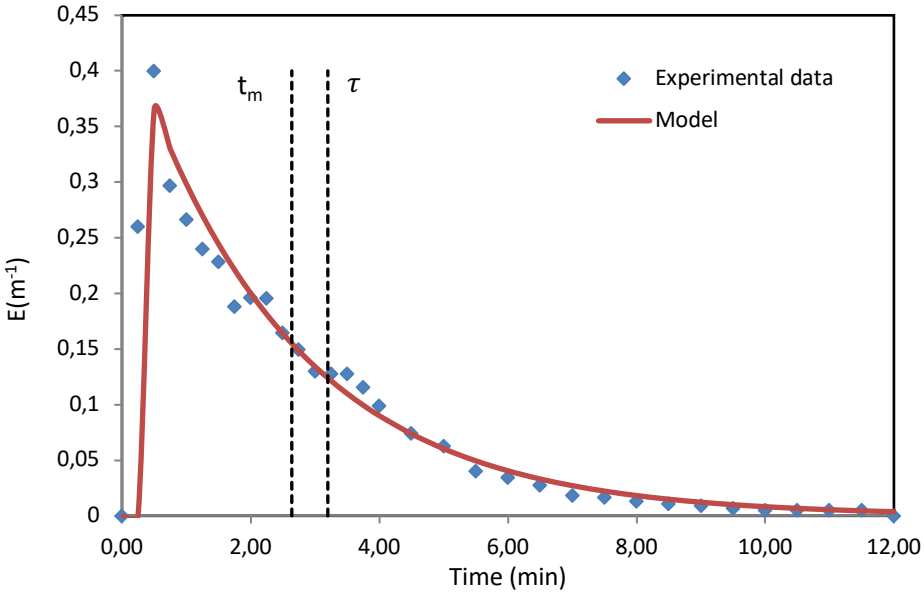

(b)

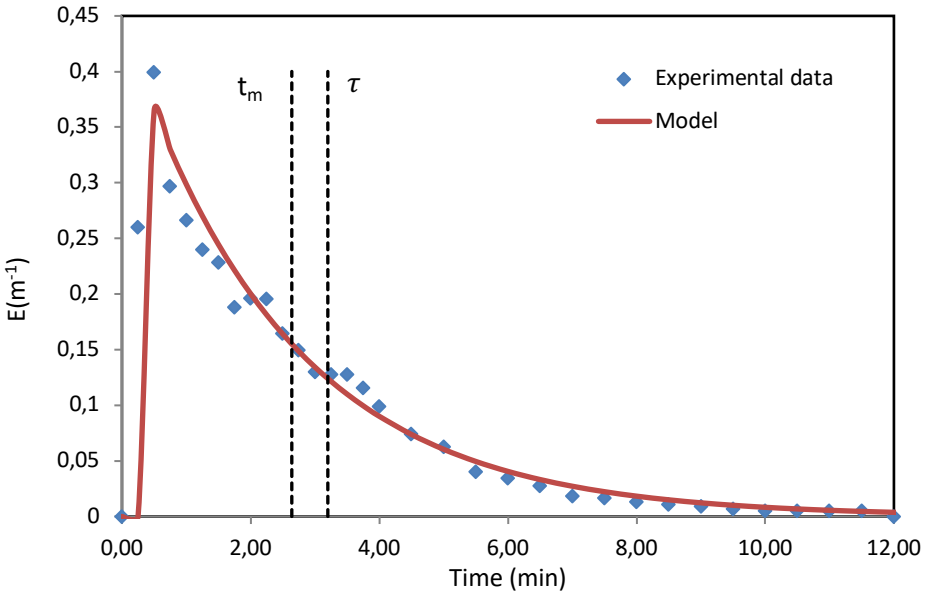

(c)

Figure 4.5: Experimental and model predicted RTD curves: a) reference case (H/D=5, U/U_{mf}=5); b) H/D=7, U/U_{mf}=5, c) H/D=5, U/U_{mf}=3.

Table 4.2 and the plotted data in Figure 4.5 illustrate that for constant time of passage (*3.2±0.1 min*), with increasing the superficial gas velocity the mixing behavior (τ_s/τ) was increased. From Kunii and Levenspiel [86], the mixing behavior and the plug flow behavior have the opposite direction. Consequently, for constant time of passage (*3.2±0.1 min*) an increase in superficial gas velocity decreases the plug flow behavior of the bed (τ_p/τ).

Table 4.2 : predicted mixing behavior and plug flow behavior from the proposed model.

Run No.	$\frac{\tau_p}{\tau}$	$\frac{\tau_s}{\tau}$	$\frac{\tau_s}{\tau_p}$
1	0.08	0.76	9.2
2	0.06	0.85	12.2
3	0.18	0.67	3.6

From the analysis of Table 4.2, the value of τ_s/τ_p is increased with increasing the solids inventory. Consequently, it is possible to conclude that the solids mixing in the bed increases with increasing the solids inventory even with increasing the mass flow rate.

Figure 4.6 also provides the parity plot comparing the predicted mean residence time from the proposed model and the experimental mean residence time for the deep fluidized bed. It could be concluded from this figure that the data points obtained based on the model are distributed uniformly

around and close to the parity line. This shows that there is a good agreement between the proposed model prediction and experimental data.

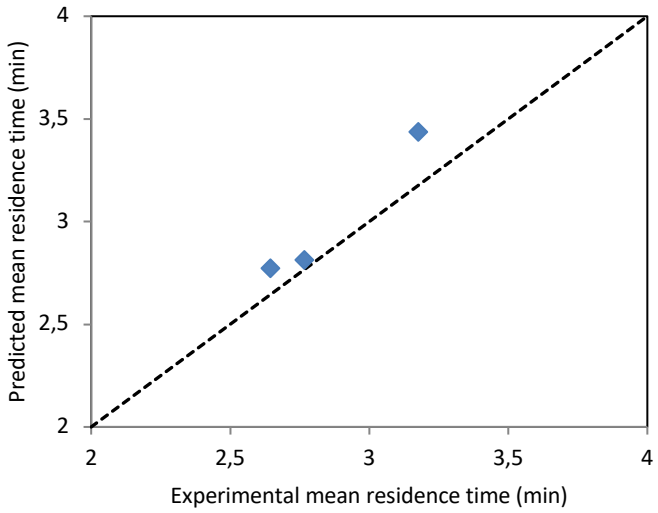

Figure 4.6: Parity plot comparing the experimental mean residence time and predicted mean residence time for the deep fluidized bed.

Tank-in-series (TIS) model:

In the present study, the tank in series (TIS) model as a one commonly used model was also considered for the comparison. To model the reactor as a series of identically sized CSTRs (tank-in-series), a single parameter model was assumed and the number of the identical CSTR in series, *N*, was evaluated. In the present study, the number of ideal tanks in series (*N*) obtained from tracer response curves:

$$N = \frac{t_m^2}{\sigma^2} \qquad (4.16)$$

where, t_m is the experimental mean residence time and σ^2 is the variance.

If the number of reactors, *N*, turns out to be small, the reactor characteristics turn out to be a single CSTR or two CSTRs in series. At the other side, when *N* turn out to be large, the reactor characteristics approach a plug flow reactor.

The assumptions made with this model include:

- There is no backflow of material in the apparatus
- The *N* stirred tanks are considered of same size.

Table 4.3 shows the values of *N* obtained for various operating conditions.

Table 4.3: The number of CSTR obtained from the experimental data.

Run No.	U/U_{mf}	Bed height (cm)	Mass flow rate (gr/s)	Experimental mean residence time (min)	Variance σ^2 (min^2)	N
1	5	31.5	7.3±0.2	2.64±0.1	4.29	1.62
2	5	44	8.8±0.2	3.17±0.1	6.91	1.46
3	3	31.5	7.3±0.2	2.76±0.1	4.66	1.64

E-function can be calculated by the following equation [86]:

$$E(t) = \frac{1}{(N-1)!\,\tau_i}\left(\frac{t}{\tau_i}\right)^{N-1}.e^{-t/\tau_i} \qquad (4.\ 17)$$

where, τ_i, is the mean residence time in each stage given by:

$$\tau_i = \frac{t_m}{N} \qquad (4.\ 18)$$

The representative comparison of experimental and two models simulated RTD curves are shown in Figure 4.7.

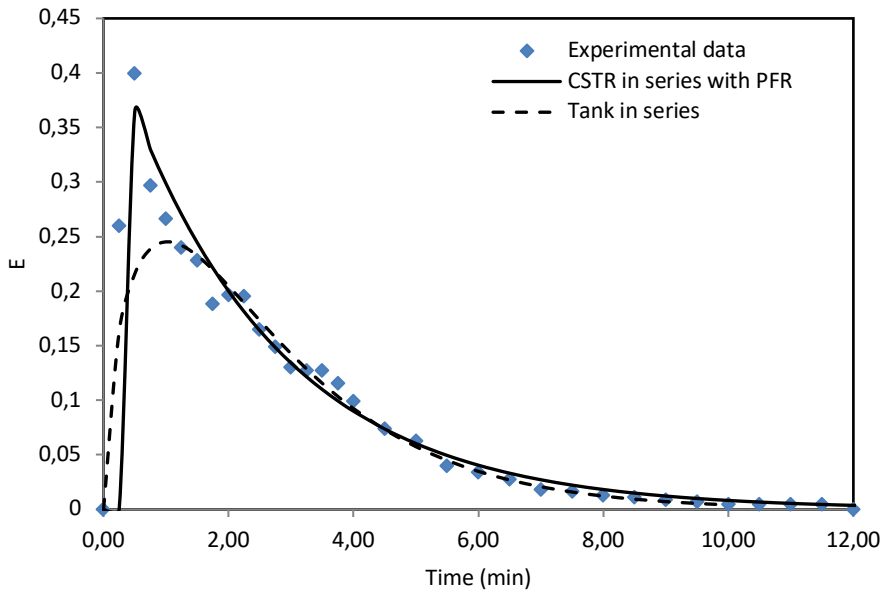

(a)

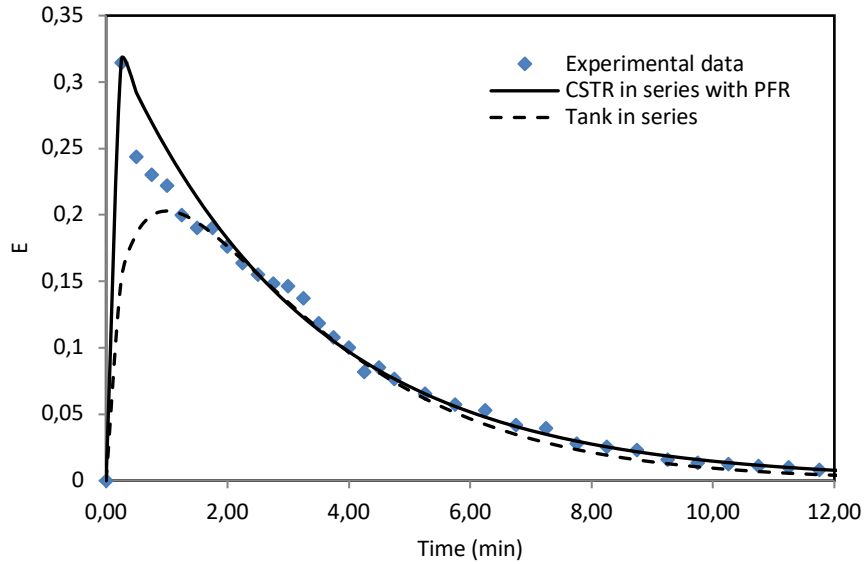

(b)

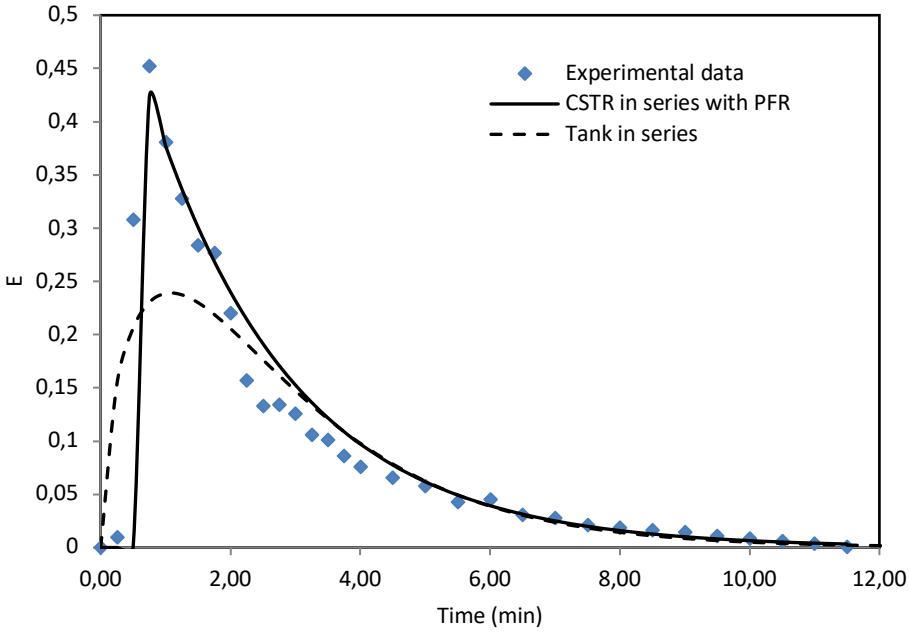

(c)

Figure 4.7: The comparison between two different model predictions (the Tank-in-series model and CSTR in series with PFR) and the experimental of the RTD curves: a) reference case (H/D=5, U/U_{mf}=5); b) H/D=7, U/U_{mf}=5, c) H/D=5, U/U_{mf}=3.

Figure 4.7 presents the comparison of the residence time distribution function, *E(t)*, between two different model predictions and experimental results. It has been observed that the "CSTR in series with PFR" model prediction generally give good agreement with the experimental results. The deep fluidized bed behavior is strongly close to the "CSTR in series with PFR" model [9]. It should be noted

that there is a recirculation of the solids in the bed which can be at the origin of the observed differences between the "Tank in series" model and the experimental results.

Table 4.4 provides the predicted mean residence time values for the "Tank-in-series" model and "CSTR in series with PFR" model comparing with the experimental mean residence time. The errors in the "CSTR in series with PFR" model is small (*4.5%* in average) whereas in the "Tank-in-series" model are highly larger (*13%* in average).

Table 4.4: Predicted mean residence time for two models (TIS model and CSTR in series with PFR model).

Run No.	Experimental mean residence time (min)	Predicted mean residence time (min)	
		Tank-in-series model	CSTR in series with PFR model
1	2.64	2.34	2.77
2	3.17	2.76	3.43
3	2.76	2.49	2.81

4.5 Conclusion

A technique for determination of solids residence time distribution has been successfully developed and described in Chapter 2. Two models using ideal reactors (plug flow reactor and CSTR reactor) have been presented (Tank-in-series model and CSTR in series with PFR model) that describe the residence time distribution of particles in a deep fluidized bed.

The following conclusions can be drawn based on results obtained in this study:

- A model consisting of a continuous stirred tank reactor in series with a plug flow reactor cross-following with a dead volume fitted well with the experimental data.
- The experimental mean residence times are in good agreement with the mean residence times predicted by the "CSTR in series with PFR" model. The average errors were calculated 4.5% and 13% for "CSTR in series with PFR" and "Tank-in-series" model respectively.
- The analysis showed that for constant mass flow rate, an increase of the superficial gas velocity causes an increase in mixing behavior (τ_s/τ).
- The CSTR fraction in the bed predicted by the "CSTR in series" model varied from 67% to 85% depending on the operating conditions. The maximum and minimum CSTR fractions were found for run no.2 (*H/D=7; U/U_{mf}=5*) and run no.3 (*H/D=5; U/U_{mf}=3*) respectively.
- In the present study, based on the experimental data, it has been also observed that the predicted value of τ_s/τ_p is increased with increasing the solids inventory. This study

emphasized the importance of the solids inventory as a critical parameter for the experimental RTD studies in the evaluation of the mixing in a flow system.

Conclusions and Recommendations

Overall conclusions

In the present study, a comprehensive investigation was conducted on hydrodynamics and particle residence time distribution determination in solid unit operations as well as model development.

This thesis can be divided into three major parts:

- Development of the novel concentration measurement technique
- Particle residence time distribution measurement in a deep fluidized bed
- Model development.

In the first part, the novel concentration measurement technique was developed based on the optical method. This technique enables RTD studies to be carried out with high accuracy in solid unit operations especially with long residence time.

Experiments were carried out with two powders, Silicon Carbide (SiC) as a bulk solid and the pigment phosphorescent (Lumilux® Green SN-F50 WS; median diameter of 70.4 µm) as tracer particles. SiC was selected due to its mechanical resistance to attrition and volumetric heat capacity that is essential in wide range applications where it is used as a heat carrier. The tracer particle (Lumilux® Green SN-F50 WS) was also chosen to have similar physical properties to the SiC particles.

The calibration procedure was conducted in an especially designed system with two transparent sections for activation of the tracer particles and detection of their intensities. With the addition of the LED-UV spot light source which fits around the maximum of the excitation spectrum of the phosphorescent tracer, the optical filter for eliminating the wavelength of the UV light detection, and using the high sensibility of the photomultiplier, the measurement sensibility was improved. The high sensibility of measurement allows the high precision detection of the pigment emission light. From the calibration results, a linear relationship between the integral of the detected intensities and pigment concentration was found and was proven to be reliable.

Since, the low consumption of the tracer particles in the experiments is desired; the measurements were carried out with high sensibility of the photomultiplier and very low pigment concentration (ranging from *0.25%wt.* to *6.25%wt.*). Due to the low consumption of the tracer, our RTD experiments can be conducted without separating the tracer particles and bulk particles.

In order to validate our RTD measurement methodology, a simple bubbling fluidized bed was used to study its particle RTD experimentally and compare it with theoretical results. Therefore, three RTD curves were determined by varying *H/D* (*1, 1.5* and *2*) with the same operating conditions. The experimental C-curves and F-curves of the fluidized bed reactor measured by the concentration measurement system fit well with the theoretical results. The experimental values of the mean residence time were also obtained close enough to the theoretical mean residence time values with a maximum relative error of less than *7%*.

The results confirmed the robustness of the methodology as a novel method for measurement of particle residence time distribution in solid unit operations.

In the second part, presented in Chapter 3, the developed technique of the concentration measurement was applied to measure the residence time distribution of a deep fluidized bed to present an application of the developed technique.

The particle RTD curves were determined experimentally in different operating conditions using Silicon Carbide (SiC) as a bulk solid and the pigment phosphorescent (Lumilux® Green SN-F50 WS) as tracer particles. In order to not perturb the flow by the injection, the amounts of tracer particles are minimized as low as possible in all experiments. A reference case (*H/D=5*; U/U_{mf}*=5*) is compared with cases in which one of the operational parameters is changed: increase height to diameter (*H/D=7*) and decrease superficial gas velocity (U/U_{mf}*=3*).

The comparison of F-curve between the reference case and ideal CSTR reactor showed that the F-curve increase more rapidly than that for perfect operation which could indicate the presence of dead volume in the bed. Consequently, the particles pass through the bed with the dead volume more quickly than that of perfect operation because there is smaller system volume.

Increasing the superficial gas velocity decreases both the mean residence time (t_m) and the variance (σ^2) of the distribution. This result is expected; the superficial gas velocity in a bed is closely related to the average particle velocity. An increase in average particle velocity corresponds to a decrease in the mean residence time.

The values of the calculated mean residence time based on the experiments were also found smaller than the theoretical mean residence time. This indicates the formation of dead regions at some locations inside the bed.

In the last part, presented in Chapter 4, a model was proposed to predict the particle residence time distribution in the deep fluidized bed described in Chapter 3. The model consists of a combination of ideal reactor models for which the E-functions are known. The measurement of RTD is required to establish a good model fitting data. Therefore, the simulated output is then compared with the experimental data.

Because of the good solids mixing in fluidization, a fluidized bed is usually modeled as tanks-in-series (TIS) model or combination of ideal plug flow and stirred tank reactors. Visual observation of the setup and the experimental data (*C*-curves and F-curves) indicated that the total volume of the bed consists of: a region where particles are mixed, a region where particles flow in the form of moving bed with insignificant mixing and a region where there is apparent absence of flow. Thus, the studied fluidized bed may be modeled as a PFR with dead volume in series with a CSTR.

Two model parameters were obtained from the model development, τ_p(mean residence time of the plug flow) and τ_s (mean residence time in the CSTR). Based on the experimental data, an increase of the superficial gas velocity cause an increase in mixing behavior (τ_s/τ). Similarly, for constant mass flow rate an increase in superficial gas velocity decreases the plug flow behavior of the bed (τ_p/τ) as expected. Furthermore, the value of τ_s/τ_p which represents the mixing behavior to plug behavior ratio is increased with increasing the solids inventory. So, it is possible to conclude that the solids mixing in the bed increases with increasing the solids inventory even with increasing the mass flow rate.

Following the modeling of the deep fluidized bed, the predicted mean residence time were obtained close enough to the measured mean residence time which indicates the existence of the good agreement between the proposed model and experimental data. It was also shown that the Tank-in-series model, as a one commonly used model, cannot describe the behavior of the studied system. The errors in the "CSTR in series with PFR" model were found small (4.5% in average) whereas in the "Tank-in-series" model were found highly larger (13% in average).

Recommendations

This thesis provides comprehensive experimental results and systematic understanding on hydrodynamics and particle residence time distribution in solid unit operations. However, there are areas which require further work:

In this study, only one type of bulk particle employed throughout the experiments, however, residence time distribution of the solid unit operations is greatly influenced by the physical properties of solid particles. Therefore, experiments using different solid particles can provide more insight into their impacts in hydrodynamics of solid unit operations and their particle residence time distributions. By using another bulk particle, another tracer particle will be needed that has identical physical properties. It is possible to coat the outside of the bulk particles using the pigment. In this way, any particles that can be coated may be used for the RTD experiments.

The RTD results in this study were obtained by sampling and subsequent measurement in laboratory using concentration measurement system. The experimental RTD curves can be obtained either by online measurement and can be monitored continuously. It will be useful to integrate the concentration measurement system with solid unit operation allowing the RTD measurement with simple online detection of the tracer.

The developed measurement technique in the present study was applied in a deep fluidized bed. Applying this developed measurement technique in other solid unit operations (Downer, extruder, cyclone, dual circulating fluidized bed…) is quite challenging and therefore further experimental works may need to be carried out.

References

[1] R. D. Abellon, Z. I. Kolar, W. den Hollander, J. J. M. de Goeij, J. C. Schouten, and C. M. van den Bleek, "A single radiotracer particle method for the determination of solids circulation rate in interconnected fluidized beds", *Powder Technol.*, vol. 92, no. 1, pp. 53–60, Jun. 1997.

[2] P. A. Ambler, B. J. Milne, F. Berruti, and D. S. Scott, "Residence time distribution of solids in a circulating fluidized bed: Experimental and modelling studies", Chemical Engineering Science, vol. 45, no. 8, pp. 2179–2186, 1990.

[3] S. Bhusarapu, M. Al-Dahhan, and M. P. Dudukovic, "Quantification of solids flow in a gas–solid riser: single radioactive particle tracking", *Chem. Eng. Sci.*, vol. 59, no. 22–23, pp. 5381–5386, Nov. 2004.

[4] W. Lin, C. E. Weinell, P. F. B. Hansen, and K. Dam-Johansen, "Hydrodynamics of a commercial scale CFB boiler-study with radioactive tracer particles", *Chem. Eng. Sci.*, vol. 54, no. 22, pp. 5495–5506, Nov. 1999.

[5] S. Mahmoudi, J. Baeyens, and J. Seville, "The solids flow in the CFB-riser quantified by single radioactive particle tracking", *Powder Technol.*, vol. 211, no. 1, pp. 135–143, Jul. 2011.

[6] H. J. Pant, V. K. Sharma, S. Goswami, J. S. Samantray, I. N. Mohan, and T. Naidu, "Residence time distribution study in a pilot-scale gas–solid fluidized bed reactor using radiotracer technique", *J. Radioanal. Nucl. Chem.*, vol. 302, no. 3, pp. 1283–1288, Sep. 2014.

[7] C. W. Chan, J. P. K. Seville, D. J. Parker, and J. Baeyens, "Particle velocities and their residence time distribution in the riser of a CFB", *Powder Technol.*, vol. 203, no. 2, pp. 187–197, Nov. 2010.

[8] A. Avidan and J. Yerushalmi, "Solids Mixing in an Expanded Top Fluid Bed", American Institute of chemical engineers (AIChE), vol. 31, no. 5, pp. 835–841, 1985.

[9] D. C. Guío-Pérez, T. Pröll, and H. Hofbauer, "Solids residence time distribution in the secondary reactor of a dual circulating fluidized bed system", *Chem. Eng. Sci.*, vol. 104, pp. 269–284, Dec. 2013.

[10] D. C. Guío-Pérez, T. Pröll, and H. Hofbauer, "Influence of ring-type internals on the solids residence time distribution in the fuel reactor of a dual circulating fluidized bed system for chemical looping combustion", *Chem. Eng. Res. Des.*, vol. 92, no. 6, pp. 1107–1118, Jun. 2014.

[11] P. Legile and Y. Gonthier, “Determination du temps de skjour des particules gaz-solide par trasage magnktique”, Powder Technology, vol. 66, pp. 69–74, 1991.

[12] R. Andreux, G. Petit, M. Hemati, and O. Simonin, “Hydrodynamic and solid residence time distribution in a circulating fluidized bed: Experimental and 3D computational study”, *Chem. Eng. Process. Process Intensif.*, vol. 47, no. 3, pp. 463–473, Mar. 2008.

[13] H. P. Cui *et al.*, “Gas and solids mixing in a dynamically scaled fluid coker stripper”, *Chem. Eng. Sci.*, vol. 61, no. 2, pp. 388–396, Jan. 2006.

[14] M. J. Rhodes, S. Zhou, T. Hirama, and H. Cheng, “Effects of Operating Conditions on Longitudinal Solids Mixing in a Circulating Fluidized Bed Riser”, American Institute of chemical engineers (AIChE), vol. 37, no. 10, 1991.

[15] K. Smolders and J. Baeyens, “Overall solids movement and solids residence time distribution in a CFB-riser”, *Chem. Eng. Sci.*, vol. 55, no. 19, pp. 4101–4116, Oct. 2000.

[16] B. Du and F. Wei, “Lateral solids mixing behavior of different particles in a riser with FCC particles as fluidized material”, *Chem. Eng. Process. Process Intensif.*, vol. 41, no. 4, pp. 329–335, Apr. 2002.

[17] A. T. Harris, R. B. Thorpe, and J. F. Davidson, “Stochastic modelling of the particle residence time distribution in circulating uidised bed risers”, Chemical Engineering Science, vol. 57, pp. 4779–4796, 2002.

[18] a. T. Harris, J. F. Davidson, and R. B. Thorpe, “Influence of exit geometry in circulating fluidized-bed risers”, *AIChE J.*, vol. 49, no. 1, pp. 52–64, Jan. 2003.

[19] a. T. Harris, J. F. Davidson, and R. B. Thorpe, “Particle residence time distributions in circulating fluidised beds”, *Chem. Eng. Sci.*, vol. 58, no. 11, pp. 2181–2202, Jun. 2003.

[20] A. Harris, J. Davidson, and R. Thorpe, “A novel method for measuring the residence time distribution in short time scale particulate systems”, *Chem. Eng. J.*, vol. 89, no. 1–3, pp. 127–142, Oct. 2002.

[21] A. T. Harris, J. F. Davidson, and R. B. Thorpe, “The influence of the riser exit on the particle residence time distribution in a circulating fluidised bed riser”, *Chem. Eng. Sci.*, vol. 58, no. 16, pp. 3669–3680, Aug. 2003.

[22] C. Huang, Z. Qian, M. Zhang, and F. Wei, “Solids mixing in a down-flow circulating fluidized bed of 0.418-m in diameter”, *Powder Technol.*, vol. 161, no. 1, pp. 48–52, Jan. 2006.

[23] F. Wei, Z. Wang, Y. Jin, Z. Yu, and W. Chen, “Dispersion of lateral and axial solids in a cocurrent downflow circulating fluidized bed”, Powder Technology, vol. 81, pp. 25–30, 1994.

[24] C. Yan *et al.*, “Solids mixing in a fluidized bed riser”, *Powder Technol.*, vol. 193, no. 1, pp. 110–119, Jul. 2009.

[25] T. Chen, W. I. Patterson, and J. M. Dealy, “On-line Measurement of Residence Time Distribution in a Twin-screw Extruder”, *Int. Polym. Process.*, vol. 10, no. 1, pp. 3–9, Mar. 1995.

[26] G. Kulah, X. Q. Song, H. T. Bi, C. J. Lim, and J. R. Grace, “A novel system for measuring solids dispersion in circulating fluidized beds”, pp. 4–9, 2003.

[27] Y. Gao, F. J. Muzzio, and M. G. Ierapetritou, “A review of the Residence Time Distribution (RTD) applications in solid unit operations”, *Powder Technol.*, vol. 228, pp. 416–423, Sep. 2012.

[28] W.-C. Yang, "Handbook of fluidization and fluid-particle systems", CRC Press, 2003.

[29] J. R. Grace, “High-velocity fluidized bed reactors”, *Chem. Eng. Sci.*, vol. 45, no. 8, pp. 1953–1966, 1990.

[30] P. V. Danckwerts, “Continuous flow systems”, *Chem. Eng. Sci.*, vol. 2, no. 1, pp. 1–13, 1953.

[31] D. C. Guío-pérez, T. Pröll, and H. Hofbauer, “Measurement of ferromagnetic particle concentration for characterization of fl uidized bed fl uid-dynamics”, Powder Technology, vol. 239, pp. 147–154, 2013.

[32] S. Mahmoudi, J. P. K. Seville, and J. Baeyens, “The residence time distribution and mixing of the gas phase in the riser of a circulating fluidized bed”, *Powder Technol.*, vol. 203, no. 2, pp. 322–330, Nov. 2010.

[33] T. Stief, U. Schygulla, H. Geider, O. U. Langer, E. Anurjew, and J. Brandner, “Development of a fast sensor for the measurement of the residence time distribution of gas flow through microstructured reactors”, *Chem. Eng. J.*, vol. 135, no. 1, 2007.

[34] H. S. Fogler, “Distributions of residence times for chemical reactors”, *Elem. Chem. React. Eng.*, pp. 867–944, 2006.

[35] T. Saruchera, “Measurement and Modelling of Particle Residence Time in a Return-Flow Cyclone”, PhD thesis, Chemical and Process Engineering , University of Canterbury, 1999.

[36] J. M. Irudayaraj, "*Food Processing Operations Modeling: Design and Analysis*", CRC Press 2001.

[37] Y. H. Hui, "*Handbook of food science, technology, and engineering- 4 Volume Set", CRC Press,* 2005.

[38] P. N. Baptista, F. A. R. Oliveira, J. Sannervik, and J. C. Oliveira, "The effect of mixing particles with different characteristics on the residence time distribution of particles in two-phase flow in a tubular system", *J. Food Eng.*, vol. 29, no. 3–4, pp. 361–373, 1996.

[39] B. Dutta and S. Sastry, "Velocity distributions of food particle suspenstions in holding tube flow: Experimental and modeling studies on average particle velocities", *Food Sci.*, vol. 55, pp. 1448–1453, 1990.

[40] L. Palmieri, D. Cacace, G. Dipollina, and G. Dall'Aglio, "Residence time distribution of food suspensions containing large particles when flowing in tubular systems", *Food Eng.*, vol. 17, pp. 225–239, 1992.

[41] M. Sancho and M. Rao, "Residence time distribution in a holding tube", *Food Eng.*, vol. 15, pp. 1–19, 1992.

[42] K. Sandeep and C. Zuritz, "Residence time of multiple particles in non-Newtonian holding tube flow: Effect of process parameters and developement of dimensionless correlations", *Food Eng.*, vol. 25, pp. 31–44, 1995.

[43] W. Chen and R. Jan, "The torsion effect on fully developed laminar flow in helical square ducts", *Fluids Eng.*, vol. 115, pp. 292–301, 1993.

[44] G. Tucker and P. Withers, "Determination of residence time distribution of non-settling food particles in viscous food carrier fluids using hall effect sensors", *Food Process eng*, vol. 17, pp. 401–422, 1994.

[45] K. Sandeep, C. Zuritz, and V. Puri, "Residence time distribution of particles during two-phase non-Newtonian flow in conventional as compared with helical holding tubes", *Food Sci.*, vol. 62, pp. 647–652, 1997.

[46] O. Levenspiel, "*Chemical reaction engineering"*. Wiley, 1972.

[47] O. Levenspiel and W. K. Smith, "Notes on the diffusion-type model for the longitudinal mixing of fluids in flow", vol. 6, pp. 227–233, 1957.

[48] N. Mostoufi and J. Chaouki, "Local solid mixing in gas–solid fluidized beds", *Powder Technol.*,

vol. 114, no. 1–3, pp. 23–31, Jan. 2001.

[49] Training cours series No. 31, “Radiotracer Residence Time Distribution Method for Industrial and Environmental Applications”, International Atomic Energy Agency (IAEA), 2008.

[50] D. J. Parker and X. Fan, “Positron emission particle tracking-Application and labelling techniques”, *Particuology*, vol. 6, no. 1, pp. 16–23, 2008.

[51] E. Talmor and R. Benenati, “Mixing and Circulation in Gas Fluidized Beds”, American Institute of chemical engineers (AIChE), vol. 9, no. 4, pp. 536–540, 1963.

[52] R. Bader, J. Findlay, and T. M. Knowlton, "*Circulating Fluidized Bed Technology*", Elsevier, 1988.

[53] J. Euzen, J.P. Fortin, “Partikelbewegung in einem dreiphaseenfliessbett”, Chemie Ingenieur Technik, vol. 5, pp. 416–419, 1987.

[54] J. Klein, O. Dolgoš, Š. Godó, M. Blažej, and J. Markoš, “Application of a Magnetic Tracer Method for the Characterization of Hydrodynamics in Internal-Loop Airlift Bioreactors”, Chem. Papers, no.54 , pp. 456–466, 2000.

[55] P. M. Heertjes, L. H. De nie and J. Verloop, “A Tracer Technique for Particles Based on Magnetic Separation”, Powder Technology, vol. 1, pp. 301-304, 1967.

[56] E. Sette, D. Pallarès, F. Johnsson, F. Ahrentorp, A. Ericsson, and C. Johansson, “Magnetic tracer-particle tracking in a fluid dynamically down-scaled bubbling fluidized bed”, *Fuel Process. Technol.*, vol. 138, pp. 368–377, 2015.

[57] W. J. Thiel and O. E. Potter, “The Mixing of Solids in Slugging Gas Fluidized Beds”, American Institute of chemical engineers (AIChE), vol. 24, no. 4, pp. 561–569, 1978.

[58] J. A. Valenzuela, “An Experimental Fluidized Bed of Solids Mixing in a Freely Bubbling”, Powder Technology, vol. 38, pp. 63–72, 1984.

[59] D. Westphalen and L. Glicksman, “Lateral solid mixing measurements in circulating fluidized beds”, Powder Technology, vol. 82, pp. 153–167, 1995.

[60] F. Wei and J. X. Zhu, “Effect of flow direction on axial solid dispersion in gas—solids cocurrent upflow and downflow systems”, *Chem. Eng. J. Biochem. Eng. J.*, vol. 64, no. 3, pp. 345–352, Dec. 1996.

[61] F. Wei and J.-X. Zhu, “Effect of flow direction on axial solid dispersion in gas-solids cocurrent upflow and downflow systems”, Chemical Engineering, vol. 64, pp. 345–352, 1996.

[62] X. Ran, F. Wei, Z. Wang, and Y. Jin, “Lateral solids dispersion in a high-density riser with swirling air flow”, *Powder Technol.*, vol. 121, no. 2–3, pp. 123–130, Nov. 2001.

[63] S. K. Kang, T. W. Kwon, and S. D. Kim, “Hydrodynamic characteristics of cyclone reactors”, *Powder Technol.*, vol. 58, no. 3, pp. 211–220, 1989.

[64] C. E. Weinell, K. Dam-Johansen, and J. E. Johnsson, “Single-particle behaviour in circulating fluidized beds”, *Powder Technol.*, vol. 92, no. 3, pp. 241–252, 1997.

[65] S. Maronga, “On the Optimization of the Fluidized Bed Particulate Coating Process”, Department of Chemical Engineering and Technology, Royal Institut of Technology, Stockholm, Sweden, 1998.

[66] A. Nienow, “Fluidized ed granulation and coating: Application to materials, Agriculture and Biotechnology”, *Chem. Eng. Commun.*, vol. 139, pp. 233–253, 1995.

[67] A. Bellil, “Méthodologie spécifique globale de caractérisation des écoulements gaz/solides pour l’optimisation d’enceintes thermiques”, PhD thesis, Université de Technologie de Compiègne, 2014.

[68] C. Wen, L.T. Fan, “Models for flow systems and chemical reactors”, *M.Dekker, New York*, p. 570, 1975.

[69] R. G. Sherritt, J. Chaouki, A. K. Mehrotra, and L. A. Behie, “Axial dispersion in the three-dimensional mixing of particles in a rotating drum reactor”, *Chem. Eng. Sci.*, vol. 58, no. 2, pp. 401–415, 2003.

[70] G. Taylor, “Dispersion of Soluble Matter in Solvent Flowing Slowly through a Tube”, *Proceedings of the Royal Society A: Mathematical, Physical and Engineering Sciences*, vol. 219. pp. 186–203, 1953.

[71] B. Régis, P. Vauchel, R. Kaas, A. Arhaliass, and J. Legrand, “Dynamical modelling of a reactive extrusion process: Focus on residence time distribution in a fully intermeshing co-rotating twin-screw extruder and application to an alginate extraction process”, Chemical Engineering Sicence, vol. 65, no. 10, pp. 3313–3321, 2010.

[72] P. M. Portillo, A. U. Vanarase, A. Ingram, J. K. Seville, M. G. Ierapetritou, and F. J. Muzzio, “Investigation of the effect of impeller rotation rate, powder flow rate, and cohesion on

powder flow behavior in a continuous blender using PEPT", *Chem. Eng. Sci.*, vol. 65, no. 21, pp. 5658–5668, 2010.

[73] O. S. Sudah, A. W. Chester, J. A. Kowalski, J. W. Beeckman, and F. J. Muzzio, "Quantitative characterization of mixing processes in rotary calciners", *Powder Technol.*, vol. 126, no. 2, pp. 166–173, 2002.

[74] P. Markström, N. Berguerand, and A. Lyngfelt, "The application of a multistage-bed model for residence-time analysis in chemical-looping combustion of solid fuel", *Chem. Eng. Sci.*, vol. 65, no. 18, pp. 5055–5066, 2010.

[75] A. H. Essadki, B. Gourich, C. Vial, and H. Delmas, "Residence time distribution measurements in an external-loop airlift reactor: Study of the hydrodynamics of the liquid circulation induced by the hydrogen bubbles", *Chem. Eng. Sci.*, vol. 66, no. 14, pp. 3125–3132, 2011.

[76] V. Shilapuram, D. Jaya Krishna, and N. Ozalp, "Residence time distribution and flow field study of aero-shielded solar cyclone reactor for emission-free generation of hydrogen", *Int. J. Hydrogen Energy*, vol. 36, no. 21, pp. 13488–13500, 2011.

[77] G. R. Ziegler and C. A. Aguilar, "Residence time distribution in a co-rotating, twin-screw continuous mixer by the step change method", *J. Food Eng.*, vol. 59, no. 2–3, pp. 161–167, 2003.

[78] L. Montastruc, J. P. Brienne, and I. Nikov, "Modeling of residence time distribution: Application to a three-phase inverse fluidized bed based on a Mellin transform", *Chem. Eng. J.*, vol. 148, no. 1, pp. 139–144, May 2009.

[79] C. Nikitine, E. Rodier, M. Sauceau, and J. Fages, "Residence time distribution of a pharmaceutical grade polymer melt in a single screw extrusion process", *Chem. Eng. Res. Des.*, vol. 87, no. 6, pp. 809–816, 2009.

[80] S. Rodríguez-Rojo, N. López-Valdezate, and M. J. Cocero, "Residence time distribution studies of high pressure fluidized bed of microparticles", *J. Supercrit. Fluids*, vol. 44, no. 3, pp. 433–440, 2008.

[81] C. J. Dittrich and S. M. P. Mutsers, "On the residence time distribution in reactors with non-uniform velocity profiles: The horizontal stirred bed reactor for polypropylene production", *Chem. Eng. Sci.*, vol. 62, no. 21, pp. 5777–5793, 2007.

[82] A. I. Yeh and Y. M. Jaw, "Modeling residence time distributions for single screw extrusion process", *J. Food Eng.*, vol. 35, no. 2, pp. 211–232, 1998.

[83] V. K. Pareek, Z. Yap, M. P. Brungs, and a. a. Adesina, “Particle residence time distribution (RTD) in three-phase annular bubble column reactor”, *Chem. Eng. Sci.*, vol. 56, no. 21–22, pp. 6063–6071, Nov. 2001.

[84] C. Zhongxi, S. Guogang, J. Jiao, Y. Zheng, G. Bing, and S. Mingxian, “Gas flow behavior and residence time distribution in a rough-cut cyclone”, *Chem. Eng. J.*, vol. 106, no. 1, pp. 43–52, Jan. 2005.

[85] C. W. A.Sarkar, “Simulation of a continuous granular mixer: effect of operating conditions on flow and mixing”, *Chem. Eng. Sci.*, vol. 11, pp. 2672–2682, 2009.

[86] D. Kunii and O. Levenspiel, "*Fluidization engineering, second edition*", Howard Brenner 1991.

[87] D. Geldart, “Types of gas fluidization”, *Powder Technol.*, vol. 7, no. 5, pp. 285–292, 1973.

[88] C. Dechsiri, *Particle Transport in Fluidized Beds: experiments and stochastic models*, University of Groningen: s.n.. 2004.

[89] L. Reh, "*Chemical Engineering Technology"*, chem.Eng.Prog. vol. 67, no. 58 1968.

[90] K. Shakourzadeh, “Techniques de fluidisation”, *Tech. l’Ingénieur*, pp. 1–20, 2002.

[91] P. Basu, "*Circulating fluidized bed boilers: Design, operation and maintenance"*, Springer international publishing, 2015.

[92] C. K. Gupta and D. Sathiyamoorthy, "*Fluid Bed Technology in Materials Processing"*, CRC Press LLC, 1999.

[93] S. Ergun, “Fluid flow through packed columns”, *Chem. Eng. Prog. symp Ser.*, vol. 48, pp. 89–94, 1952.

[94] H. J. Subramani, M. B. Mothivel Balaiyya, and L. R. Miranda, “Minimum fluidization velocity at elevated temperatures for Geldart’s group-B powders”, *Exp. Therm. Fluid Sci.*, vol. 32, no. 1, pp. 166–173, 2007.

[95] C. Y. Wen and Y. H. Yu, “Mechanics of fluidization”, *Chem. Eng. Prog. symp Ser.*, vol. 62, no. 62, pp. 100–111, 1966.

[96] M. Leva, “Fluidization”, *McGraw Hill, New York*, 1959.

[97] J. Baeyens, PhD thesis,University of Bradford, 1973.

[98] V. Thonglimp and N. H. C. Laguerie, “Vitesse Minimale de Fluidisation et Expansion des Couches Fluidiques par un gaz”, *Powder Technol.*, vol. 38, pp. 233–253, 1984.

[99] Y. Lu *et al.*, “Minimum fluidization velocities for supercritical water fluidized bed within the range of 633-693K and 23-27MPa”, *Int. J. Multiph. Flow*, vol. 49, pp. 78–82, 2013.

[100] C. Y. Wen and L. H. Chen, “Fluidized bed freeboard phenomena: Entrainment and elutriation”, *AIChE J.*, vol. 28, no. 1, pp. 117–128, 1982.

[101] W.-C. Yang, “Mechanistic models for transitions between regimes of fluidization”, *AIChE J.*, vol. 30, no. 6, pp. 1025–1027, 1984.

[102] H. L. D. Liu, M. Kwauk, “Aggregative and particulate fluidization—the two extremes of a continuous spectrum”, *Chem. Eng. Sci.*, vol. 51, pp. 4045–4063, 1996.

[103] N. K. G. Keller, “Mixing and Segregation in 3D Multi-Component Two-Phase Fluidized Beds Using X-Ray Computed Tomography”, PhD thesis, Iowa state university, 2012.

[104] E. R. Monazam, L. J. Shadle, J. S. Mei, and J. Spenik, “Identification and characteristics of different flow regimes in a circulating fluidized bed”, *Powder Technol.*, vol. 155, no. 1, pp. 17–25, 2005.

[105] L.-S. Fan and C. Zhu, “Principles of gas solid flows”, Cambridge university press, 1998.

[106] R. Zarghami, N. Mostoufi, R. Sotudeh-gharebagh, and J. Chaouki, “Particle-Wall Contact Time in Fluidized Beds”, Int. Conf. on Heat transfer, thermal engineering and environment, pp. 85–90, 2005.

[107] J. Yerushalmi and N. T. Cankurt, “Further studies of the regimes of fluidization”, *Powder Technology*, vol. 24, no. 2, pp. 187–205, 1979.

[108] H. T. Bi and J. R. Grace, “Flow regime diagrams for gas-solid fluidization and upward transport”, *Int. J. Multiph. Flow*, vol. 21, no. 6, pp. 1229–1236, 1995.

[109] R. C. Zijerveld, F. Johnsson, A. Marzocchella, J. C. Schouten, and C. M. Van Den Bleek, “Fluidization regimes and transitions from fixed bed to dilute transport flow”, *Powder Technol.*, vol. 95, no. 3, pp. 185–204, 1998.

[110] D. Bai, A. S. Issangya, and J. R. Grace, “A novel method for determination of choking velocities”, *Powder Technol.*, vol. 97, no. 1, pp. 59–62, 1998.

[111] C. X. R. Rowe, P. N., and Yacono, “The Bubbling Behaviour of Fine Powders When Fluidised”,

Chem. Eng. Sci., vol. 31, pp. 1179–1192, 1976.

[112] L. Macchi, A., Bi, H., Grace, J. R., McKnight, C. A., and Hackman, "Effect of gas Density on the Hydrodynamics of Bubble Columns and Three-Phase Fluidized Beds", *Can. J. Chem. Eng.*, vol. 81, pp. 846–852, 2003.

[113] T. Nienow, A. W., Rowe, P. N., and Chiba, "Mixing and Segregation of a Small Proportion of Large Particles in Gas Fluidized Beds of Considerably Smaller Ones", *AIChE J.*, vol. 74, pp. 45–53, 1978.

[114] E. R. Monazam and L. J. Shadle, "A transient method for characterizing flow regimes in a circulating fluid bed", *Powder Technol.*, vol. 139, no. 1, pp. 89–97, 2004.

[115] W. Namkung, S. W. Kim, and S. D. Kim, "Flow regimes and axial pressure profiles in a circulating fluidized bed", *Chem. Eng. J.*, vol. 72, no. 3, pp. 245–252, 1999.

[116] M. Louge and H. Chang, "Pressure and voidage gradients in vertical gas-solid risers", *Powder Technol.*, vol. 60, no. 2, pp. 197–201, 1990.

[117] C. Wang, "High-density gas-solid circulating fluidized bed riser and downer reactors", PhD thesis, The University of Western Ontario, 2013.

[118] Y. Jin and F. Wei, "*Multi-phase chemical reaction and technology (Part 1)"*, 1911.

[119] D. Bai, E. Shibuya, N. Nakagawa, and K. Kato, "Characterization of gas fluidization regimes using pressure fluctuations", *Powder Technol.*, vol. 87, no. 2, pp. 105–111, 1996.

[120] D. R. Bai, Y. Jin, Z. Q. Yu, and J. X. Zhu, "The axial distribution of the cross-sectionally averaged voidage in fast fluidized beds", *Powder Technol.*, vol. 71, no. 1, pp. 51–58, 1992.

[121] B. Boissière, "Etude hydrodynamique et thermique d'un nouveau concept de recepteur solaire à suspensions de denses gas-particules", PhD thesis, L'institut National Polytechnique de Toulouse (INP), 2015.

[122] F. Yang, B. Henderson, and K. P. O'donnell, "The origin of the Stokes shift: The line shapes of quantum well exciton absorption and photoluminescence spectra A2 - Walle, Chris G. Van de BT - Wide-Band-Gap Semiconductors", Amsterdam: Elsevier, 1993, pp. 362–365.

[123] W. L. McCabe, J. C. Smith, P. Harriott, "Unit operation of chemical engineering- fifth edition", McGRAW-HILL international editions, 1993.

[124] J. Richardson, "Incipient fluidization and particulate systems", *Fluidization*, New york:

Academic Press, pp. 25–64, 1971.

[125] H. S. Fogler “Elements of Chemical Reaction Engineering, 3rd Ed”, 2006.

[126] D. C. Guío-pérez, T. Pröll, and H. Hofbauer, “Non-intrusive online detection of ferromagnetic particles for measurement of bed density and residence time distribution in circulating”

[127] E. Arriola, C. F. Cruz-Fierro, K. H. Alkhaldi, B. P. Reed and G. Jovanovic, “Residence time distribution of solids in staged spouted beds”, The Canadian Journal of Chemical Engineering, vol.82, pp. 94-101, 2004.

[128] E. B. Naumann and B. A. Buffham, “Mixing in Continuous Flow Systems”,,The University of Michigan, Wiley, 1983.

Annexes

Annex I: Pigment phosphorescent:

Honeywell

Europe : Phone : + 49 (5137) 999-525
Fax : + 49 (5137) 999-121
USA : Phone : + 1 (973) 455-2189
Fax : + 1 (973) 455-2561
Asia : Phone : + 82-2-3483-5103

www.honeywell-lumilux.com

Product Data Sheet
50101 Lumilux® Green SN-F50 WS

Main use	Long afterglow products according to DIN 67510 part 4
Useable for	Solvent-based paints and inks, thermoplastics, thermosetting plastics

Typical chemical properties

Composition	Strontium aluminate : Eu, Dy
Insoluble in	organic solvents
Decomposition by	water, acids
	A processing of the pigment in dispersion paints or in waterbased inks does not create a loss of glow brightness within a time frame of a few hours. A storing and warehousing of the finished waterbased system is not recommended due to a slowly ongoing decomposition of the pigment.

Typical physical properties

Appearance	yellow-green
Specific gravity	3.4 g/cm³
Particle size distribution	d_{50} = max. 75 µm as determined by COULTER Lasersizer 230
Screen analysis	max. 1 % oversized particles on 125 µm testing screen

Typical luminescent properties

Excitation	white light, UV radiation
Color of fluorescence	green
Color of phosphorescence	green
Reference criterion to DIN 67510, part 1	min. 500/70-6500-W-K

Typical decay curve

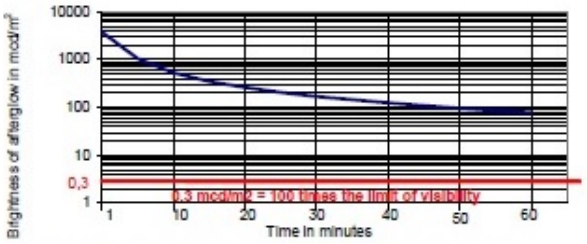

Typical intensity of afterglow according to the German norm DIN 67510-1:
Photoluminescent pigments and products - Part 1: Measurement and marking at the producer

after	5 minutes	990 mcd/m²
after	10 minutes	500 mcd/m²
after	60 minutes	70 mcd/m²
after	120 minutes	30 mcd/m²

Typical excitation (left) and phosphorescence (right) spectra

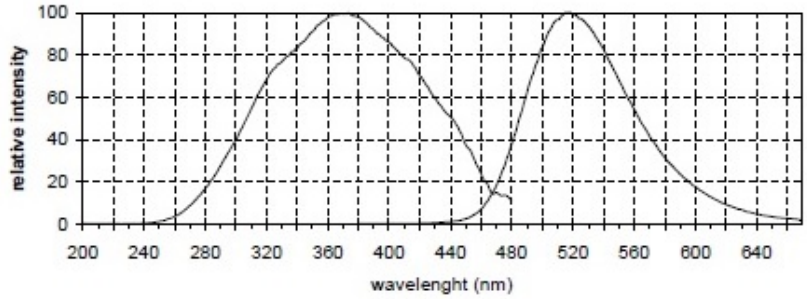

Annex II: Characteristics of UV-LED light source

Characteristics of UV-LED light source

PARAMETERS	**UV-LED SPOT LIGHT SOURCE**	**UNIT**
Maximum UV irradiation	14000	mW/cm^2
Peak wavelength	365 ± 5	nm
LED design life	20000	h
Input voltage	9 ± 0.5	V
Power consumption (Max)	25	W
Operating temperature range	+5 to +35	°C
Operating humidity range	20% to 80%	-
Control method	Front panel control/ external control/ communication control	-